Insights into cardiac remodelling by multi-modal magnetic resonance imaging and spectroscopy

Steffen E. Petersen

MD

Christ Church

Department of Cardiovascular Medicine

John Radcliffe Hospital

Oxford

OX3 9DU

Thesis submitted for the degree of
Doctor of Philosophy

Trinity Term 2005

Table of Contents

Acknowledgements

My two supervisors, Professor Stefan Neubauer and Professor Hugh Watkins, have been invaluable throughout the past three years. They supported me through excellent professional guidance for my project. I was always encouraged – both through good times and bad. I am sincerely grateful for their mentorship. My experience in Oxford has provided tremendous inspiration for my future career plans.

I would like to thank my colleagues at the University of Oxford Centre for Clinical Magnetic Resonance Research (OCMR), who all contributed to make the research project very enjoyable and memorable. I owe special thanks to my closest collaborators at OCMR: Dr. Lucy Hudsmith, Dr. Matthew Robson, Jane Francis, Dr. Joseph Selvanayagam and Dr. Damian Tyler. Dr. Frank Wiesmann deserves to be mentioned separately. Frank has become an important and indispensable friend. He proved to be an excellent housemate, fellow traveller, listener and adviser in private and professional matters. All my thoughts are with Frank and his family in this difficult time for them.

I feel immensely fortunate to have had the opportunity to work on this project at Oxford. To this end, I am very grateful to Dr. Barbara Casadei and her enthusiasm to discuss evolving project ideas and to help with patient recruitment. Dr. Helen Doll's statistical advice was similarly outstanding and has formed an integral part of my DPhil project. This research project benefited from national and international collaborations. Without Professor Robert H. Anderson's (London) unparalleled enthusiasm and optimism, our data and ideas on left ventricular non-compaction may never have got off the

ground. My perspective with regards to diagnosing and managing, particularly paediatric, hypertrophic cardiomyopathy patients was broadened by Professor Ingegerd Őstman-Smith (Gothenburg). Professor Jűrgen Hennig and Dr. Bernd Jung have kindly provided us with the tissue phase mapping sequences. Bernd has also been an excellent host and introduced me to the pleasant sides of “sunny” Freiburg. This three year project would not have been possible without the financial support from the German Academic Exchange Service (DAAD), the Medical Research Fund of Oxford University and the British Heart Foundation.

My parents are ultimately responsible for the opportunity to carry out this project. I have received complete and generous support through my days as school pupil, student and junior doctor. It was incredibly important that they were there for me. Very special thanks to both of them. A D.Phil. project is a full-time job, but it is important to recharge one’s batteries in the company of good friends and our regular “SIBS meetings”. I would particularly like to thank Clare, Krissie, Petra, Catherine, Michael and Zilli.

In summer 2003 I met Amy, my fiancée. I cannot express how much I appreciate her never-ending support and understanding. Although cardiac magnetic resonance imaging and spectroscopy enables new insights into hearts, it is thanks to Amy that I realized that no imaging modality can be perfect.

“It is only with the heart that one can see rightly; what is essential is invisible to the eye.”

“The little Prince”, Antoine de Saint Exupéry

Manuscripts arising from this work

Petersen SE, Selvanayagam JB, Francis JM, Robson MD, Wiesmann F, Myerson SG, Ostman-Smith I, Casadei B, Watkins H, Neubauer S. Differentiation of various forms of cardiac hypertrophy by means of geometric indices derived from Cardiovascular Magnetic Resonance. J Cardiovasc Magn Reson 2005;7:551-558.

Petersen SE, Jung BA, Wiesmann F, Selvanayagam JB, Francis JM, Hennig J, Neubauer S, Robson MD. Three-Dimensional Myocardial Tissue Motion – Quantitative Regional Wall Motion Analysis in Healthy Volunteers using Cine Phase Contrast Velocity Magnetic Resonance Imaging. Radiology in press.

Petersen SE, Selvanayagam JB, Wiesmann F, Robson MD, Francis JM, Anderson RH, Watkins H, Neubauer S. Left Ventricular Non-Compaction: Insights from Cardiovascular Magnetic Resonance Imaging. J Am Coll Cardiol 2005; 46(1):101-105.

Petersen SE, Timperley J, Neubauer S. Left ventricular thrombi in a patient with left ventricular non-compaction – Visualisation of the rationale for anticoagulation. Heart. 2005 Jan;91(1):e4.

Petersen SE, Hudsmith LE, Robson MD, Doll HA, Francis JM, Wiesmann F, Jung, BA, Hennig J, Watkins H, Neubauer. Sex-specific characteristics of cardiac function, geometry and mass in young adult elite athletes. Submitted.

Hudsmith LE[*], Petersen SE[*], Francis JM, Robson MD, Neubauer S. Normal human left and right ventricular and left atrial dimensions using steady state free precession magnetic resonance imaging. J Cardiovasc Magn Reson (in press).

[*]Both authors contributed equally to the work

Declaration

I declare that the work presented in this thesis is my own and has not been submitted for any other degree in this or any other University or Institute of learning.

The work presented in chapter 3 has been accepted for publication in the Journal of Cardiovascular Magnetic Resonance Imaging with a joint first authorship for Dr. Lucy E. Hudsmith and me. We have contributed equally to this specific work.

Abbreviations

ACC = American College of Cardiology

AHA = American Heart Association

ATP = adenosinetriphosphate

B_0 = symbol for external magnetic field

B_1 = denotes the rotating magnetic field generated by an RF pulse

^{13}C = carbon

CMR = cardiovascular magnetic resonance

CSI = chemical shift imaging

D = dimensional

DCM = dilated cardiomyopathy

DENSE = displacement encoding with stimulated echos

DPG = diphosphoglycerate

ECG = electrocardiogram

EDV(I) = end-diastolic volume (index)

EF = ejection fraction

ESV(I) = end-systolic volume (index)

FID = free induction decay

FLASH = fast low angle shot

^{1}H = hydrogen

HCM = hypertrophic cardiomyopathy

LA = left atrium/atrial

LV = left ventricle/ventricular

LVNC = left ventricular non-compaction

MRI = magnetic resonance imaging

MRS = magnetic resonance spectroscopy

^{23}Na = sodium

NC/C ratio = ratio of non-compacted to compacted myocardium

NYHA = New York Heart Association

^{31}P = phosphorus

PCr = phosphocreatine

PDE = phosphodiesters

PPA = phenylphosphonic acid

RF = radiofrequency

ROC = receiver operating characteristics

RV = right ventricle/ventricular

SD = standard deviation

SSFP = steady-state free precession

SV(I) = stroke volume (index)

T = Tesla

TE = echo time

TR = repetition time

TSE = turbo spin echo

T_1 = longitudinal or spin-lattice relaxation

T_2 = transverse or spin-spin relaxation

TPM = tissue phase mapping

Venc = velocity encoding

Abstract

Insights into cardiac remodelling by multi-modal magnetic resonance imaging and spectroscopy

Steffen E. Petersen, Christ Church, DPhil, Trinity Term, 2005

Cardiac remodelling, defined as a change in cardiac shape and size in response to myocardial injury or external stimuli (pressure- or volume-overload), can be physiological or pathological in nature. Physiological remodelling may occur in athletes and pathological left ventricular hypertrophy can be found in hypertrophic and dilated cardiomyopathy, in left ventricular non-compaction (LVNC) and in left ventricular hypertrophy secondary to hypertension or aortic stenosis. Cardiovascular magnetic resonance (CMR) allows for detailed characterisation of structural and functional cardiac changes using imaging and spectroscopy techniques.

This thesis aimed to achieve several goals: First, we aimed to establish normal databases for left and right ventricular volume studies, geometric cardiac indices, as well as three-dimensional contraction and relaxation patterns. Second, based on these, we aimed to establish CMR-specific diagnostic criteria for the differentiation of physiological and pathological left ventricular hypertrophy, and for the detection of LVNC. Third, in a cross-sectional study of elite athletes and age-and sex-matched sedentary volunteers, we tested for sex-specific cardiac structural and functional changes to long-term exercise training. The final aim was to investigate cardiac energy metabolism in a group of LVNC patients with preserved cardiac function. It is unknown which pathophysiological mechanisms may be

responsible for the development of heart failure in this condition. One attractive mechanism which may explain progression into cardiac dysfunction in patients with LVNC may be altered cardiac high-energy phosphate metabolism since this has been described in hypertrophic and dilated cardiomyopathy.

Healthy sedentary controls and volunteers with physiological (athletes) and patients with pathological cardiac remodelling (hypertrophic cardiomyopathy, left ventricular non-compaction and left ventricular hypertrophy secondary to aortic stenosis or hypertension) underwent steady state free precession cine imaging. Tissue phase mapping to assess three-dimensional myocardial velocities was performed in sedentary controls and athletes. High-energy phosphates were determined by cardiac magnetic resonance spectroscopy in left ventricular non-compaction patients and in age- and sex-matched healthy controls.

We established databases in healthy volunteers for cardiovascular magnetic resonance volume studies and systolic and diastolic myocardial velocities. Based on these databases, we were able to lend further evidence to the benign nature of athlete's heart in demonstrating the absence of sex-specific cardiac structural and functional differences due to long-term exercise. We found that athlete's heart can be reliably distinguished from all forms of pathological cardiac hypertrophy using left ventricular volume and geometric indices, but pathological forms of left ventricular hypertrophy present with overlapping cardiac hypertrophy phenotypes. In addition to showing high diagnostic accuracy of cardiovascular magnetic resonance

imaging in left ventricular non-compaction, we demonstrated, for the first time, altered cardiac energetics in such patients at an early disease stage with maintained ejection fraction.

In summary, we established normal ranges for cardiac volume studies and systolic and diastolic myocardial velocities using magnetic resonance imaging. We provided further evidence for the benign nature of athlete's heart. MR-specific criteria for the differentiation of physiological from pathological LV (left ventricular) hypertrophy as well as for the diagnosis of left ventricular non-compaction were developed. Using MR spectroscopy, we documented reduced cardiac energy metabolism in left ventricular non-compaction, which may contribute towards the development of heart failure in this condition. Multi-modal magnetic resonance allows new insights into chronic cardiac remodelling processes.

CHAPTER 1: Introduction

1.1 Multi-modal magnetic resonance imaging and spectroscopy

Magnetic resonance imaging (MRI) and spectroscopy (MRS) are based on complex physics. Bloch (Bloch, 1946) and Purcell (Purcell et al., 1946) shared the Nobel Price in Physics for discovering the phenomenon of nuclear magnetic resonance. 30 years after describing the use of magnetic field gradients to encode for spatial distribution of nuclear spins, a paramount prerequisite for creating two- and three-dimensional images, Lauterbur and Mansfield were awarded the 2003 Nobel Price in Medicine (Lauterbur, 1973). Radda's (Garlick et al., 1977) and Jacobus' (Jacobus et al., 1977) groups were the first to record an MR signal from the heart, in the form of a ^{31}Phosphorus-spectrum. Cardiac MRI and MRS are challenging, as the heart is constantly moving due to breathing, cardiac contraction and relaxation. Major improvements in hardware (high-field, highly homogenous magnets, coil design, computing speed) and software, i.e. sequence development (steady-state free precession, SSFP), have contributed to the widely accepted role of CMR for growing numbers of clinical applications. This development has not come to a standstill and it is conceivable that CMR may become the primary diagnostic tool in cardiovascular medicine, due to its non-invasiveness and versatility.

1.1.1 Cardiac magnetic resonance imaging

Nuclear spin is a property of atomic nuclei with an odd number of protons, neutrons or both, such as Hydrogen (^{1}H), Phosphorus (^{31}P) and Sodium (^{23}Na) and Carbon (^{13}C). Magnetic resonance imaging is commonly

based on the ^{1}H nuclei of water and fat, which is the preferential atomic nucleus due to its high concentration in the human body (up to 110 Molar) coupled with its high “relative MR sensitivity”.

Typical clinical MRI systems possess field strengths of 1.5 Tesla (T), which is about 20000 to 50000 times stronger than the earth’s magnetic field. Nuclei possessing net spin behave as minute radio-frequency receivers and transmitters in a magnetic field. The frequency ω_0 of the transmitter is defined by the Larmor equation ($\omega_0 = \gamma B_0$; with γ being the gyromagnetic ratio and B_0 being the external magnetic field strength) and thus increases with increasing field strength. Radiofrequency (RF) pulses, if transmitted at the resonance frequency of the nuclei under investigation, elevate these spins to a higher energy level, from which they subsequently re-emit a RF signal on their return to the initial lower energy level. This re-emitted signal can be received and recorded.

One valuable consequence of the Larmor equation is that protons transmit at slightly different frequencies, if they are exposed to different field strengths. By applying a linearly increasing magnetic field within the magnet, the location of the protons will be encoded within the re-emitted RF frequencies. The mathematical transformation from a sampled signal to the component frequencies is known as a Fourier transform and the amplitude of the signal at a specific frequency will represent the number of protons at that specific location. The direction of this gradient is described as the ‘read-out’ or ‘frequency encoding’ direction in the MR image. To extend acquisition to two or more dimensions, additional switched magnetic field gradients (or gradients

for short) need to be applied in the directions perpendicular to the read-out direction. For two-dimensional imaging, the above process is repeated with different gradients applied in the second dimension for short intervals prior to acquisition, and the position is this time encoded in the phase of the signal rather than the frequency. The number of these ‘phase encoding’ steps is generally equal to the number of pixels in the phase-encode direction. The time required for each phase-encoding step is known as the repetition time (TR).

For slice selection, a magnetic field gradient is applied perpendicular to the frequency- and phase-encoding direction when an RF excitation pulse is played out. By using a RF excitation pulse that only contains a narrow range of frequencies, only nuclei within a narrow slice are excited. Frequency-encoding, phase encoding and slice selection are the processes necessary to obtain a two-dimensional image from a discrete slice of the sample. A feature particularly important for cardiac imaging is the ability to select even oblique views. This is achievable by modifying the frequency of the RF pulse, and by adaptations to the gradients.

The term “pulse sequence” or “imaging sequence” describes the way in which the scanner plays out RF pulses and gradient fields and how it acquires and reconstructs the resultant data to form an image. Different orders of these pulses have defined names to describe them, such as FLASH (Fast Low Angle SHot), SSFP (Steady-State Free Precession) and TSE (Turbo Spin Echo).

As mentioned before, a challenge for CMR remains the acquisition of high spatial and temporal resolution images of a constantly moving structure within an acceptable scan time. Cardiac motion is compensated for by cardiac gating. An electrocardiogram (ECG) signal is co-registered throughout the MR examination and can be used prospectively to trigger the image acquisition to the R-wave of the ECG. Typically, 80-90% of the cardiac cycle is covered by this method, i.e. a short part of the end-diastolic phase is missing. In retrospective cardiac gating, the co-registered ECG is used to later assign data, continuously acquired throughout the cardiac cycle, to specific cardiac frames or phases (this term is not equivalent to the phase of a spin, but relates to a temporal stage of the cardiac cycle). To compensate for respiratory motion, two fundamentally different methods have been applied in CMR. The most commonly used method is the data acquisition within a single breath-hold. Alternatively, navigator techniques can be used obviating the need for breath-holding. A navigator, typically placed over the dome of the diaphragm, allows co-registration of the position of the diaphragm and generally only accepts acquired MR signals within a narrow diaphragm position window. The advantages of navigator based imaging is that it allows patients to breathe freely and to achieve high temporal and spatial resolution; however this is at the cost of substantially longer scan time. As the duration of a breath-hold is limited, a number of clever methods have been developed to achieve high quality images within the length of a breath-hold. As already discussed, the number of acquisitions per R-R interval (one heart beat to next) is determined by the MR scanner capabilities. However, one must choose the number of temporal cardiac phases or frames to image as well as

the number of excitations per frame (also known as the number of views per segment). For each cardiac phase, the scanner can only gather data to fill a fraction or segment of k-space (k-space is an array of numbers whose Fourier transformation is the MR image); hence the term segmented k-space filling. For each R-R interval, similar segments of k-space can be filled in many different cardiac phases. For example, if a resolution of 128 is desired in the phase-encoding direction, and the number of excitations per segment is 8 (i.e. 8 lines of k-space are filled in a certain cardiac frame per R-R interval), thus requiring 16 heartbeats (8x16=128) to completely fill k-space. However, since many more RF excitations are performed per heartbeat, segments of k-space during other cardiac phases are also collected, as shown in **Figure 1.1**. The number of cardiac phases that can be acquired depends on the heart rate, number of lines of k-space per segment, and the TR. Shortening the breath-hold time by increasing the number of lines acquired per cardiac phase to fill k-space comes at a cost. Increasing the number of lines acquired per segment or cardiac phase results in more blurring of the image and at the same time provides less time to collect data for other cardiac phases, i.e. reducing the temporal resolution. A clever method of increasing the number of temporal frames without changing the acquisition is called view sharing (**Figure 1.2**). With this technique frames are interpolated between the acquired frames, thereby almost doubling the temporal resolution without changing the spatial resolution. For example, if one is acquiring four excitations per segment for each frame, the last two views of one segment are combined with the first two views of the next segment to make another image frame.

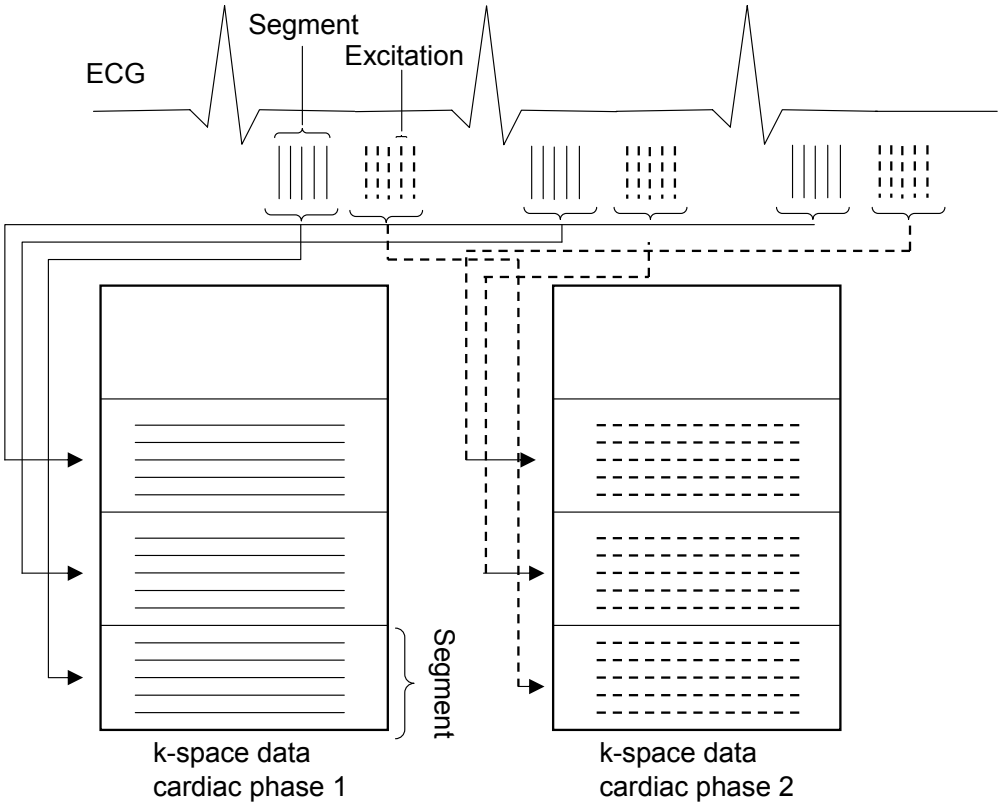

Figure 1.1: *Single slice, multiple-frame (or phase) gated segmented k-space technique. Number of excitations per segment = 5. ECG=electrocardiogram. Adapted from Elster and Burdette (Elster and Burdette, 2001).*

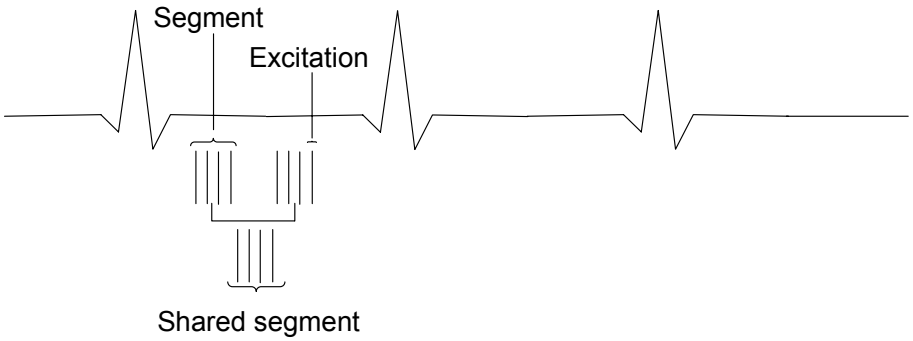

Figure 1.2: *View sharing almost doubles the temporal resolution of cine images without changing the spatial resolution. Excitations from two adjacent segments are shared to make an additional cardiac frame or phase. Adapted from Elster and Burdette (Elster and Burdette, 2001).*

If all the nuclei behaved identically, then the intensity at a pixel would depend solely on the concentration of that nucleus at that location in the body. However, several additional mechanisms make MRI a fundamentally more powerful technique.

The longitudinal relaxation time (T_1) is the time it takes for the signal to recover after an excitation pulse. Consequently, in pulse sequences with a short TR, tissue components with a long T_1 will not recover fully and will be darkened in the image (this effect is known as saturation), whereas tissues with a short T_1 will be brighter in the image. T_1 contrast can also be manipulated by changing the size of the excitation pulse (this parameter is known as the flip angle), as the spins will require more time to recover from the application of a large flip angle than from a small one. Consequently, decreasing TR and increasing the flip angle will both increase the amount of T_1-weighting and vice versa.

The transverse relaxation time (T_2) results from spins losing their phase coherence in the transverse plane and thus relates to the time that the signal is available for sampling after excitation. In T_2-weighted images the signal is acquired a short period after the excitation of the nucleus, termed echo time (TE). Tissue with a short T_2 will be darkened almost completely in the image, whereas tissue components with a long T_2 will be brighter. Increasing TE will lead to images being more T_2-weighted.

Phase velocity methods allow quantification of either flow or myocardial velocities (Bryant et al., 1984). The field gradients are used to encode the position of the blood or myocardium in the phase of the signal and then

decode this position at a later time. Stationary signal is unaffected by this encoding and decoding, but moving structures undergo a change in the phase of their signal which provides quantitative information on flow and velocity.

1.1.2 Cardiac magnetic resonance spectroscopy

CMR imaging uses the ^{1}H nucleus in water and fat molecules as its only source. In contrast, in cardiac MR spectroscopy (MRS) many additional nuclei which have a net nuclear spin, can be studied, as well summarized in recent reviews and book chapters (Neubauer, 2003; Neubauer and Clarke, 2003). The most extensively studied nucleus in cardiac MRS is ^{31}P, but ^{1}H (protons from metabolites other than water and fat), ^{13}C and ^{23}Na can be used. MRS is the only available method for the non-invasive study of cardiac metabolism without external radioactive tracers (as used for example in positron emission tomography), but is limited by low spatial and temporal resolution. The nuclei studied with MRS have low MR sensitivity (e.g. for ^{31}P, 6.6% that of ^{1}H) and are present in much lower concentrations than those of ^{1}H nuclei of water and fat (e.g. for ^{31}P, 1 to $15x10^{-3}$ Molar vs. 110 Molar). Therefore, the resolution of MRS is several orders of magnitude lower than that of CMR imaging.

There are hardware requirements that usually do not come with a standard CMR system for human cardiac ^{31}P-MRS studies: The radiofrequency (RF) generator has to be able to produce frequencies other than for ^{1}H (broadband capability), and a nucleus-specific (here ^{31}P) RF cardiac surface coil is used for MR excitation and signal reception. Corresponding to the basic principles described for CMR imaging, a RF pulse

causes spin excitation and the resulting MR signal, the free induction decay (FID), is then recorded. The FID is subjected to Fourier transformation, which results in an MR spectrum. For practical patient comfort reasons, the acquisition time is limited to about 30-45 minutes. Thus, the resolution of MRS cannot be simply improved by lengthening the acquisition time. ECG gating is required, whilst respiration gating is currently not employed given the large voxel sizes and the already extended acquisition time. It is currently recommended to perform MRS studies prone rather than supine, as this reduces respiratory motion artefacts and brings the heart closer to the surface coil, improving sensitivity. The cardiac muscle lies behind the chest wall skeletal muscle, whose ^{31}P-signal requires suppression by means of spectroscopic localisation techniques (Bottomley, 1994), such as 3-dimensional (D)-CSI (chemical shift imaging), the technique used in our studies. Pohmann and von Kienlin (Pohmann and von Kienlin, 2001), have recently implemented acquisition-weighted ^{31}P-chemical shift imaging, which reduces the signal contamination between adjacent voxels. For the first time, ^{31}P-spectra from the posterior wall could be obtained. Acquisition-weighting should thus be implemented for all cardiac MRS protocols, although the analysis of spectra most distant from the surface coil still remain a challenge and are highly dependent on the signal-to-noise ratio available in a given voxel.

A typical ^{31}P-MR spectrum from a healthy volunteer is shown in **figure 1.3.** A human ^{31}P-spectrum shows six resonances, corresponding to the three ^{31}P-atoms of adenosinetriphosphate (ATP) (labelled as α-, β- and γ-ATP), phosphocreatine (PCr), 2,3-Diphosphocglycerate (2,3-DPG, arising from

erythrocytes) and phosphodiesters (PDE, a signal due to membrane as well as serum phospholipids). Chemical shift causes different metabolites to resonate at specific frequencies, and this is quantified relative to the external magnetic field B_0 (in ppm=parts per million). Different positions of the atoms under investigation within the molecule lead to subtle alterations in the local magnetic field strength, spreading the resonance frequencies of ^{31}P-metabolites over a range of ~30 ppm. From the fully relaxed state, the area under each ^{31}P-resonance is proportional to the amount of each ^{31}P-nucleus in the sample, and metabolite resonances are quantified by measuring peak areas. Relative metabolite levels are calculated, such as the PCr/ATP ratio. The PCr/ATP ratio is a powerful indicator of the energetic state of the heart.

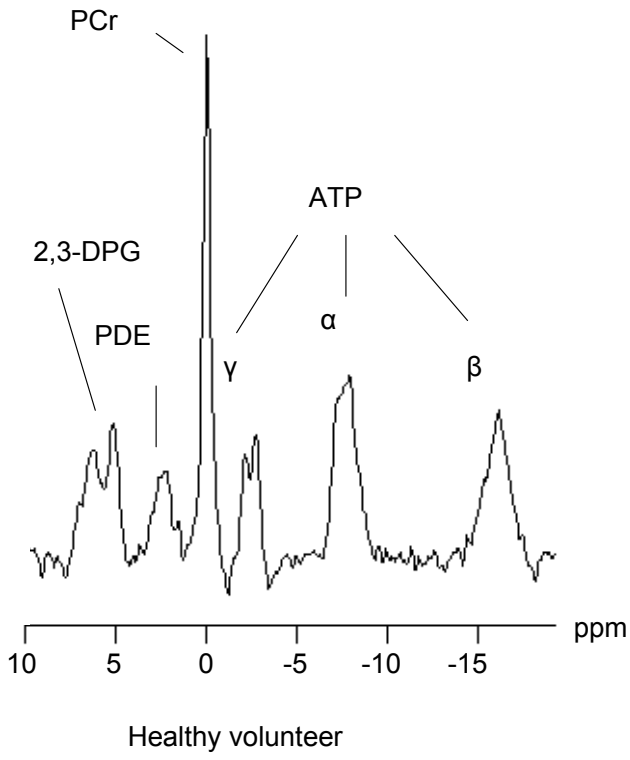

Figure 1.3: *^{31}P spectra from the basal anterior myocardium of a healthy volunteer, obtained from ^{31}P acquisition weighted chemical shift imaging datasets.*

In MRS, it is important to account for the effects of partial saturation when selecting pulse angles and TR: a full MR signal can only be obtained when the nucleus is excited from a fully relaxed spin state, i.e., when a time of at least 5 x T_1 has passed since the previous excitation (for example, T_1 of PCr at 1.5 Tesla ~4.4 s requiring TR of 22 s). Fully relaxed spectra can therefore only be obtained with long TR, leading to prohibitively long acquisition times. In practice, a shorter TR is used, leading to partially saturated spectra. Since the T_1 of ^{31}P-metabolites such as PCr and ATP differs (T_1 of PCr is ~ twice as long as T_1 of ATP), the degree of saturation also varies for different ^{31}P-resonances. Thus, when quantifying partially saturated spectra, saturation factors need to be used for correction. These factors are determined for each metabolite by comparing fully relaxed and saturated spectra. In addition, to account for saturation, either adiabatic pulses (creating identical flip angles across the entire sample volume) or B_1 (B_1 denotes the rotating magnetic field generated by an RF pulse) field characterisation (taking into account variations in flip angle) are required. Blood contributes signal to the ATP-, 2,3-DPG- and PDE-resonances of a cardiac ^{31}P-spectrum. As human blood spectra show an ATP/2,3-DPG area ratio of ~0.11 and a PDE/2,3-DPG area ratio of ~0.19, for blood correction, the ATP resonance area of cardiac spectra is reduced by 11% of the 2,3-DPG resonance area, and the PDE resonance area is reduced by 19% of the 2,3-DPG resonance area (Neubauer et al., 1992).

1.2 Cardiac remodelling

The consensus paper from an international forum on cardiac remodelling distinguishes physiological remodelling, a compensatory adaptive

change to long-term exercise, from pathological forms. Pathological forms of cardiac remodelling are defined as “genome expression, molecular, cellular and interstitial changes that are manifested clinically as changes in size, shape and function of the heart after cardiac injury” (Cohn et al., 2000). Traditionally, the term cardiac remodelling was used to describe compensatory cardiac changes in size, shape and function after a myocardial infarction as the primary cardiac injury. However, cardiac remodelling is now used in a much broader sense, including conditions with pressure-overload (aortic stenosis, hypertension), volume-overload (valvular regurgitation), inflammatory heart muscle disease (myocarditis) or idiopathic dilated cardiomyopathy. In this thesis, the focus is on primarily non-ischaemic (i.e. not coronary artery disease) cardiac remodelling, including athlete’s heart as the physiological form of remodelling and left ventricular (LV) hypertrophy secondary to hypertension and aortic stenosis, hypertrophic and dilated cardiomyopathy and left ventricular non-compaction as the pathological forms of cardiac remodelling.

1.2.1 Physiological remodelling in athlete’s heart

Athlete’s heart represents a physiological adaptation either to pressure- (strength-trained athletes, e.g. weight lifting) or volume-overload (endurance-trained athletes, e.g. cycling), leading to concentric or eccentric LV hypertrophy, respectively. Most sporting disciplines yield a combination of both mechanisms (Morganroth et al., 1975; Pelliccia et al., 1991; Maron et al., 1995; Pelliccia et al., 1999; Pluim et al., 2000; Maron, 2003; Whyte et al., 2004b). Cardiac dimensions are closely related to body size and composition (Henry et al., 1980; Gardin et al., 1987), an important factor to be taken into

account when interpreting echocardiographies or CMR scans of athletes. In the literature, female athletes have typically been underrepresented: Recent meta-analyses included male athletes in 59 studies and female athletes in only 13 studies (Pluim et al., 2000; Whyte et al., 2004a). Female athletes have larger LV cavity dimensions and maximal wall thickness compared with sedentary controls (Pelliccia et al., 1996). Nevertheless, and not surprisingly, women show smaller absolute LV cavity dimensions and wall thicknesses in comparison with male athletes (Pelliccia et al., 1991; Pelliccia et al., 1996). Furthermore, little data exist addressing the degree of right ventricular (RV) adaptive changes to exercise training, mainly due to the limited echocardiographic access to the right ventricle (Scharhag et al., 2002; D'Andrea et al., 2003a; D'Andrea et al., 2003b). Whether sex-specific differences in physiological LV and RV cardiac remodelling exist cannot be answered with confidence due to the lack of studies in athletes with age- and sex-matched sedentary controls. We performed such a study and the data are presented in Chapter 5. A genetic influence in the cardiac remodelling of athletes has been demonstrated for the renin-angiotensin system (Montgomery et al., 1997; Karjalainen et al., 1999). Recent findings have indicated that physiological hypertrophy may result from the activation of Akt through a phosphoinositide 3-kinase (PI3K) pathway (McMullen et al., 2003), a finding not observed in pathological forms of LV hypertrophy. In contrast to pathological forms of cardiac hypertrophy, upper limits of LV remodelling appear to exist for changes seen in athletes. Athletes with average training programmes almost never exceed the range of normal LV dimensions: An average of 10% increase for cavity size and 15% for wall thickness has been

reported compared with matched untrained controls (Maron et al., 1986). Elite athletes, however, can present with cardiac dimensions in a grey area or overlap area with hypertrophic and dilated cardiomyopathy. 2% of such highly trained athletes present with substantial wall thickening (≥ 13 mm), suggestive of hypertrophic cardiomyopathy (Pelliccia et al., 1991) and 15% show marked LV dilatation (end-diastolic diameter of LV cavity ≥ 60 mm), compatible with a diagnosis of dilated cardiomyopathy (Pelliccia et al., 1999).

1.2.2 Pathological remodelling

1.2.2.1 Hypertrophic cardiomyopathy

Hypertrophic cardiomyopathy (HCM) is a disease entity characterised by the development of cardiac hypertrophy without obvious cause (Spirito et al., 1997). It is one of the most common single-gene disorders of the heart, affecting up to 1 in 500 of the population and is inherited in an autosomal dominant pattern (Redwood et al., 1999; Seidman and Seidman, 2001). Many patients are asymptomatic, though dyspnoea and chest pain are common clinical features (Spirito et al., 1997). Sudden cardiac death, however, is a well recognised feature of the disease, and HCM is the most common cause of sudden death in the younger population (Maron et al., 1996). Apart from a variable degree of cardiac hypertrophy, the typical pathological features of the disease are the development of myocyte and myofibrillar disarray and increased interstitial fibrosis (**Figure 1.4**).

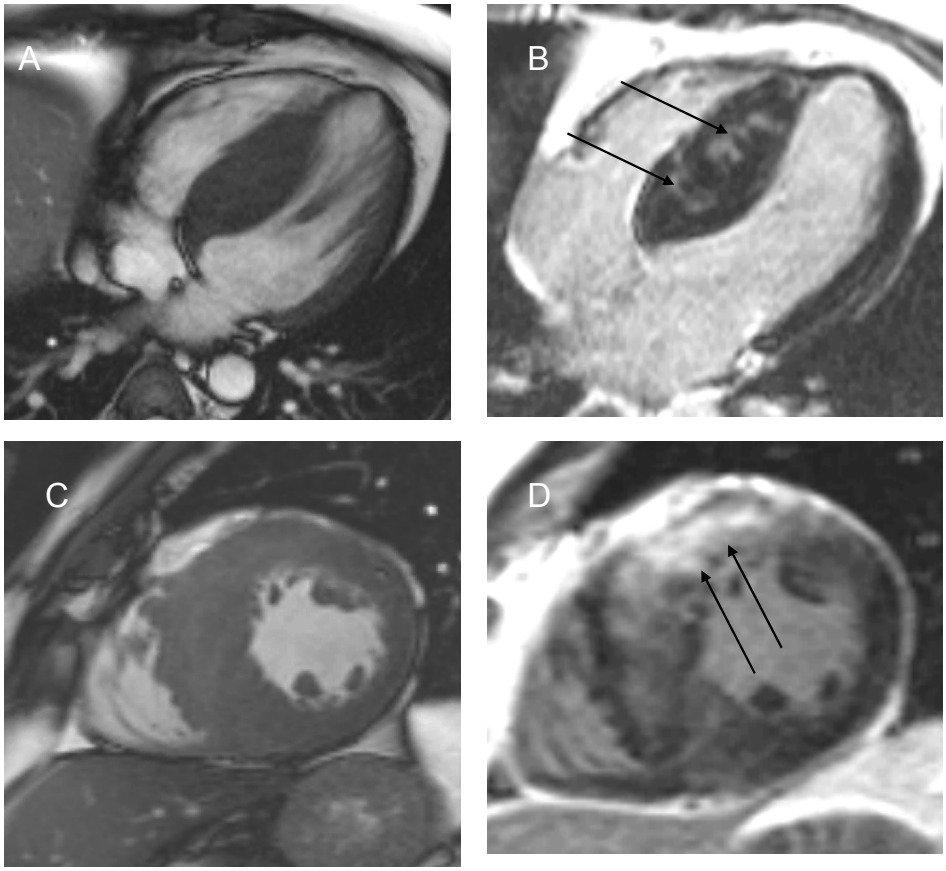

Figure 1.4: *31-year old patient with HCM. A/B horizontal long axis and C/D short axis views. A and C are end-diastolic images for the analysis of geometry, myocardial mass, volumes and function using steady-state free precession cine-sequences. B and C are corresponding end-diastolic images obtained with the delayed enhancement technique, where signal-intense areas represent fibrotic tissue and the normal myocardium appears dark. Note the patchy signal-intense areas in the anteroseptal wall (black arrows). Overall, fibrotic tissue accounts for 69.5 g in this patient. This translates to 19% of total left ventricular mass (365 g).*

The molecular genetic basis of HCM is now largely known as, in the majority of families, the disease results from mutations in genes encoding components of the cardiac contractile apparatus; thus, for the last decade HCM has been considered a “disease of the sarcomere” (Thierfelder et al., 1994). To date, nine sarcomeric disease genes have been identified in which

mutations cause HCM, and this genetic heterogeneity contributes to the clinical heterogeneity of the disease.

In most instances, HCM results from single nucleotide substitutions resulting in missense mutations, i.e. causing the substitution of a single amino acid in the protein generated. There is extensive evidence that these mutant proteins incorporate into the sarcomere, which presumably then malfunctions in some critical way (Redwood et al., 1999). The initial assumption was that a fundamental perturbation of contractility caused HCM. Early experimental evidence implicated depressed contractile function, suggesting that the cardiac hypertrophy was a compensatory response mediated by mechanical and neuroendocrine signalling. However, subsequent data suggested that different sarcomeric mutations have opposing influences, with many (probably the majority) resulting in hypercontractility; there is thus no consistent change in contractility on which to base models of disease pathogenesis. Instead, analysis of empirical data from biophysical studies of the different classes of mutant proteins lead to the suggestion that the unifying abnormality amongst HCM mutant proteins was reduced mechanical efficiency that would increase the energy cost of force production (Sweeney et al., 1998; Redwood et al., 1999; Ashrafian et al., 2003). These theoretical predictions have since been supported by experimental measurements of the amount of ATP consumed per unit force generated by HCM mutant sarcomeres (Montgomery et al., 2001).

1.2.2.2 Left ventricular non-compaction

Left ventricular non-compaction (LVNC) is characterized by the presence of an extensive myocardial trabecular layer lining the cavity of the left ventricle, and potentially leads to cardiac failure, thromboembolism (**Figure 1.5**), and malignant arrhythmias (Chin et al., 1990; Ritter et al., 1997; Ichida et al., 1999; Oechslin et al., 2000; Stollberger et al., 2002). Within this trabecular layer, it is frequently possible to find thick and prominent coarse trabeculations separated by deep intertrabecular recesses (Feldt et al., 1969; Dusek et al., 1975; Chin et al., 1990; Michel et al., 1998; Angelini et al., 1999; Jenni et al., 1999; Oechslin et al., 2000; Jenni et al., 2001; Finsterer et al., 2002; Oechslin and Jenni, 2002; Finsterer et al., 2003a; Stollberger and Finsterer, 2004; Weiford et al., 2004). Histological specimens show that the deep recesses are lined by endothelium, which extends close to the surface of the persisting compacted ventricular layer.

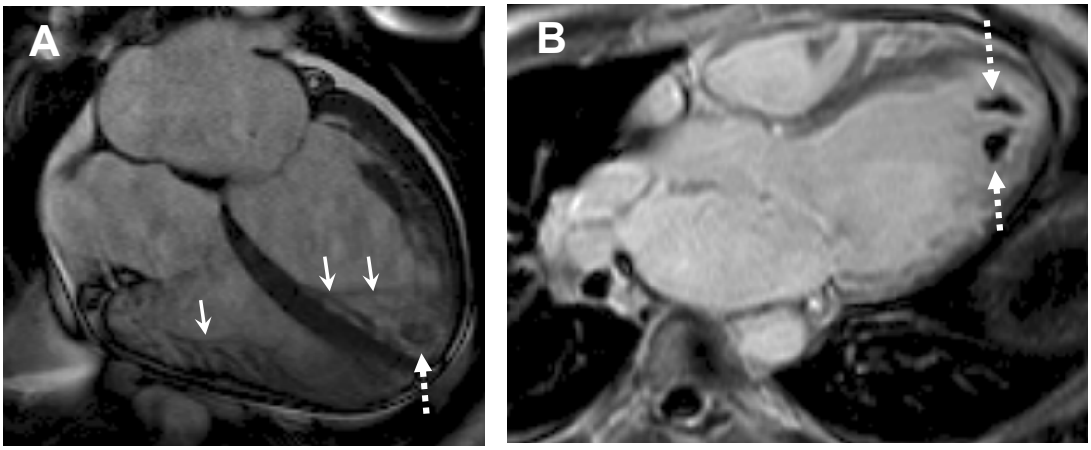

Figure 1.5: *A 46 year old previously fit and healthy male was admitted with a right femoral artery embolus, which was immediately removed by percutanous thrombectomy. Cardiovascular magnetic resonance imaging showed severely reduced left and right ventricular global function with marked biventricular dilatation. Both left and right ventricle showed a thick non-compacted and a thin compacted layer with a diagnostic left ventricular systolic non-compaction-to-compaction ratio of 3.6 (A). Thrombus imaging early after Gadolinium-DTPA administration revealed two apical left ventricular thrombi within the non-compacted layer of myocardium (B).*

The condition can be associated with a wide variety of neuromuscular disorders (Chin et al., 1990; Stollberger et al., 1996; Ichida et al., 1999; Finsterer et al., 2001; Ichida et al., 2001; Stollberger et al., 2002) and other cardiac malformations (Ichida et al., 1999; Oechslin et al., 2000). Dusek and his colleagues provided one of the earliest substantial descriptions of the entity that represents what is now called LVNC (Dusek et al., 1975). The isolated form was first described in 1990 by Chin and colleagues (Chin et al., 1990). As based on echocardiographic studies, the prevalence is estimated at 0.05% in the general population (Ritter et al., 1997). In this regard, Jenni and co-workers (Jenni et al., 2001) suggested the echocardiographic finding of a ratio of greater than two between the non-compacted and compacted myocardium in systole to be diagnostic. Echocardiography, however, poses

inherent problems in assessing the left ventricular apex, known to be the most common non-compacted area (Moon et al., 2004). Furthermore, patients with the condition may be misdiagnosed as apical hypertrophic cardiomyopathy using echocardiography (Ichida et al., 1999). Similarly, involvement of the right ventricle remains controversial, first because of the more trabeculated nature of the right ventricle itself, and second, due to problems with echocardiographic access to the right ventricle behind the sternum. Previous echocardiography studies have reported right ventricular involvement in less than half the patients with LVNC (Ritter et al., 1997; Zambrano et al., 2002), but whether this reflects the true prevalence of concomitant right ventricular non-compaction remains to be determined. In Chapter 7 we present our data on diagnostic accuracy for LVNC using cardiovascular magnetic resonance imaging.

LVNC is not currently classified as a distinct form of cardiomyopathy by the Word Health Organisation (Richardson et al., 1996), and its underlying pathophysiological mechanisms remain controversial and ultimately unknown (Finsterer et al., 2003b). LVNC may be a developmental abnormality, reflecting either impaired or arrested compaction of the developing myocardium (Dusek et al., 1975; Chin et al., 1990; Steiner et al., 1996; Angelini et al., 1999; Jenni et al., 1999; Victor et al., 1999; Jenni et al., 2001; Stollberger and Finsterer, 2004; Weiford et al., 2004). Stollberger, Finsterer and their colleagues, suggest suggest considering other mechanisms, including dissection of the myocardium, frustrated attempt to myocardial hypertrophy, myocardial tearing caused by dilatation, a metabolic defect, or compensatory hypervascularisation (Stollberger and Finsterer, 2004).

Amongst Japanese children with LVNC (Ino et al., 1993), more patients are asymptomatic on presentation and have fewer systemic embolic events and episodes of ventricular tachycardia when compared to the observations of Chin et al (Chin et al., 1990). Ichida and colleagues (Ichida et al., 1999) suggest that this difference may be accounted for by the fact that LVNC in their patients was detected incidentally during a screening study of an entire population of Japanese children. Whether the extent or degree of hypertrabeculation has a role in determining the timing of presentation, and severity of clinical course, is also uncertain, although this has been suggested (Chin et al., 1990; Wald et al., 2004). Because of the known genetic heterogeneity (Digilio et al., 1999), it is yet to be determined if a specific genetic marker may contribute to either the severity or timing of presentation. One attractive mechanism for the progression into cardiac dysfunction in LVNC may lie in altered cardiac energetics, similar to the situation in hypertrophic (Jung et al., 1998; Crilley et al., 2003) or dilated cardiomyopathy (Neubauer et al., 1992; Beer et al., 2002). Confirmation of such a mechanism would have two clinical implications: First, this would suggest treatment strategies aimed to improve myocardial energetics. Second, PCr/ATP ratios offer the hope of serving as a discriminator of a benign vs. malignant course in LVNC cases, as was shown in dilated cardiomyopathy (Neubauer et al., 1997a). Thus, we aimed to investigate cardiac energetics in a group of LVNC patients who have not or not yet developed cardiac dysfunction, to study whether cardiac energetics derangement can be demonstrated early in the disease process suggesting altered energetics as a factor contributing to the development of heart failure in LVNC. We present our findings of deranged

cardiac metabolism in LVNC patients with preserved LV ejection fraction in Chapter 8.

Ichida and colleagues (Ichida et al., 1999) reported several years ago that, in patients with isolated LVNC, familial recurrence is high, being found in approximately two-fifths of patients, a conclusion shared by others (Chin et al., 1990; Oechslin et al., 2000; Jenni et al., 2001; Neudorf et al., 2001; Stollberger and Finsterer, 2004). Mutations in the gene G4.5, which encodes taffazin, and maps to chromosome Xq28, are responsible for this myocardial disorder in some patients, being allelic with Barth Syndrome (Bione et al., 1996; Bleyl et al., 1997a; Bleyl et al., 1997b; Matsuda et al., 1999; Ichida et al., 2001; Chen et al., 2002). G4.5 was initially identified as the gene responsible for Barth syndrome, an X-linked mitochondrial disease affecting cardiac and skeletal muscle (Neustein et al., 1979; Barth et al., 1983). These mutations produce a wide phenotypic spectrum of cardiomyopathies, including dilated cardiomyopathy, X-linked infantile cardiomyopathy, and X-linked endocardial fibroelastosis (Ichida et al., 2001). Ichida and colleagues (Ichida et al., 2001) found a mutation in α-dystrophin in some of their patients. A novel mutation of intron 8 of G4.5 in one family with severe X-linked LVNC, but without the other usual findings of Barth Syndrome has been reported (Chen et al., 2002). Deletion of chromosome 5q has been identified in a child with previously repaired congenital heart disease, facial dysmorphism, and LVNC (Pauli et al., 1999). Vatta and co-workers have shown that a mutation in Cypher-Zasp, a gene encoding a protein that is a component of the Z-line in both skeletal and cardiac muscle, may be causal (Vatta et al., 2003). Interestingly, mice lacking FKBP12 have normal skeletal muscle, but have a

severe dilated cardiomyopathy and a condition suggestive of LVNC (Shou et al., 1998).

In adults identified with the sporadic form of isolated LVNC, it is an autosomal dominant disorder rarely caused by mutations in G4.5, and hence is genetically distinct from the X-linked cases seen in infancy (Kenton et al., 2004; Sasse-Klaassen et al., 2004). Sasse-Klaassen and colleagues mapped the responsible gene to chromosome 11p15 in a family with an autosomal dominant form of LVNC (Sasse-Klaassen et al., 2003). Interestingly, this study describes family members with a partial expression of the phenotype for LVNC. LVNC may also be associated with mutations in the lamin A/C gene (Hermida-Prieto et al., 2004).

1.2.2.3 Hypertensive heart disease

Hypertension affects approximately 50 million individuals in the United States and approximately 1 billion individuals worldwide (Chobanian et al., 2003). In a cross-sectional population-based study of 734 essential hypertensive patients, the prevalence of LV hypertrophy ranged from approximately 50% to 70% depending on the LV hypertrophy definition (Conrady et al., 2004). The traditional concept of heart failure development via hypertension, concentric LV hypertrophy, myocardial fibrosis and contractile dysfunction, albeit attractive, may be too simplistic and is not supported by a large body of evidence. As hypertension is an independent risk factor for coronary artery disease, at least a substantial proportion of hypertensive hearts with systolic impairment will be caused by a mismatch of increased oxygen demand (hypertrophy) and reduced oxygen supply

(coronary artery disease). Hypertensive heart disease patients were studied in this thesis as a model of pressure-overload LV hypertrophy.

1.2.2.4 Aortic stenosis

A degenerative process is the most common cause of aortic stenosis in adults. The aortic valve area must be reduced to one fourth its normal size before significant changes in haemodynamics occur. In adults with aortic stenosis, the obstruction develops gradually. During this time, the LV adapts to pressure overload through a concentric hypertrophic process with increase in LV mass and wall thickness, while chamber size and ejection fraction are preserved (Bonow et al., 1998). The hypertrophied heart may have reduced coronary flow and coronary flow reserve, even in the absence of epicardial coronary artery disease (Bache et al., 1981; Marcus et al., 1982). LV hypertrophy secondary to aortic stenosis was investigated in this thesis as another model of pressure-overload hypertrophy.

1.3 Cardiac energetics in physiological and pathological left ventricular hypertrophy

^{31}P-Magnetic resonance spectroscopy studies support the notion that cardiac remodelling due to long-term exercise training behaves differently from pathological forms of LV hypertrophy. Myocardial PCr/ATP ratios remain normal at rest and during stress in athletes (Pluim et al., 1996; Pluim et al., 1998). Experimental work in rats had predicted this finding (Spencer et al., 1997).

Increasing evidence based on data from animal models and patients strongly supports the energy depletion hypothesis as a unifying mechanism

leading to hypertrophy in HCM. Impaired energetics (decreased PCr/ATP-ratios in cardiac ^{31}P-MRS) have been documented in genetically modified animal models (Spindler et al., 1998; Javadpour et al., 2003) of HCM as well as in asymptomatic patients with clinical features of HCM (Jung et al., 1998) and in genotyped, phenotypically affected and phenotypically unaffected (gene carrier), HCM patients (Crilley et al., 2003).

Only three ^{31}P-MRS studies have examined patients with LV hypertrophy due to chronic hypertension. Lamb et al (Lamb et al., 1999) demonstrated reduced PCr/ATP ratios in patients with hypertension both at rest and during dobutamine stress testing. Furthermore, PCr/ATP ratio showed a negative correlation with diastolic function indices. In contrast, two other studies showed no significant changes in cardiac energetics in hypertension (Okada et al., 1998; Beer et al., 2002). A possible explanation for these discrepant findings may lie in different severity of LV hypertrophy and different duration of hypertension in the studied populations. Experimental work clearly suggests that cardiac energetics are impaired in long-standing hypertension (Perings et al., 2000).

Experimental studies suggest alterations in myocardial energy metabolism for advanced LV hypertrophy (Wexler et al., 1988; Zhang et al., 1993). Conway et al demonstrated reductions of PCr/ATP ratios by 36% in patients with LV hypertrophy due to aortic stenosis or incompetence only if clinical signs of heart failure were present, while PCr/ATP ratios remained unchanged for asymptomatic cases (Conway et al., 1991). These findings were confirmed by another study documenting reduced PCr/ATP ratios in

patients with aortic valve disease in NYHA (New York Heart Association) stage III and IV, but not in stage I and II (Neubauer et al., 1997b). Interestingly, this study showed that for patients with the same degree of LV hypertrophy cardiac energetics were more severely altered in patients with pressure-overload hypertrophy, i.e. due to aortic stenosis, when compared to those with overload-hypertrophy, i.e. due to aortic valve incompetence. A further interesting aspect of this study was the finding of an inverse correlation between PCr/ATP ratios and LV end-diastolic pressures and wall stress. In a study performing absolute quantification of PCr and ATP in patients with aortic stenosis, ATP concentration remained unchanged with a 28% reduction in PCr concentration (Beer et al., 2002). A follow-up study determined cardiac PCr/ATP ratios in patients undergoing aortic valve surgery due to severe aortic stenosis before and 40 weeks after surgery, when LV hypertrophy had regressed. PCr/ATP ratios, which were decreased by 12% before surgery compared to healthy controls, returned to normal after successful surgery (Beyerbacht et al., 2001).

1.4 Differentiation of physiological and pathological left ventricular hypertrophy

The athlete's heart was first described and observed in cross-country skiers by carefully performed percussion of the chest at the end of the 19th century (Rost and Hollmann, 1983). For decades, determination of outer cardiac contours by physical examination and chest X-rays were the only available diagnostic tools for assessment of athlete's heart. The introduction of echocardiography has enabled in vivo morphological assessment of athlete's hearts, and subsequently diagnostic markers to distinguish

physiological from hypertrophic cardiomyopathy have been proposed (Maron et al., 1995). Hypertrophic cardiomyopathy is more likely than physiological hypertrophy if the hypertrophy is asymmetric and presents with an unusual pattern of abrupt changes in wall thickness between adjacent segments. A small LV cavity (≤ 45 mm) and abnormal LV filling pattern both suggest hypertrophic cardiomyopathy rather than athlete's heart, in which the LV cavity would be expected to be enlarged (≥ 55 mm) with normal LV filling patterns (Maron et al., 1995). However, a grey area exists, so that in clinical practice, the distinction of pathological and physiological LV hypertrophy remains a frequent clinical dilemma. Various pathological forms of LV hypertrophy, such as due to hypertrophic cardiomyopathy (HCM), hypertensive heart disease or aortic stenosis, and physiological forms of LV hypertrophy, such as in athlete's hearts, can present with overlapping cardiac hypertrophy phenotypes as determined by 2D-echocardiography or ECG. In clinical practice, the distinction between physiological hypertrophy occurring in athletes and pathological hypertrophy is critical because HCM accounts for about one-third of exercise-related sudden deaths in young competitive athletes (Maron et al., 1980; Maron et al., 1986; Burke et al., 1991; Corrado et al., 1998). Furthermore, in athletes with hypertension, the relative contributions of increased blood pressure and physical training to the degree of LV hypertrophy detected need to be clarified, and this has implications as to the recommendation of treatment with antihypertensive agents in this situation.

In current clinical practice, one strategy of distinguishing athlete's heart from pathological LV hypertrophy is to document the deconditioning effect

after training cessation for several months (Martin et al., 1986; Maron et al., 1993; Pelliccia et al., 2002). However, this is often not acceptable to athletes. Metabolic exercise testing has been shown to facilitate the differentiation between athlete's hearts and HCM (Sharma et al., 2000). We studied a novel approach to distinguish athlete's heart from various forms of pathological LV hypertrophy by means of three-dimensional CMR-derived LV volume and geometric indices, obviating the need for 'de-training' to make this distinction. These data are presented in Chapter 6.

1.5 Study aims and hypotheses

In chapter 3, we aimed to establish a large database of reference values for left and right ventricles of healthy volunteers using steady-state free precession techniques (SSFP), the preferred technique of choice for assessment of volume data in current clinical practice.

In chapter 4, we aimed to demonstrate that tissue phase mapping, an MR technique to assess 3D myocardial velocities, would allow quantitative measurement of motion parameters which are reproducible and independent of analysers. Further, given the high resolution of tissue phase mapping, we hypothesized that this method would show differences between endo- and epicardium for radial, circumferential and longitudinal velocity parameters in healthy volunteers. Thus, the purpose of our study was to prospectively establish a database of normal, three-dimensional, systolic and diastolic, endo- and epicardial velocities of all myocardial segments in healthy volunteers using cine phase contrast velocity magnetic resonance imaging (tissue phase mapping or TPM).

In chapter 5, we aimed to study male and female young adult elite athletes with age- and sex-matched sedentary controls to assess sex-specific differences for LV and RV dilatation and hypertrophy as well as for LV contraction and relaxation. We hypothesized that structural and functional adaptive changes to exercise training would be sex-specific.

In chapter 6, we employed CMR imaging to test whether CMR-derived LV volume parameters and geometric indices accurately predict the underlying aetiology of LV hypertrophy. This hypothesis was tested in groups of patients with HCM, hypertension and aortic stenosis, and in athletes.

It is necessary to establish specific CMR criteria for the diagnosis of pathological non-compaction. To this end, we examined healthy volunteers as well as patients with potential differential diagnoses for LVNC. Findings from this group were compared with unequivocal LVNC cases in whom the diagnosis was supported by other clinical features. Data on diagnostic accuracy for LVNC are presented in chapter 7.

LVNC is characterised by the presence of an extensive non-compacted layer of myocardium, which can lead to chronic cardiac failure. The non-compacted myocardium likely represents an embryological arrest of compaction, i.e., a mechanism distinct from other forms of cardiomyopathy with known alteration of cardiac energetics, such as dilated or hypertrophic cardiomyopathy. We hypothesized that patients with LVNC and maintained ejection fraction show reduced cardiac high-energy phosphate metabolism, suggesting altered energetics as a factor contributing to the development of heart failure in LVNC. Our findings are presented in chapter 8.

CHAPTER 2: Methods

All individuals underwent a clinical study with two subsequent CMR scans performed on a 1.5 Tesla MR system (Sonata Maestro Class, Siemens Medical Solutions, Erlangen, Germany)) equipped with a high performance gradient system (40mT/m peak strength, 200T/m/s maximum slew rate), and multi-nuclear capabilities enabling ^{31}P MRS of the heart.

2.1 Cardiac magnetic resonance imaging protocol

Multi-modality CMR imaging, was designed to measure cardiac morphology, function and mass. After piloting, steady-state free precession cine images (SSFP, TE/TR 1.5/3.0 ms, flip angle 60°, in-plane resolution 1.5 x 1.5 mm, slice thickness 7 mm, 3 mm inter-slice gap, temporal resolution 45 ms,15 lines of k-space per heartbeat, 14-17 heartbeats per breath-hold, prospective ECG-gating) were acquired in long-axis views, i.e. horizontal and vertical long axis, and the LV outflow tract views. A short axis stack was obtained, parallel to the atrioventricular groove, covering the entire left ventricle.

Phase contrast images (tissue phase mapping, TPM) were acquired with a prospectively triggered black blood k-space segmented gradient echo sequence (TE/TR=4.5/6.2 ms, flip angle=15°) with first-order flow compensation in all dimensions to minimize artefacts from flow or motion described in detail elsewhere (Hennig et al., 1998b; Markl and Hennig, 2001). The pixel size was 2.7 x 1.3 mm (field of view 255 x 340 mm, 96 x 256 matrix interpolated to 192 x 256) with a slice thickness of 8 mm. Velocity encoding was performed by adding a bipolar gradient in read, phase and slice direction

after each RF pulse to the otherwise identical sequence (velocity encoding (venc) in-plane=20 cm/s, venc through-plane=30 cm/s). The temporal resolution was 37 ms to 87 ms in a single breath-hold (baseline, x-, y- and z-velocity components) over 17 to 29 heartbeats (adjustable to breath-holding capability). The quoted temporal resolution was achieved using view sharing techniques for which the resulting velocity errors have been shown to be small in structures the size of the myocardium (Markl and Hennig, 2001). The temporal resolution used for our study population (mean ± standard deviation (SD) of 62 ± 12 ms) showed very low correlation coefficients for mid-ventricular radial peak systolic (r= 0.003) and diastolic (r=0.19) velocities suggesting that the temporal resolution applied would not significantly confound the acquired velocity parameters. Three short axis slices at basal (between the LV outflow tract and the papillary muscles), mid-ventricular and apical levels were acquired according to recommended guidelines by the American Heart Association (AHA) and the American College of Cardiology (ACC) to assess myocardial segments (**Figure 2.1**) (Cerqueira et al., 2002). The typical distance between the basal and the apical short axis slice was 4 to 6 cm and positioning of the slices, expressed as percentage of the distance of the atrioventricular groove to the apex in the horizontal long axis, showed low variability.

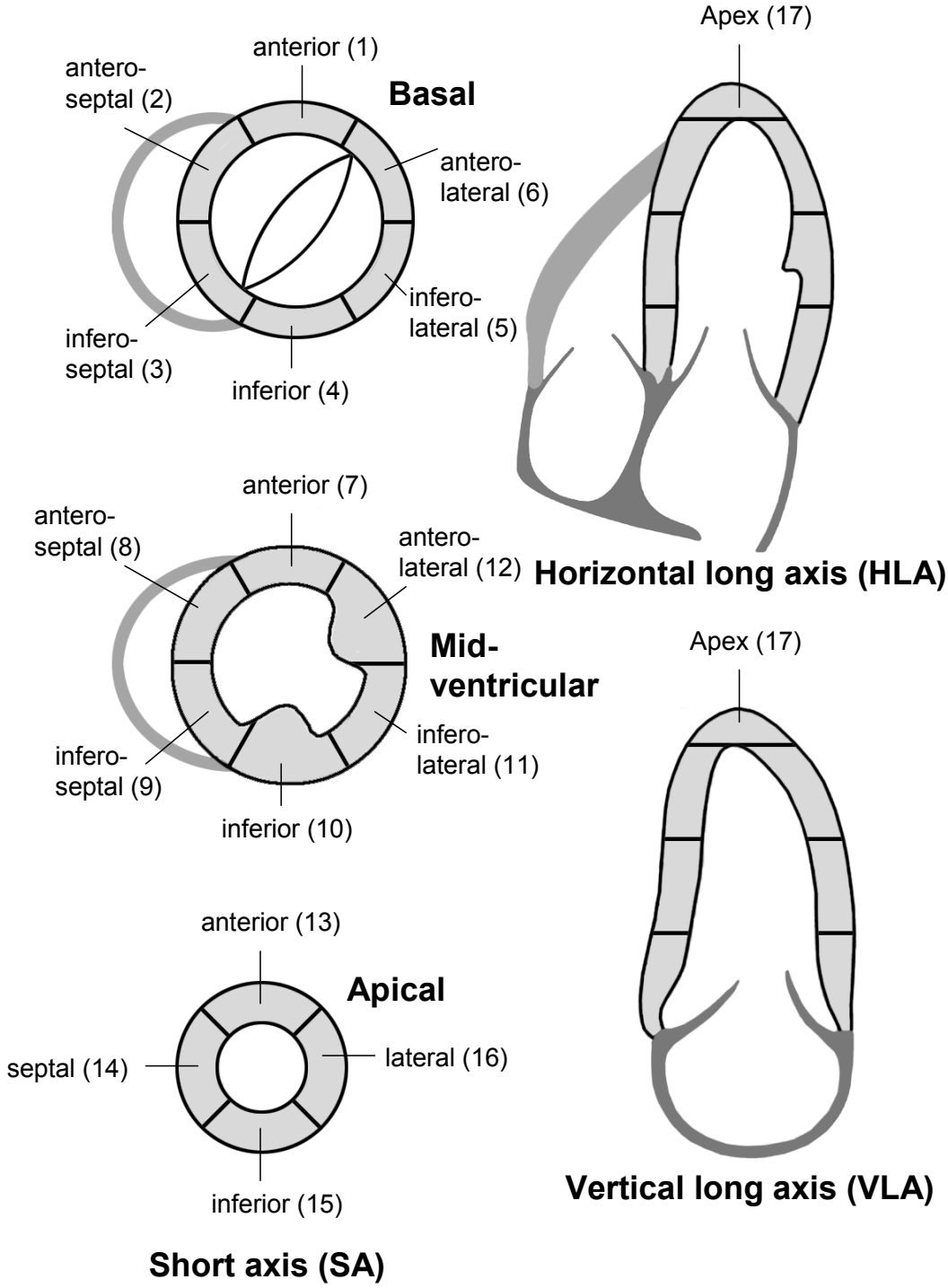

Figure 2.1: *Standardized myocardial 17 segment model (segment number given in brackets) and nomenclature for tomographic imaging of the heart: Adapted from a statement for healthcare professionals from the Cardiac Imaging Committee of the Council on Clinical Cardiology of the American Heart (Cerqueira et al., 2002).*

2.2 Cardiac ^{31}Phosphorus magnetic resonance spectroscopy protocol

In order to detect possible changes in cardiac high-energy phosphate metabolism, cardiac ^{31}P-MRS was performed at rest. All data were acquired with a commercially available heart/liver ^{31}P/^{1}H surface coil (Siemens Medical Systems, Erlangen, Germany). This coil contains a large single loop for excitation at both phosphorous (^{31}P) and proton (^{1}H) frequencies and for detection of ^{1}H signals. It also contains a quadrature coil for detection of ^{31}P signals, which comprises a figure-of-eight shaped loop and a circular coil.

The ^{31}P B_1 fields of these coils (transmit and receive) were calculated according to the Biot-Savart law and verified by experiment. To enable determination of the coil position for field map orientation purposes, capsules of cod liver oil were placed within the four corners of the coil casing. By imaging these capsules at the beginning of each experiment, it was possible to map the coil profiles onto the individual volunteer position.

All volunteers were positioned in a head first prone position, so that their heart was placed as close to the centre of the coil as possible. Correct positioning was confirmed with the use of a stack of limited field of view proton scout images. Following positioning and measurement of the cod liver oil markers, a series of unlocalised ^{31}P inversion recovery FID acquisitions were acquired at different inversion times to measure the actual flip angle of a reference vial of phenylphosphonic acid (PPA) positioned inside the coil casing. Knowledge of this flip angle allows for calculation, via the calculated excitation B_1 field map, of the localised flip angle at all points in the subsequently acquired spectra.

After piloting, a series of 32 double oblique SSFP images, oriented along the short axis of the heart were acquired. Image dimensions were 300 x 225 mm (Matrix size 128 x 96), with a slice thickness of 8 mm. The images were cardiac gated, with acquisition occurring during the early part of diastole. A ^{31}P 3D acquisition weighted CSI spectral data set was then acquired with the same position as the anatomical images but dimensions of 320 x 200 x 240 mm, a Matrix size of 12 x 8 x 8 (zero-filled to 16 x 16 x 8). Hence, the spatial resolution was 26.7 x 25 x 30 mm3 (20 ml) interpolated to 20 x 12.5 x 30 mm3 (7.5 ml).

2.3 Analysis of cardiac magnetic resonance images

CMR cine image analysis was performed with Argus software (Version 2002B, Siemens Medical Solutions, Erlangen, Germany). Manual tracing of the endocardial and epicardial borders of successive short-axis slices at end-diastole and end-systole (image with the smallest left and right ventricular cavity) was performed. Both epicardial and endocardial borders were traced on the end-diastolic frame, with only an endocardial border on end-systolic frame. The contour tracing was monitored by reviewing the movie with contours attached.

The basal slice was selected for the left ventricle when at least fifty percent of the blood volume was surrounded by myocardium in both end-diastole and end-systole. The apical slice was defined as the last slice showing intracavity blood pool.

For the right ventricle, volumes below the pulmonary valve were included. From the inflow tract, RV volumes were excluded if the surrounding muscle was thin and not trabeculated, suggestive of right atrium (**Figure 2.2**).

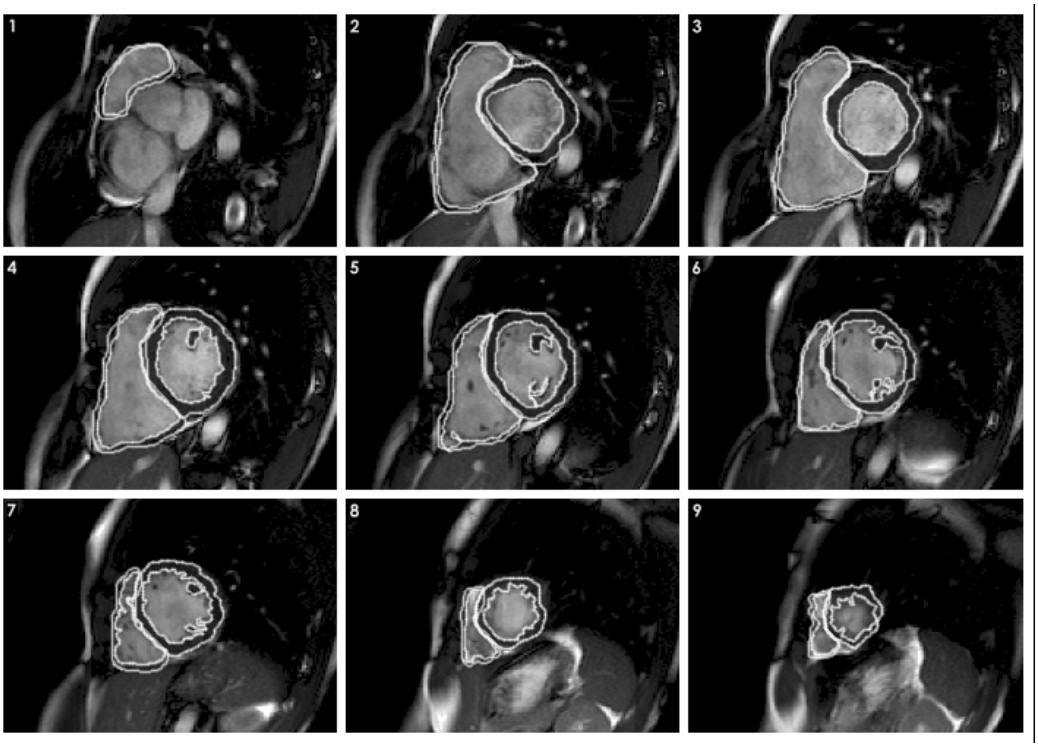

Figure 2.2: *End-diastolic short-axis images from base to apex in a healthy volunteer with endocardial and epicardial contours drawn for both the left and right ventricles. The basal slice was selected for the left ventricle when at least fifty percent of the blood volume was surrounded by myocardium in both end-diastole and end-systole. The apical slice was defined as the last slice showing intracavity blood pool. For the right ventricle, volumes below the pulmonary valve were included. From the inflow tract, RV volumes were excluded if the surrounding muscle was thin and not trabeculated, suggestive of right atrium. Papillary muscles were included in the LV mass.*

Papillary muscles were included in the mass and excluded from the volume calculations. The interventricular septum was included as part of the left ventricle. From these data, the mass, ejection fraction, end-systolic and end-diastolic volumes could be calculated. Myocardial mass was determined

by multiplication of the tissue volume by 1.05g/cm^3 (specific density of myocardium). Functional parameters, normalised to body surface area were also calculated.

TPM data analysis was performed on a personal computer using customized software programmed in Matlab Version 6.5 (The Mathworks Inc., Natick, MA) (Markl et al., 2002). After manual endo- and epicardial contour segmentation and a correction for translational motion components of the LV in the image plane (Hennig et al., 1998b), radial and circumferential velocities were calculated from in-plane velocities for each pixel based on an internal polar coordinate system positioned at the centre of mass of the LV. The longitudinal velocities were already encoded in the acquisition and were used without correction. The average velocity was computed for pixels within the epicardial (inner half of wall thickness), endocardial (outer half of wall thickness) and transmural regions for each of the 16 segments of the 17 segment model according to the AHA/ACC recommendations (Cerqueira et al., 2002). The temporal axis of the three-dimensional systolic velocity information obtained was then normalized to the end-systolic time as defined by the smallest LV cavity on mid-ventricular cine images to avoid temporal jitter. Diastolic velocity information was similarly normalized to the duration of diastole (RR interval minus duration of systole). For each of the radial and longitudinal velocities, two systolic and two diastolic parameters were computed: systolic peak velocity, systolic time to peak velocity, diastolic peak velocity and diastolic time to peak velocity. These parameters were computed for endocardial, epicardial and transmural velocities in 16 segments (Cerqueira et al., 2002) and for averaged global basal, mid-ventricular and

apical velocities. In addition, the relative speed of motion between the basal and apical slice was plotted over the cardiac cycle as the difference between the circumferential (torsion-rate [$rad.s^{-1}.cm^{-1}$] defined as the rate of change of angular velocity along the heart) and longitudinal (longitudinal strain-rate [s^{-1}]) velocities of the global basal and apical slices normalized to mid-ventricular short axis diameter and to ventricular length. Peak systolic torsion-rate, peak diastolic torsion-rate, systolic time to peak torsion-rate, diastolic time to peak torsion-rate and peak systolic longitudinal strain-rate, peak diastolic longitudinal strain-rate, systolic time to peak systolic longitudinal strain-rate and diastolic time to peak longitudinal strain-rate were then derived from those graphs.

2.4 Analysis of cardiac ^{31}Phosphorus magnetic resonance spectroscopy

Cardiac high-energy phosphate metabolites (blood and T_1 corrected PCr/ATP ratio, an index of the energetic state of the heart) were measured at rest using ^{31}P-MR spectroscopy in the basal anterior myocardium. The processing was carried out using home-written software in Matlab (MathsWorks Inc, Natick, MA). The proton images and the ^{31}P spectra were initially loaded and reregistered to one another, and to the previously calculated B_1-field maps, using the images of the cod liver oil tablets. The flip angle at the PPA reference was then measured by fitting the inversion recovery data, after correcting for the off resonance position of the PPA, for the local flip angle and the T1 of the reference.

The spectra produced were quantified using the AMARES, time-domain fitting algorithm within jMRUI (www.mrui.uab.es/mrui/mruiHomePage.html). This takes into account the j-couplings and amplitude ratios of the different peaks as prior knowledge. The fitted amplitudes were then individually corrected for blood contamination and saturation effects using T1 and contamination values from the literature.

CHAPTER 3: Normal human left and right ventricular and left atrial dimensions using steady state free precession magnetic resonance imaging

3.1 Introduction

Cardiovascular magnetic resonance imaging (CMR) has become the gold standard method for the characterisation of cardiac anatomy, function and mass (Pennell, 2003). It is an accurate and reliable technique for the serial monitoring of patients, particularly in response to therapeutic intervention (Grothues et al., 2002).

CMR is a well-tolerated, non-invasive technique without exposure to radiation with no known side-effects and is becoming increasingly available to the clinician. Establishment of a normal healthy reference database is essential for measurements to be useful and relevant in clinical practice. There are a number of different vendors and acquisition techniques, which may reflect some of the discrepancies in normal values for left and right ventricular parameters published in the literature (Lorenz et al., 1999; Sandstede et al., 2000; Alfakih et al., 2003). Furthermore, information regarding the left atrial size, volume and function is clinically important in the management of patients, particularly those with atrial fibrillation. Assessment of left atrial volumes using CMR has not yet become routine because it is not straightforward and the standard short-axis method of measuring left atrial volume and ejection fraction is very time-consuming. Echocardiography is currently the gold standard for assessing left atrial volumes but relies on a number of geometric assumptions.

It has been demonstrated that, when compared to the short-axis method in CMR, the biplane area-length method for ellipsoid bodies is a more rapid alternative in both healthy volunteers and patients which is both accurate and reproducible (Dulce et al., 1993; Sievers et al., 2004).

We aimed to establish a large database of reference values for left and right ventricles of healthy volunteers using steady-state free precession techniques (SSFP), the preferred technique of choice for assessment of volume data in current clinical practice. Previously only one large series of SSFP values has been reported, using one specific vendor, which did not examine right ventricular mass in combination with left and right ventricular volumes in a single clinical examination (Alfakih et al., 2003). In addition, we aimed to study left atrial end-systolic and end-diastolic volumes, stroke volume and ejection fraction.

3.2 Methods

Study population

108 healthy volunteers (63 male; mean age 38 ± 12 years, range 21-68 years) were recruited with no history of cardiac disease, hypertension or cardiac risk factors and a normal baseline ECG. Volunteers with contraindications to CMR were not enrolled. The study was carried out according to the principles of the Declaration of Helsinki and was approved by our institutional ethics committee. Each subject gave informed written consent. Baseline characteristics of the healthy volunteers are shown in **Table 3.1**.

Table 3.1: *Characteristics of healthy volunteers*

	Mean ± SD (n = 108)
Age (years)	38 ± 12
Gender	63 male/45 female
Height (cm)	174 ± 9
Weight (kg)	73.4 ± 12.3
Body Surface Area (m^2)	1.88 ± 0.18
Heart Rate (bpm)	65 ± 10
Systolic Blood Pressure (mmHg)	123 ± 17
Diastolic Blood Pressure (mmHg)	81 ± 16

Cardiovascular magnetic resonance imaging protocol and image analysis

The details of the CMR acquisition protocol and of the analysis of the LV and RV volume studies are described in detail in chapter 2.

In addition to the LV and RV volume analysis, the left atrial (LA) volumes, ejection fraction and stroke volume were measured using the biplane area-length method in the horizontal and vertical long axes (**Figure 3.1**). The left atrial appendage was included in the atrial volume, but the pulmonary veins were excluded. Left atrial stroke volume and ejection fraction:

Stroke Volume (SV) = End-Diastolic Volume (EDV) – End- Systolic Volume (ESV) and Ejection Fraction (EF) = Stroke Volume (SV) /End-Diastolic Volume (EDV) x 100%.

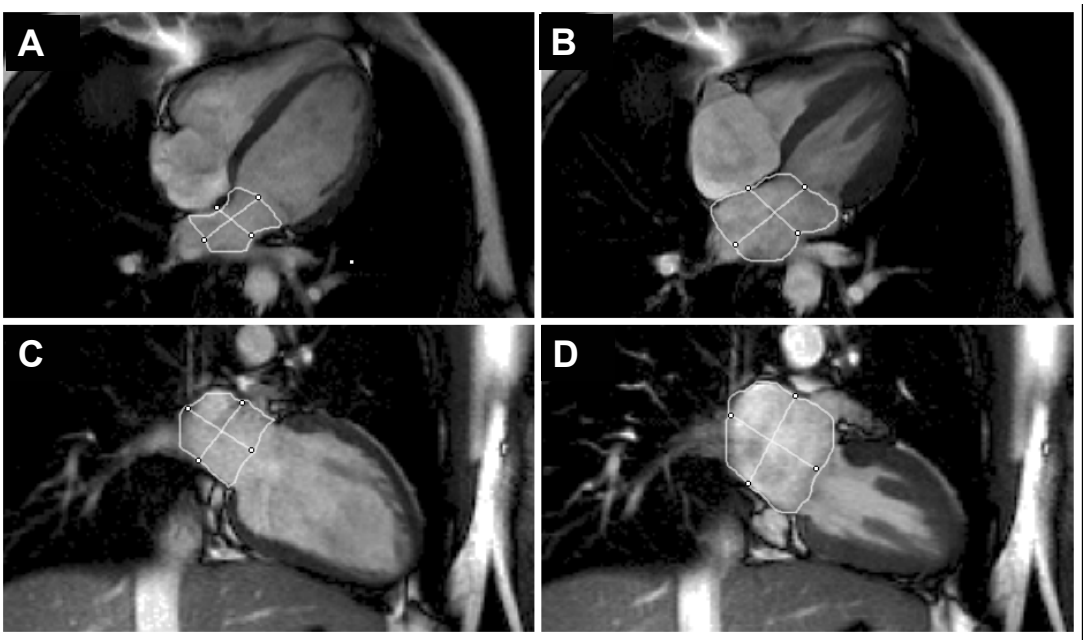

Figure 3.1: *Horizontal long axis (HLA) in end-diastole (A) and end-systole (B), vertical long axis (VLA) in end-diastole (C) and end-systole (D) illustrating contouring for the biplane are-length method for left atrial volumes and ejection fraction. The left atrial appendage was included in the atrial volume but the pulmonary veins were excluded.*

Reproducibility

To assess inter-study reproducibility, 12 subsequent subjects underwent a second identical scan, separated by at least one week from the first study.

Inter-observer variability was assessed by a second investigator analysing 12 of the data sets. One observer analysed the first 12 volunteer images twice, leaving a 6 week gap and blinded to the previous results, providing intra-observer variability.

Statistical Analysis

All data are presented as mean ± standard deviation (SD) unless stated otherwise.

For inter-study reproducibility, inter- and intra-observer variability was assessed using the method of Bland and Altman (Bland and Altman, 1986). The coefficient of variability was calculated as the SD of the differences between the two sets of measurements divided by the mean value of the parameter under consideration. All computations were performed with SPSS 11.5 (SPSS Inc., Chicago, United States).

3.3 Results

Cardiovascular magnetic resonance scanning was well tolerated by all participants. All datasets were of sufficient quality to be included in the study. The values for left and right ventricular function and mass are shown in **Table 3.2**.

Table 3.2: *LV and RV measurements in 108 healthy volunteers*

	Mean ± SD (n = 108)	Male (n = 63)	Female (n = 45)	P value
LV ejection fraction (%)	69 ± 6	69 ± 6 (57-81)	69± 6 (57-81)	0.80
LV mass (g)	112 ± 27	123 ± 21 (81-165)	96 ± 27 (42-150)	**<0.001**
LV mass index (g/m^2)	59.2 ± 11	62.5 ± 9.0 (45-81)	54.6 ± 12 (31-79)	**<0.001**
LV end-diastolic volume (ml)	150 ± 31	160 ± 29 (102-218)	135 ± 26 (83-187)	**<0.001**
LV end-diastolic volume index (ml/m^2)	80 ± 13	82 ± 13 (56-108)	78 ± 12 (54-102)	0.16
LV end-systolic volume (ml)	47 ± 15	50 ± 16 (18-82)	42 ± 12 (18-66)	**0.007**
LV end-systolic volume index (ml/m^2)	25 ± 7	25 ± 8 (9-41)	24 ± 6 (12-36)	0.53
LV stroke volume (ml)	104 ± 21	112 ± 19 (74-150)	91 ± 17 (57-125)	**<0.001**
LV stroke volume index (ml/m^2)	55 ± 8	56 ± 8 (40-72)	54 ± 9 (36-72)	0.12
RV ejection fraction (%)	61 ± 6	59 ± 6 (47-71)	63 ± 5 (53-73)	**0.002**
RV mass (g)	38 ± 8	41± 8 (25-57)	35± 7 (21-49)	**<0.001**
RV mass index (g/m^2)	20.3 ± 3.6	20.6 ± 3.7 (13-28)	20.0 ± 3.5 (13-27)	0.371
RV end-diastolic volume (ml)	173 ± 39	190 ± 33 (124-256)	148 ± 35 (78-218)	**<0.001**
RV end-diastolic volume index (ml/m^2)	91 ± 16	96 ± 15 (66-126)	84 ± 17 (50-118)	**<0.001**
RV end-systolic volume (ml)	69 ± 22	78 ± 20 (38-118)	56 ± 18 (20-92)	**<0.001**
RV end-systolic volume index (ml/m^2)	36 ± 10	39 ± 10 (19-59)	32 ± 10 (12-52)	**<0.001**
RV stroke volume (ml)	104 ± 21	113 ± 19 (75-151)	90 ± 19 (52-128)	**<0.001**
RV stroke volume index (ml/m^2)	55 ± 9	57 ± 8 (41-73)	53 ± 9 (35-71)	**0.02**

Values are given as mean ± SD; reference ranges in brackets, calculated as ± 2SD of the mean.

End-diastolic and end-systolic volumes were smaller in females than in males by about 15% for the left and about 25% for the right ventricle ($p < 0.01$ for all values). Left and right ventricular masses were larger in males than in females (22% for LV mass and 15% for RV mass, $p < 0.001$ for both). After indexing to body surface area, the differences for the left, but not for right ventricular volumes, and also for right, but not left, ventricular mass were no longer statistically significant. Right ventricular ejection fraction was 7% higher in females ($p = 0.002$) but left ventricular ejection fraction was not significantly different ($p = 0.80$).

The normal values for male and female left and right ventricular volumes in older and younger age groups are shown in **Table 3.3**. In males, with increasing age, there were significantly smaller right and left ventricular volumes. These differences remained after normalisation to body surface area. Left and right ventricular mass and mass indices were also lower with increasing age in males. Both left and right ventricular ejection fractions significantly increased with increasing age in males ($p=0.01$ for both). In females, only left ventricular end-diastolic volume index was significantly different ($p=0.03$) and stroke volume index showed a trend for smaller values with increasing age ($p=0.05$).

Table 3.3: *Myocardial mass and function by age and gender*

	Male (n = 63)			Female (n = 45)		
	< 35 years (n =31)	**≥ 35 years (n =32)**	**p**	**< 35 years (n =23)**	**≥ 35 years (n =22)**	**p**
LV ejection fraction (%)	67 ±5 (57-77)	71 ± 6 (59-83)	**0.01**	69±6 (57-81)	69 ±6 (57-81)	0.90
LV mass (g)	131 ±21 (89-173)	120 ±23 (74-166)	**0.05**	92±20 (52-132)	92 ±19 (54-130)	0.94
LV mass index (g/m^2)	67 ±10 (47-87)	60 ±9 (42-78)	**0.005**	53±9 (35-71)	52 ±9 (34-70)	0.76
LV end-diastolic volume (ml)	173 ±29 (115-231)	149 ±25 (99-199)	**0.001**	137±25 (87-187)	128 ±23 (82-174)	0.23
LV end-diastolic volume index (ml/m^2)	90 ±11 (68-112)	75 ±11 (53-97)	**<0.001**	80±9 (62-98)	73 ±11 (51-95)	**0.03**
LV end-systolic volume (ml)	57 ±15 (27-87)	43 ±13 (17-69)	**<0.001**	43±11 (21-65)	40 ±12 (16-64)	0.30
LV end-systolic volume index (ml/m^2)	30 ±7 (16-44)	22 ±6 (10-34)	**<0.001**	25±6 (13-37)	23 ±6 (11-35)	0.20
LV stroke volume (ml)	118 ± 18 (82-154)	106 ± 19 (68-144)	**0.015**	96 ± 18 (60-132)	89 ± 16 (57-121)	0.19
LV stroke volume index (ml/m^2)	60 ± 8 (44-76)	53 ± 8 (37-69)	**0.001**	55 ± 6 (43-67)	51 ± 8 (35-67)	0.05
RV ejection fraction (%)	57 ±5 (47-67)	61 ±6 (49-73)	**0.01**	61±3 (55-67)	64 ±7 (50-78)	0.20
RV mass (g)	42 ±8 (26-58)	39 ±7 (25-53)	0.06	36±7 (22-50)	33 ±7 (19-47)	0.13
RV mass index (g/m^2)	22 ±4 (14-30)	20 ±3 (14-26)	**0.03**	21±3 (15-27)	19 ±3 (13-25)	0.08
RV end-diastolic volume (ml)	203 ±33 (137-269)	181 ±28 (125-237)	**0.006**	152±27 (98-206)	140 ±37 (66-214)	0.23
RV end-diastolic volume index (ml/m^2)	104 ±15 (74-134)	89 ±11 (67-111)	**<0.001**	89±11 (67-111)	80 ±19 (42-118)	0.09
RV end-systolic volume (ml)	87 ±20 (47-127)	71 ±17 (37-105)	**0.001**	59±12 (35-83)	52 ±22 (8-96)	0.23
RV end-systolic volume index (ml/m^2)	44 ±9 (26-62)	34 ±7 (20-48)	**<0.001**	35±5 (25-45)	30 ±12 (6-54)	0.08
RV stroke volume (ml)	116 ± 19 (78-154)	110 ± 18 (74-146)	0.20	93 ± 17 (59-127)	93 ± 17 (50-126)	0.33
RV stroke volume index (ml/m^2)	59 ± 9 (41-77)	55 ± 8 (39-71)	0.06	54 ± 7 (40-68)	54 ± 7 (32-68)	0.15

The values for end-diastolic (maximal volume), end-systolic (minimal volume), stroke volume and ejection fraction for the left atrium are shown in **Table 3.4**. Males showed significantly larger end-systolic left atrial volumes and stroke volumes than females. There was a trend for males to have larger end-diastolic left atrial volumes (p = 0.055). There was no significant gender difference in left atrial ejection fraction.

Table 3.4: *Left atrial (LA) parameters and comparison between males and females*

	Mean ± SD (n=108)	**Males mean ± SD (n=63)**	**Females mean ± SD (n=45)**	**P value**
Maximal LA volume (ml)	97 ± 27	103 ± 30	89 ± 21	0.01
Minimal LA volume (ml)	44 ± 13	46 ± 14	41 ± 11	0.055
LA ejection fraction (%)	54 ± 12	55 ± 13	53 ± 9	0.47
LA stroke volume (ml)	53 ± 21	58 ± 23	48 ± 15	0.01

Intraobserver, interobserver and interstudy variability was higher for right ventricular compared with the left (**Table 3.5**). For right and left ventricular parameters, intraobserver variability was lowest, followed by interobserver and then interstudy variability (**Figure 3.2**). Variability was generally larger for left atrial measurements.

Table 3.5: *Reproducibility of measurements*

	Intraobserver		Interobserver		Interstudy	
	Bias (95% Limits of Agreement)	**CoV**	**Bias (95% Limits of Agreement)**	**CoV**	**Bias (95% Limits of Agreement)**	**CoV**
LV EF	0.5 (-2.6 to 3.5)	2.3	1.6 (-2.8 to 6.0)	3.3	0.5 (-9.1 to 10.1)	7.5
LV EDVI	4.6 (-4.4 to 13.7)	5.6	0.4 (-3.8 to 4.6)	2.7	-1.4 (-9.7 to 6.9)	5.2
LV mass	5.4 (-6.8 to 17.5)	6.1	5.8 (-4.4 to 16.0)	5.2	1.8 (-17.9 to 21.6)	9.4
RV EF	0.1 (-6.2 to 6.4)	5.3	-2.8 (-15.2 to 9.1)	10.7	1.9 (-11.48 to 15.2)	11.4
RV EDVI	-3.2 (-18.8 to 12.5)	9.0	-0.1 (-16.7 to 16.5)	9.6	0.7 (-21 to 4.3)	7.4
LA EF	-1 (-18 to 17)	16.4	4.4 (-6 to 15)	9.6	-3 (-19 to 12)	14.7

CoV = Coefficient of Variability; LA = left atrial; LV = left ventricular; RV = right ventricular; EF = ejection fraction; EDVI = end-diastolic volume index;

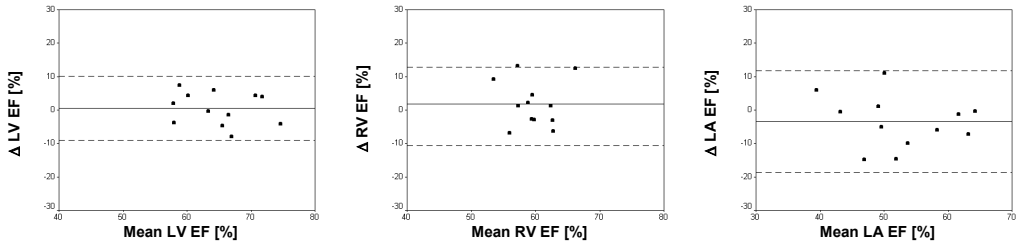

Figure 3.2: *Interstudy reproducibility for LV ejection fraction (LV EF), RV ejection fraction(RV EF) and left atrial ejection fraction (LA EF) for 12 healthy volunteers (Bland-Altman plot (Bland and Altman, 1986)). Solid lines represent the mean (bias) and dotted lines represent the limits of agreement (95% limits of agreement).*

3.4 Discussion

Over the past five years, a number of studies have reported on the use of CMR to establish normal values for ventricular function for comparison with clinical patients. These have been limited by the use of free-breathing, small numbers of subjects over a narrow age range, the focussing on either the left or the right ventricle and the use of different acquisition techniques and vendors (Lorenz et al., 1999; Sandstede et al., 2000; Grothues et al., 2002; Moon et al., 2002; Grothues et al., 2004).

Recently, the steady-state free precession (SSFP) technique has allowed more accurate definition of the endocardial and epicardial borders and a shorter acquisition time.

In this study, we have used this technique to establish a large database of ventricular and left atrial volumes in healthy volunteers in a single, clinically realistic examination.

Our values show volumes, normalised volumes, stroke volumes and ejection fractions for the left ventricle similar to Grothues et al (Grothues et al., 2002; Grothues et al., 2004). However, our right ventricular volumes are slightly larger (RVEDV 173± 39 versus 153± 34 ml, RVESV 69± 22 versus 58± 20ml) and our masses smaller (38±8g versus 60 ± 14g). These differences may be explained by the use of segmented FLASH breath-hold cines with contiguous 10mm slices on a Picker Edge 1.5 T Marconi system in Grothues' study.

Lorenz and co-workers published the first normal range of CMR mass and volumes (Lorenz et al., 1999). Their data show smaller volumes, which may be explained by the use of acquisition with a conventional cine gradient echo sequence and the inclusion of children. Moon et al have previously shown significantly higher left ventricular volume measurements using SSFP imaging when compared with FLASH imaging which is explained as being due to better definition of the endocardial and epicardial borders and improved basal slice selection (Moon et al., 2002). The normal range published by Alfakih using a Phillips 1.5 T breath-hold SSFP sequence with 6mm slices and a 4 mm interslice gap showed left and right ventricular volumes comparable to our study (Alfakih et al., 2003). Left ventricular mass index was also similar, males 64.7 ± 9.3g and females 52.0 ± 7.4g compared with 62.5 ± 9.0g and 54.6 ± 11.9g in our study. However, our study also provides information on right ventricular mass and left atrial volumes and function. Furthermore, we have acquired this in a clinically realistic setting with three different operators scanning in a larger population of healthy volunteers.

In the present study, we showed a significant gender difference for left and right ventricular volume indices, left ventricular mass index and right ventricular ejection fraction. We also demonstrated a significant decrease in volume indices of both ventricles with age in males. However, females only showed a statistically significant difference in LV end-diastolic volume and left ventricular stroke volume indices. These observations closely reflect autopsy findings with decreasing left ventricular mass and progressive left ventricular myocyte loss with increasing age in males with values remaining constant in females (Olivetti et al., 1995). These findings may reflect gender differences in ventricular remodelling with increasing age in healthy volunteers (Sandstede et al., 2000). Such differences may result from age-related hormonal changes, in particular reduced testosterone levels with increasing age in males, which may explain the reduced ventricular mass. In animal models, supraphysiological testosterone levels have been shown to induce cardiac hypertrophy and increases in left ventricular weight (Nahrendorf et al., 2003). The age-specific gender differences may also be explained by a reduction in physical activity with age. Our data suggest that in clinical practice, indexed age and sex specific values should be used, particularly in males.

Our results confirm that the interstudy reproducibility is lower for the right ventricle than for the left, similar to previous results (Grothues et al., 2004). This may be explained by the difficulty in defining the most basal slice and also in drawing endocardial contours around the increased trabeculations and moderator band of the right ventricle. Our volunteers underwent repeat scans at least one week apart, appropriately reflecting changes in physiology

and ensuring repositioning and replanning. The scans within our study were acquired by three operators. This explains why our interstudy variability is slightly larger than other studies where subjects underwent repeat scanning within 15 minutes by a single operator. However, we feel this acquisition reflects real clinical practice more closely.

Intraobserver and interobserver variability was higher for the right than for the left ventricle, again illustrating the complexity of the right ventricle. Our variability measurements were comparable to others reported in the literature (Lorenz et al., 1999; Rominger et al., 1999).

Left atrial function is impaired in a number of cardiac conditions, including atrial fibrillation, the commonest arrhythmia. Echocardiographic methods of measuring the left atrium rely on geometric assumptions and are user-dependent. The standard acquisition of left atrial volumes and ejection fraction with CMR uses the short-axis stack for which both acquisition and post-processing is time-consuming (Sievers et al., 2004). The biplane area-length method has previously been shown to correlate well with the short axis stack, and to be significantly faster, but it requires geometric assumptions similar to echocardiography (Matsuoka et al., 1993; Sievers et al., 2004). It also relies upon the use of pilot images acquired to optimise left ventricular imaging rather than primarily focussing on the left atrium in these views.

Our left atrial ejection fractions are similar to those previously reported. However, there was a high interobserver variability of these left atrial measurements, reflecting the difficulty in drawing contours, particularly when including the left atrial appendage but excluding the pulmonary veins. A small

difference between observers in drawing contours or measuring the left atrial length will have a large effect on left atrial volume when using the biplane area-length method. However, the left atrial ejection fraction variability was acceptable. The interstudy reproducibility for the left atrial measurements was again relatively low, reflecting the additional dependence of the volumes on slice positioning and variable cardiac physiology. However, when using comparable values to those in the literature, our reproducibility values compare favourably (Sievers et al., 2004).

We have shown the normal range of left atrial volumes, stroke volumes and ejection fraction using the biplane area-length method in healthy volunteers. These data are routinely obtained from a clinical scan and hence provide a normal range of values for a time-saving method of acquiring left atrial volumes. However, in view of the high observer variability, we would recommend the use of an additional short-axis method for a more reproducible and accurate assessment of the left atrium when this is clinically required.

Conclusion

We have produced a large database for left and right ventricular and left atrial volumes of healthy volunteers using SSFP images at 1.5 T. This will be of particular use for reference in both clinical and research studies.

We have shown significantly different volumes with gender, and significant differences in age-specific left and right ventricular volumes, mass and ejection fraction in males but not in females. We have also demonstrated

the use and limitations of the biplane area-length method to acquire left atrial volumes and ejection fraction.

CHAPTER 4: Three-dimensional myocardial tissue motion – quantitative regional wall motion analysis in healthy volunteers using cine phase contrast velocity magnetic resonance imaging

4.1 Introduction

Assessment of myocardial regional wall motion plays a key role in many diagnostic and therapeutic decisions in current clinical practice. Studies of both stress induced ischemia and of viability, i.e. high dose and low dose dobutamine stress echocardiography (Mazur and Nagueh, 2001), respectively, or cardiovascular magnetic resonance imaging (Nagel et al., 1999) (CMR), are based on regional wall motion analysis. Semi-quantitative grading of regional wall motion is the most frequently applied technique, but is highly subjective with limited reproducibility. Despite dramatic improvements in echocardiography and CMR technology, permitting quantitative and objective regional wall motion analysis, none has yet been widely applied in clinical practice. A possible explanation for this is that no existing single technique has yet provided non-invasive, quantitative, reproducible, three-dimensional, systolic and diastolic regional wall motion analysis with sufficient spatial resolution to identify transmural variation (endo- and epicardial differences) in all myocardial segments (Cerqueira et al., 2002).

Tissue doppler, strain and strain-rate imaging using echocardiography are highly dependent on transducer angulation and have, thus, inherent limitations regarding complete, three-dimensional myocardial coverage and reproducibility (Pellerin et al., 2003; Voigt and Flachskampf, 2004). CMR offers different techniques for regional wall motion analysis: myocardial

tagging (Zerhouni et al., 1988; Maier et al., 1992; McVeigh and Atalar, 1992; Rademakers et al., 1994; Young et al., 1994a; Young et al., 1994b; Reichek, 1999; Henson et al., 2000), phase velocity ('tissue phase mapping') (Karwatowski et al., 1994a; Pelc et al., 1994; Hennig et al., 1998a; Hennig et al., 1998b; Markl et al., 1999; Henson et al., 2000; Markl and Hennig, 2001; Markl et al., 2002), phase displacement (Aletras et al., 1999a; Aletras et al., 1999b; Kim et al., 2004), and optical flow methods (Amartur and Vesselle, 1993). Tagging approaches deliberately obliterate lines or grids of signal and watch grid deformation as these regions move during the cardiac cycle. Phase velocity based methods directly observe the velocity of the tissue using the phase of the signal, hence the term 'tissue phase mapping', and can determine the displacement by integration over time. Traditionally, tissue phase mapping methods have measured the displacement over short time intervals yielding measurements of instantaneous velocity, this interval can be extended with use of the displacement encoding with stimulated echos (DENSE) approach (Aletras et al., 1999a; Aletras et al., 1999b; Kim et al., 2004) that allows it to measure displacements over most of the cardiac cycle. Optical flow provides an alternative approach for defining cardiac velocities and displacements and uses high-resolution cine MR images that are not encoded with additional displacement information. Computerized algorithms are used to generate motion fields that explain the evolution of the images from one frame to the next. Such an approach is an extension of the method that is performed naturally by the human brain (Amartur and Vesselle, 1993).

We hypothesized that tissue phase mapping would allow quantitative measurements of motion parameters which are reproducible and independent

of analysers. Further, given the high resolution of tissue phase mapping, we hypothesized that this method would show differences between endo- and epicardium for radial, circumferential and longitudinal velocity parameters in healthy volunteers. Thus, the purpose of our study was to establish prospectively a database of normal, three-dimensional, systolic and diastolic, endo- and epicardial velocities of all myocardial segments in healthy volunteers using cine phase contrast velocity magnetic resonance imaging (tissue phase mapping or TPM).

Study participants

96 healthy volunteers (mean±SD age=38±12 years, 57 (59%) men) with normal electrocardiograms were enrolled to undergo CMR imaging. The mean±SD age of males (n=57; 39±13 years) was similar to females (n=39; 37±12 years) ($p>0.05$). None of the subjects indicated a history of cardiovascular disease, diabetes, cardiovascular symptoms or chronic medication other than contraceptives. The study was carried out according to the principles of the Declaration of Helsinki and was approved by our institutional ethics committee. Each subject gave informed written consent. Baseline characteristics of the healthy volunteers are given in **Table 4.1**.

4.2 Methods

MR imaging

Acquisition of SSFP cine images and of tissue phase mapping data are described in detail in chapter 2. All acquired datasets were of sufficient image

quality, without respiration artefacts in the magnitude images, and could be included in the analysis (Figure 4.1).

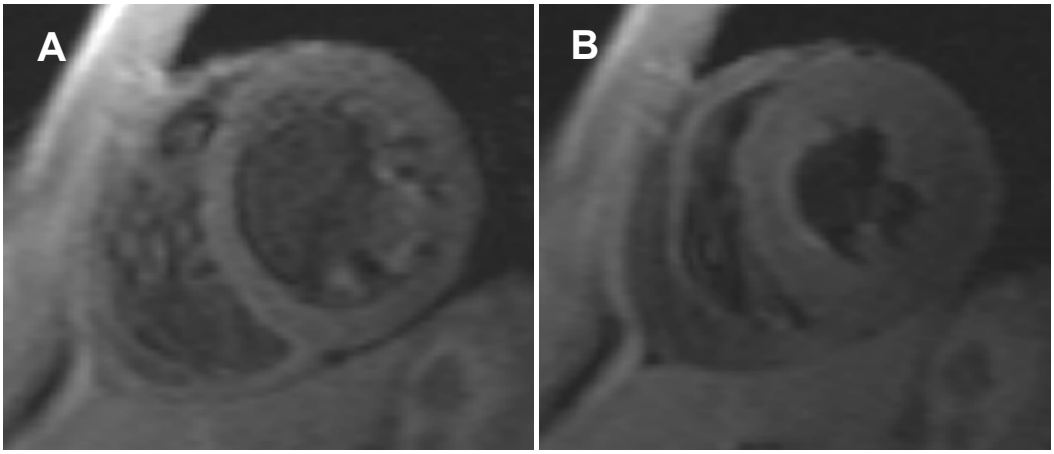

Figure 4.1: *End-diastolic (A) and end-systolic (B) magnitude images at mid-ventricular level in a healthy volunteer using a black blood k-space segmented gradient echo sequence (tissue phase mapping).*

The first consecutive 18 of 96 healthy volunteers were scanned twice within one week to determine the inter-study reproducibility. The mean ± SD of males (n=8; 36 ± 15 years) was similar to females (n=10; 37 ± 14 years) ($p>0.05$). These 18 repeat sets of tissue phase mapping data were acquired with an initial sequence providing only radial and circumferential velocity information. Consequently, no variability information was available for longitudinal velocity and strain-rate.

Data Analysis

Cine images were analyzed manually as described in detail in chapter 2. For each set of cine studies, standard LV volume parameters were generated to further document normalcy of the volunteers (**Table 4.1**): LV ejection fraction (LVEF), LV mass index, LV end-diastolic (LVEDVI), end-

systolic (LVESVI) and stroke volume index (LVSVI). All parameters were within normal limits. TPM data analysis was performed on a personal computer using customized software programmed in Matlab Version 6.5 (The Mathworks Inc., Natick, MA) as described in chapter 2 (Markl et al., 2002). One observer analysed the first 18 volunteer images twice, after a 6 months gap, and these data were also analysed by a second observer to allow intra- and inter-observer variability, respectively.

Statistical Analysis

All data are presented as mean ± standard deviation (SD) unless stated otherwise. To establish differences for continuous data between the base, the mid-ventricle and the apex and to compare endo- and epicardial parameters (transmural gradient), mixed effects models were fitted in STATA 8.0 (StataCorp LP, College Station, Texas US), with a random intercept for volunteer and categorical fixed effects for sector and transmural gradient. Throughout the analyses, a two-sided p-value of <0.05 was considered statistically significant.

For inter-study reproducibility, inter- and intra-observer variability the mean difference ± the standard deviation of the mean difference were determined (Bland and Altman, 1986). All other computations were done with SPSS 11.5 (SPSS Inc., Chicago, US) and Matlab Version 6.5 (The Mathworks Inc., Natick, MA).

Table 4.1: *Baseline characteristics and left ventricular volume results. Normal range for males (m) and females (f) in brackets (Alfakih et al., 2003).*

	Mean ± SD (n=96)
Age [years]	38 ± 12
Gender	57 male/ 39 female
Height [cm]	174 ± 8
Weight [kg]	73.0 ± 12.9
Body surface area [m^2]	1.87 ± 0.19
Heart rate [bpm]	65 ± 10
Systolic blood pressure [mmHg]	123 ± 18
Duration of systole [ms]	324 ± 34
Diastolic blood pressure [mmHg]	81 ± 17
LV ejection fraction [%]	69 ± 6 (m: 55-73; f: 54-74)
LV mass index [g/m^2]	58.7 ± 10.5 (m: 46-83; f: 37-67)
LV end-diastolic volume index [ml/m^2]	80 ± 12 (m: 53-112; f: 56-99)
LV end-systolic volume index [ml/m^2]	25 ± 7
LV stroke volume index [ml/m^2]	55 ± 8

4.3 Results

Radial velocity

Contraction (positive radial velocities) and expansion (relaxation, negative radial velocities) patterns in the base, at mid-ventricular and apical level were characterized by an increase in contraction velocity during early systole, followed by a slowing down of contraction velocity later in systole. The inverse pattern was observed in diastole. Similarly, an initial increase in radial expansion velocities was followed by a decrease later during diastole (**Figure 4.2**). Systolic peak radial velocity was lowest in the apex (mixed effects model $z=-10.38$, $p<0.001$), but the systolic time to peak radial velocity was similar at all levels ($z=-1.21$, $p=0.23$., **Table 4.2, Figure 4.3**). The diastolic time to peak radial velocity was shorter in the basal compared to the mid-ventricular and to the apical slices ($z=8.44$, $p<0.001$), which was accompanied by similar diastolic peak radial velocities at those myocardial levels ($z=0.35$, $p=0.73$). Transmural gradients for systolic and diastolic peak radial velocities could be observedin each myocardial slice ($p<0.001$ across levels for both systolic and diastolic velocities) with higher endo- than epicardial velocities (**Figure 4.3**).

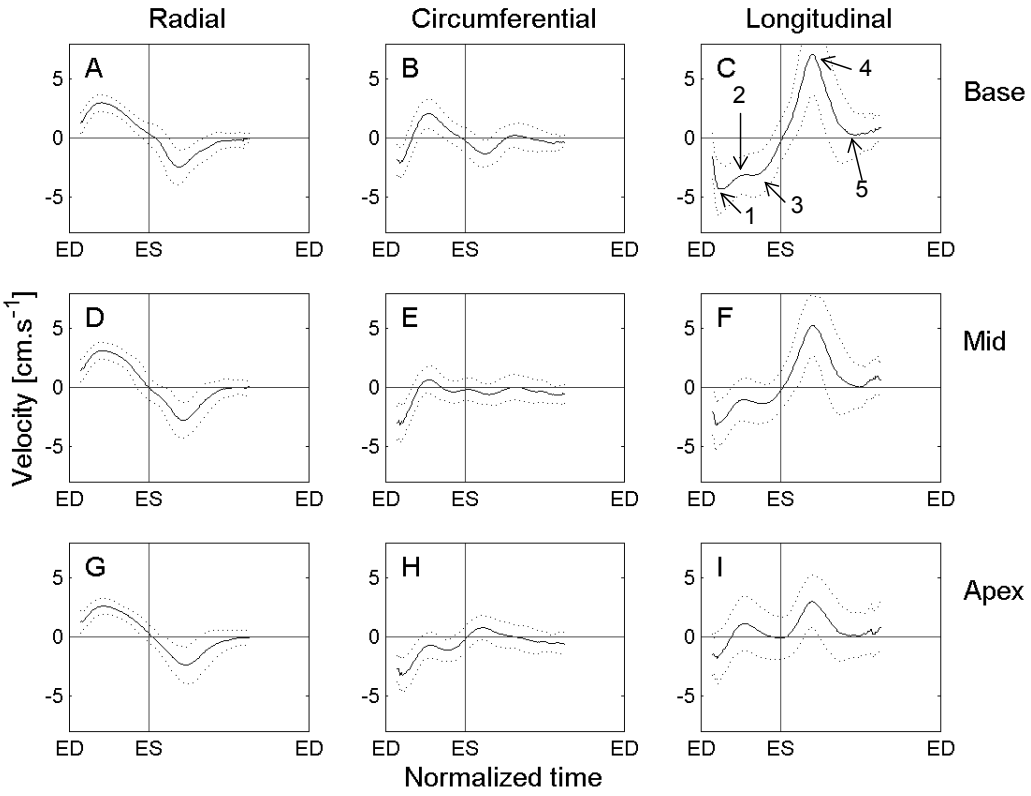

Figure 4.2: *Three-dimensional tissue phase mapping of basal (top row), mid-ventricular (middle row) and apical short axis views (bottom row). Graphs are presented as mean (solid line) ± SD (dashed lines) after piecewise cubic Hermite interpolation. Panels A, D and G show radial velocity (n=96) information with positive velocities representing contraction and negative velocities expansion. Panels B, E and H display circumferential velocities (n=96) with positive velocities representing clockwise rotation and negative velocities counter-clockwise rotation. Panels C, F and I plot longitudinal velocities (n=78) with positive velocities indicating base movement away from the apex and negative velocities showing base movement towards the apex. Longitudinal velocities during the cardiac cycle can be divided into 5 steps: The base of the heart undergoes an initial displacement towards the apex (1) followed by a velocity drop (2). At end-systole a small increase in velocity directed towards the apex occurs (3) before rapid motion of the base away from the apex during early diastole (4). This is followed by a rapid decrease in velocity (5).*

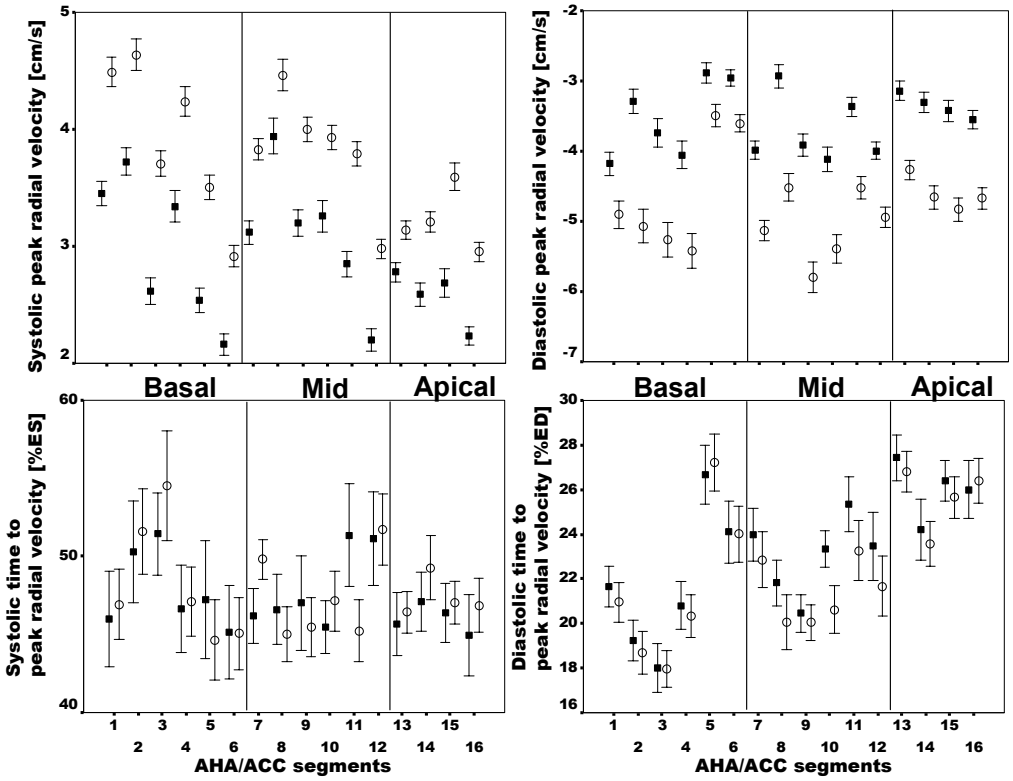

Figure 4.3: *Segmental and myocardial layer distribution of radial velocity parameters (n=96). Segments 1-6 are basal, 7-12 mid-ventricular and 13-16 apical according to the AHA/ACC recommendation (Cerqueira et al., 2002). Epicardial (solid squares) and endocardial (circles) velocity parameters are shown as mean ± standard error of the mean. Positive radial velocities indicate contraction and negative radial velocities expansion. Transmural gradients for systolic and diastolic peak radial velocities are observed in each of the three myocardial levels ($p<0.001$ for both) with higher absolute endo- than epicardial velocities. The basal, mid-ventricular and apical slices were located at 28 ± 5%, 51 ± 4% and 74 ± 5%, respectively.*

Table 4.2: *Mean±SD segmental and myocardial layer distribution of radial and longitudinal velocity parameters*

	Basal	**Mid**	**Apical**	**Basal**	**Mid**	**Apical**
Systolic peak radial velocity [cm/s]				**Diastolic peak radial velocity [cm/s]**		
Epicardium	2.97±1.22	3.09±1.27	2.57±0.96	-3.52±1.71	-3.72±1.54	-3.36±1.37
Endocardium	3.92±1.26	3.83±1.12	3.22±0.94	-4.62±2.13	-5.05±1.80	-4.61±1.56
Transmural	3.44±1.33	3.46±1.25	2.90±1.00	-4.07±2.01	-4.38±1.80	-3.98±1.60
Systolic time to peak radial velocity [%ES]				**Diastolic time to peak radial velocity [%ED]**		
Epicardium	47.8±29.9	48.0±25.3	46.0±20.8	21.7±11.2	23.1±11.1	26.0±11.5
Endocardium	48.3±25.6	47.4±18.5	47.4±16.1	21.5±10.5	21.4±11.7	25.6±9.56
Transmural	48.1±27.8	47.7±22.1	46.7±18.6	21.6±10.8	22.2±11.4	25.8±10.6

	Basal	**Mid**	**Apical**	**Basal**	**Mid**	**Apical**
Systolic peak longitudinal velocity [cm/s]				**Diastolic peak longitudinal velocity [cm/s]**		
Epicardium	-5.59±2.73	-4.14±3.01	-2.66±2.71	9.25±3.04	6.94±2.80	4.27±2.49
Endocardium	-5.65±2.61	-4.11±2.82	-2.71±2.65	9.59±3.18	7.28±2.80	4.35±2.45
Transmural	-5.62±2.67	-4.12±2.92	-2.68±2.68	9.42±3.11	7.11±2.80	4.31±2.47
Systolic time to peak longitudinal velocity [%ES]				**Diastolic time to peak longitudinal velocity [%ED]**		
Epicardium	37.3±38.8	50.6±61.0	64.4±67.4	21.7±7.36	22.7±8.19	15.2±17.7
Endocardium	38.4±41.8	54.4±62.8	65.5±67.2	21.5±7.54	22.2±8.90	11.7±19.4
Transmural	37.9±40.3	52.5±61.9	65.0±67.3	21.6±7.45	22.4±8.55	13.4±18.7

Circumferential velocity and torsion-rate

During systole, a counter-clockwise rotation (negative velocities in **Figure 4.2**) as viewed from the apex was followed by a clockwise rotation (positive velocities in **Figure 4.2**) in the base and at mid-ventricular level. The apical myocardium, however, showed a counter-clockwise rotation during the entire length of systole. Circumferential velocities were generally lower during diastole. The base revealed a counter-clockwise rotation in contrast to a clockwise rotation in the apex during diastole. Consequently, peak velocities and time to peak parameters for clockwise and counter-clockwise rotation were systolic or diastolic depending on the location of the myocardial

segments. Therefore, we plotted the torsion-rate over the cardiac cycle (**Figure 4.4a**). A relative counter-clockwise rotation during systole was followed by a relative clockwise rotation of the apex against the base. Peak systolic torsion-rate, peak diastolic torsion-rate, systolic time to peak torsion-rate, diastolic time to peak torsion-rate are shown in **Table 4.3**.

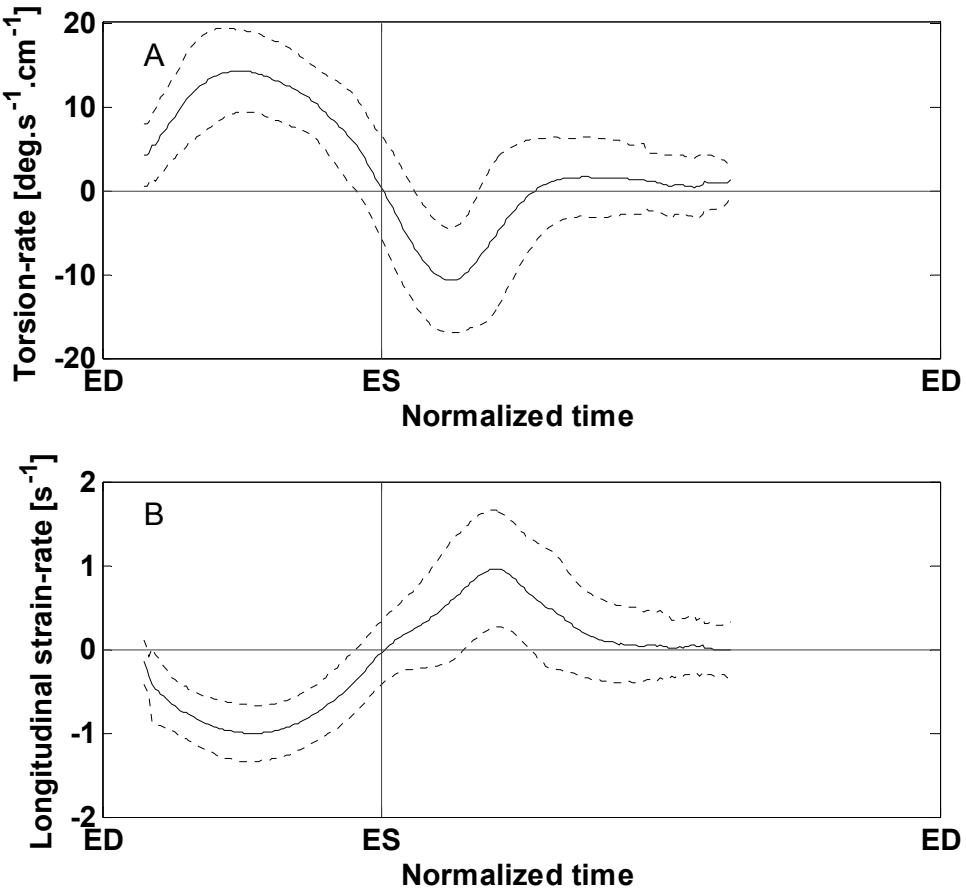

Figure 4.4: *A: Myocardial torsion-rate (n=96). Graphs are presented as mean (solid line) and 1x SD (dashed lines) after piecewise cubic Hermite interpolation. A relative counter-clockwise rotation during systole is followed by a relative clockwise rotation of the apex against the base. B: Myocardial longitudinal strain-rate (n=78). Basal movement towards the apex occurs during systole and away from the apex during diastole. ED=end-diastole, ES=end-systole.*

Table 4.3: *Mean ± SD myocardial torsion-rate and longitudinal strain-rate in 96 healthy volunteers*

Peak systolic torsion-rate [deg.s^{-1}.cm^{-1}] (n=96)	16.2 ± 4.7
Time to peak systolic torsion-rate [%ES, i.e. time from R-wave/time from R-wave to ES] (n=96)	53 ± 21
Peak diastolic torsion-rate [deg.s^{-1}.cm^{-1}] (n=96)	- 15.0 ± 5.7
Time to peak diastolic torsion-rate [%ED, i.e. time from ES to time from ES to R-wave] (n=96)	13 ± 8
Peak systolic longitudinal strain-rate [s^{-1}] (n=78)	- 1.09 ± 0.32
Time to peak systolic longitudinal strain-rate [%ES, i.e. time from R-wave/time from R-wave to ES] (n=78)	51 ± 13
Peak diastolic longitudinal strain-rate [s^{-1}] (n=78)	1.49 ± 0.60
Time to peak diastolic longitudinal strain-rate [%ED, i.e. time from ES to time from ES to R-wave] (n=78)	23 ± 8

No statistically significant differences between endo- and epicardial velocities were observed for clockwise and counter-clockwise peak velocities and time to peak circumferential velocities ($p>0.05$ for all).

Longitudinal velocity and longitudinal strain-rate

Longitudinal velocities during the cardiac cycle could be divided into 5 steps (numbers of steps in brackets correspond to those in **Figure 4.2**): The base of the heart underwent an initial displacement towards the apex (1, peak systolic longitudinal velocity -5.3 ± 2.0 cm/s) followed by a velocity drop (2). At end-systole a small increase in velocity directed towards the apex occurred

(3) before rapid motion of the base away from the apex during early diastole (4, peak diastolic longitudinal velocity 9.2 ± 2.5 cm/s). This was followed by a rapid decrease in velocity away from the apex (5). The same pattern of motion was present at the mid-ventricular (peak systolic and diastolic longitudinal velocities -3.7± 2.1 and 7.0 ± 2.3 cm/s, respectively) and apical level (peak systolic and diastolic longitudinal velocities -2.2 ± 2.1 and 4.1± 2.0 cm/s, respectively) with decreasing amplitudes. Maximal basal movement towards the apex occurred during systole and away from the apex during diastole (Figure 4.4b).

Systolic peak ($z=-0.25$, $p=0.81$) and time to peak ($z=1.04$, $p=0.30$) longitudinal velocities were similar in the endocardial and epicardial layers, while diastolic peak ($z=3.12$, $p=0.002$) and time to peak ($z=-2.72$, $p=0.006$) longitudinal velocities differed. Both diastolic ($z=-44.64$, $p<0.001$) and systolic ($z=27.11$, $p<0.001$) peak longitudinal velocities decreased from base to apex (**Table 4.2, Figure 4.5**).

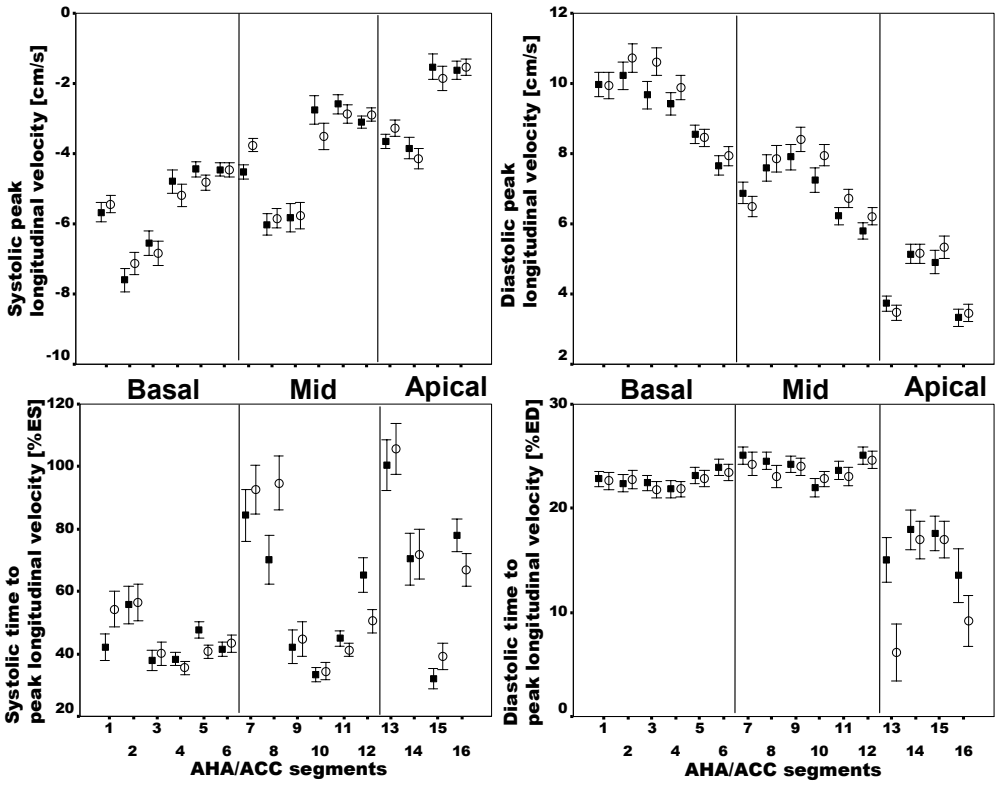

Figure 4.5: *Segmental and myocardial layer distribution of longitudinal velocity parameters (n=78). Segments 1-6 are basal, 7-12 mid-ventricular and 13-16 apical according to the AHA/ACC recommendation (Cerqueira et al., 2002). Epicardial (solid squares) and endocardial (circles) velocity parameters are shown as mean ± standard error of the mean. Positive longitudinal velocities indicate base movement away from the apex and negative values base movement towards the apex. Systolic peak (z=-0.25, p=0.81) and time to peak (z=1.04, p=0.30) longitudinal velocities were similar in the endocardial and epicardial layers, while diastolic peak (z=3.12, p=0.002) and time to peak (z=-2.72, p=0.006) longitudinal velocities differed. Both diastolic (z=-44.64, p<0.001) and systolic (z=27.11, p<0.001) peak longitudinal velocities decreased from base to apex.*

Inter- and intra-observer variability and inter-study reproducibility

Intra-observer and inter-observer variability were low and inter-study reproducibility was high for all velocity parameters at apical, mid-ventricular and basal level (**Table 4.4 and Figure 4.6**).

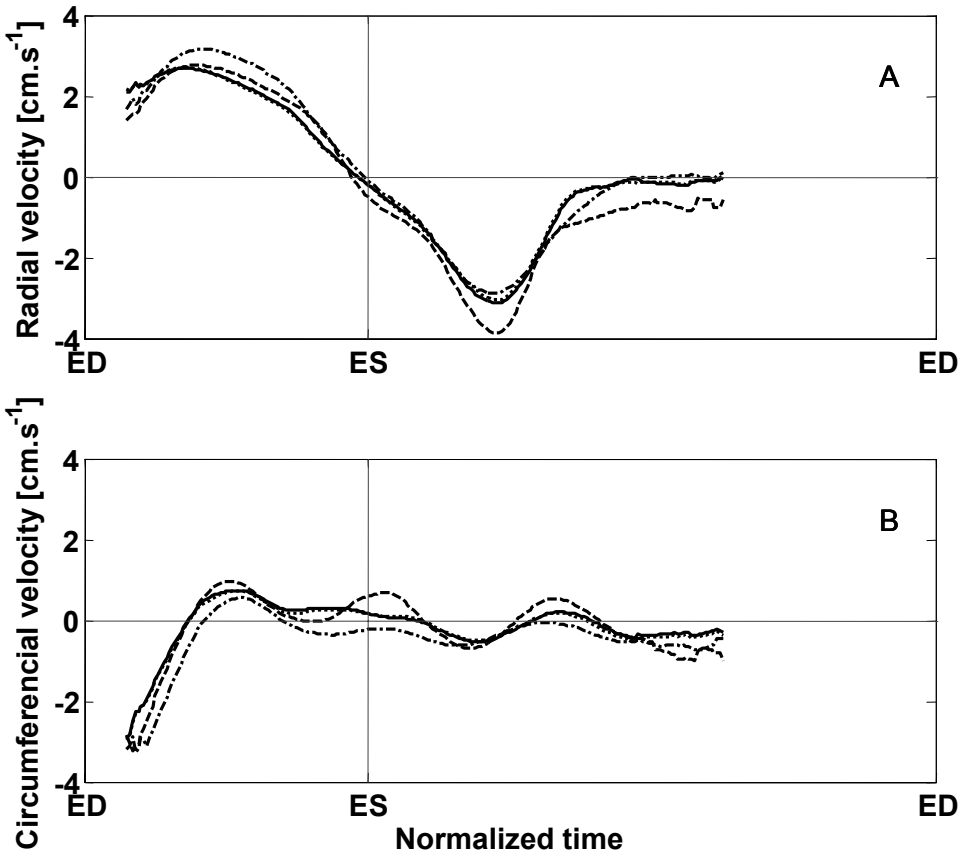

Figure 4.6: *Intra- and inter-observer variability and inter-study reproducibility for radial and circumferential velocities during the cardiac cycle at mid-ventricular level shown as the mean for the first 18 consecutive healthy volunteers. Observer 1, measurement 1 (solid line), observer 1, measurement 2 (dashed-dotted line), observer 2 (dashed line) and second scan (dotted line). Note the small variation in systolic and diastolic peak velocities and systolic and diastolic time to peak velocities. ED=end-diastole, ES=end-systole.*

Table 4.4: *Intra-and inter-observer variability and inter-study reproducibility at basal, mid-ventricular and apical level*

	Healthy volunteers (mean for n=18)		Intra-observer variability	Inter-observer variability	Inter-study reproducibility
Systolic peak radial velocity [cm.s^{-1}]	basal	2.70±0.63	-0.009±0.17	0.02±0.13	-0.003±0.59
	mid	2.94±0.71	-0.07±0.29	0.005±0.31	-0.12±0.84
	apical	2.40±0.75	-0.04±0.13	0.02±0.13	0.18±0.76
Diastolic peak radial velocity [cm.s^{-1}]	basal	-3.05±1.06	-0.04±0.37	-0.05±0.36	-0.72±1.46
	mid	-3.88±1.33	-0.10±0.25	-0.06±0.21	-0.76±1.84
	apical	-4.03±1.33	-0.08±0.17	0.04±0.13	-0.37±1.55
Clockwise peak circumferential velocity [cm.s^{-1}]	basal	2.48±0.55	-0.16±0.34	0.04±0.11	0.51±1.03
	mid	1.61±0.69	-0.04±0.41	-0.05±0.23	0.29±0.87
	apical	1.80±0.66	0.02±0.11	0.05±0.13	0.14±0.87
Counter-clockwise peak circumferential velocity [cm.s^{-1}]	basal	-2.55±1.03	-0.14-0.65	-0.006±0.10	-0.22±1.43
	mid	-2.99±1.37	0.02±0.49	-0.03±0.24	-0.72±1.18
	apical	-2.97±1.31	-0.03±0.09	0.04±0.12	-0.56±1.12
Peak systolic torsion-rate [deg.s^{-1}.cm^{-1}]	12.6±.4.6		0.3±1.1	0.2±0.6	0.1±5.7
Peak diastolic torsion-rate [deg.s^{-1}.cm^{-1}]	-14.3±5.7		0.2±1.1	-0.1±0.6	-3.4±7.4

Variability and reproducibility data are presented as mean difference ± standard deviation.

4.4 Discussion

Both of the mature CMR based methods, tagging and tissue phase mapping essentially evaluate myocardial motion. Tissue phase mapping offers the better spatial resolution, whereas tagging has a better temporal resolution and may thus be superior in terms of identifying peak deformation. Tissue phase mapping covers most of the cardiac cycle allowing for quantification of endo- and epicardial wall motion in both systole and a large portion of diastole with consistent data quality, whereas tag fading prevented diastolic motion assessment until newer tagging sequences were introduced. Tissue phase mapping data acquisition and post-processing are quick and simple in contrast to the time-consuming tagging analysis, although the latter is continually being improved (Osman et al., 1999; Garot et al., 2000). The temporal resolution for tissue phase mapping could potentially be improved with a navigator sequence, although such an approach would remove the need for breath-holding, but might increase the total scan time. Within the temporal resolution applied in our study population, no dependency was found for peak systolic and diastolic mid-ventricular radial velocity suggesting that the current range of temporal resolution for tissue phase mapping might be sufficient.

Typical transmural radial velocity patterns in healthy hearts have been described by Markl and co-workers using tissue phase mapping (Markl et al., 2002) and are in keeping with our findings. In addition, we report transmural differences with higher systolic and diastolic endo- than epicardial radial velocities. Hashimoto and colleagues found an increase in systolic and diastolic strain-rate from endocardium to mid-myocardium to epicardium in an

animal model, but did not observe significant differences in myocardial velocities using tissue doppler imaging (Hashimoto et al., 2003). This discrepancy might be partly explained by the slightly better spatial resolution for tissue phase mapping (2.7 x 1.3 mm for TPM vs. <3 x <2 mm for tissue doppler imaging (Hashimoto et al., 2003)) and more likely by the fact that our study only compared two rather than three myocardial layer velocities. The lower systolic peak radial velocities at the apex might reflect the fact that the this region is constrained by the diaphragm. Smaller diastolic peak radial velocities in the basal compared to the mid-ventricular and apical myocardium might be explained by the proportionally smaller myocardium-to-cavity area at the base of the heart.

Our findings of a counter-clockwise rotation followed by a clockwise rotation in the base of the heart during systole and the apical counter-clockwise rotation during the entire length of systole as viewed from the apex are consistent with reports using CMR tagging (Moore et al., 2000). This pattern of circumferential velocity in the myocardium is responsible for the fact that peak circumferential clockwise and counter-clockwise velocities occur quite variably during either systole or diastole. Plotting the “torsion-rate” as the difference between the basal and apical circumferential velocities by normalizing by the distance between these slices, we obtain the basic system independent measure of this motion. This allows determination of true systolic and diastolic parameters, such as peak systolic torsion-rate, time to peak systolic torsion-rate, peak diastolic torsion-rate and time to peak diastolic torsion-rate. We did not find a transmural gradient of circumferential velocities

which is in keeping with three-dimensional tagging results reported by Moore and colleagues (Moore et al., 2000).

Our diastolic peak longitudinal velocity at the myocardial base (9.2 ± 2.5 cm/s) results match basal longitudinal velocities reported by Karwatowski et al (Karwatowski et al., 1994b) using tissue phase mapping (8.2 ± 2.2 cm/s). Similarly, the decrease in longitudinal velocities from base to apex observed in our cohort is confirmed by a previous echocardiography study (Peak systolic and diastolic longitudinal velocities at base (-9.3 ± 1.3 and 14.8 ± 3.2 cm/s, respectively) and mid-ventricular (-7.7 ± 1.6 and 12.3 ± 2.8 cm/s, respectively)) (Galiuto et al., 1998). Longitudinal velocities were generally smaller using tissue phase mapping compared to echocardiography, which might be explained by the better temporal resolution. Surprisingly, we could not detect a statistically significant transmural gradient for peak systolic longitudinal velocities, although longitudinally directed fibres are mainly located in the subendocardium (Rushmer et al., 1953; Simpson, 1997). A possible explanation might lie in the helical orientation of the epicardial fibres (Torrent-Guasp et al., 1997), potentially only inhibiting systolic transmural velocity differences, as peak diastolic longitudinal velocities were greater in the endocardial layers.

Our results suggest that tissue phase mapping is a reproducible, comprehensive modality to assess regional wall motion, and intra- and inter-observer variabilities are low. A previous report has suggested high reproducibility assessing patients twice but within the same scan for longitudinal velocities (Karwatowski et al., 1994b). The variation seen in true

inter-study reproducibility, however, should not only reflect variability in measurement, but also varying pre-load, blood pressure and different slice selection, which necessitates separate scans. The variability in slice positioning in our study population was very low (≤ 5%, standard deviation of position/distance from apex to mitral valve plane). Inter-observer variability found in our study compares favourably with those obtained for echocardiographic strain and strain-rate imaging (in the order of 15%) (Voigt et al., 2000).

Limitations

Our study was performed in young healthy volunteers and was not designed to investigate effects of age, pre-load and medication on myocardial velocities. The effects on the described parameters will have to be addressed in future studies.

Tissue phase mapping is currently limited by a lower temporal resolution when compared to echocardiographically determined strain and strain-rate (Pellerin et al., 2003) (one order of magnitude) and CMR tagging (Moore et al., 2000) (2- to 3-fold). Furthermore, the prospectively triggered tissue phase mapping naturally misses about 10-20% of the cardiac cycle in late diastole. Higher field-strength magnets, improved gradient systems and implementation of parallel imaging may further improve temporal resolution.

An inherent problem in using myocardial velocity parameters is caused by the nature of continuous structures, such as the myocardium, to transmit deformation to adjacent tissue, often referred to as “tethering”. Any locally measured myocardial velocity might reflect active or passive motion (Urheim

et al., 2000; Abraham et al., 2002; Kukulski et al., 2002). As described in detail elsewhere (Hennig et al., 1998b), tissue phase mapping is acquired in breath-hold to avoid bulk motion of the internal organs and it corrects for in-plane translational motion. Furthermore, our measures of torsion-rate and longitudinal strain-rate are independent of tethering effects.

Conclusions

Tissue phase mapping is a reproducible, comprehensive modality to assess regional wall motion, and intra- and inter-observer variabilities are low. Our results may potentially serve as a reference with which abnormal hearts can be compared, allowing tissue phase mapping to be used as part of a multi-parametric CMR approach in clinical practice.

CHAPTER 5: Sex-specific characteristics of cardiac function, geometry and mass in young adult elite athletes

5.1 Introduction

Principal differences between male and female hearts are at least partly a reflection of the sex specific hormonal milieu (Silver, 1991). Experimental studies suggest opposing modulating effects of oestrogen and testosterone, with oestrogen having an anti-proliferative and testosterone a proliferative stimulus in situations of cardiac remodelling (Marsh et al., 1998; Xin et al., 2002; Cavasin et al., 2003; Nahrendorf et al., 2003; Babiker et al., 2004; Pedram et al., 2005; Skavdahl et al., 2005). However, recent molecular studies have indicated a fundamental difference in calcium-sensitive signalling pathways leading to pathological vs. physiological hypertrophy (McMullen et al., 2003). Little data exist for sex-specific effects on chronic physiological cardiac remodelling. Athlete's heart represents a physiological adaptation either to pressure- (strength-trained athletes) or volume-overload (endurance-trained athletes), leading to concentric or eccentric LV hypertrophy, respectively. Most sport disciplines yield a combination of both mechanisms (Morganroth et al., 1975; Pelliccia et al., 1991; Maron et al., 1995; Pelliccia et al., 1999; Pluim et al., 2000; Maron, 2003; Whyte et al., 2004b). In the literature, female athletes have typically been underrepresented: Recent meta-analyses included male athletes in 59 studies and female athletes in only 13 studies (Pluim et al., 2000; Whyte et al., 2004a). Furthermore, little data exist addressing the degree of right ventricular adaptive changes to exercise training, mainly due to the limited

echocardiographic access to the right ventricle (Scharhag et al., 2002; D'Andrea et al., 2003a; D'Andrea et al., 2003b).

Cardiac magnetic resonance (CMR) provides high image quality and is intrinsically three-dimensional, not relying on geometric assumptions, and is, thus, the currently accepted gold-standard method for the measurement of both LV and RV cardiac volumes and mass (Bellenger et al., 2000). CMR phase velocity imaging ('tissue phase mapping') allows three-dimensional assessment of cardiac contraction and relaxation with good inter-study reproducibility (chapter 4). We aimed to study male and female young adult elite athletes with age- and sex-matched sedentary controls to assess sex-specific differences for LV and RV dilatation and hypertrophy as well as for LV contraction and relaxation. We hypothesized that structural and functional adaptive changes to exercise training would be sex-specific.

5.2 Methods

Study Population

23 male elite athletes (mean age 25±4 years, training 22±7 hours/week in rowing, swimming or triathlon) and 20 female elite athletes (mean age 24±4 years, training 19±5 hours/week in rowing, swimming or triathlon) and age- and sex-matched sedentary healthy controls (21 male, mean age 26±3 years and 17 female, mean age 26±3 years) were enrolled into the study. None of the subjects had any of the following: history of cardiac disease, hypertension or other cardiac risk factors. All sedentary controls had normal electrocardiograms (ECG) and no athlete presented with pathological ECG changes other than voltage criteria for LV hypertrophy. Subjects with

contraindications for CMR were not enrolled. The study was carried out according to the principles of the Declaration of Helsinki and was approved by our institutional ethics committee. Each subject gave informed written consent.

Cardiovascular Magnetic Resonance Imaging Protocol

Details of the SSFP cine imaging and tissue phase mapping protocol are given in chapter 2. All acquired datasets were of sufficient image quality, without respiration artefacts in the magnitude images, and could be included in the analysis.

Image Analysis

LV and RV volumes, masses and ejection fractions were determined as outlined in chapter 2.

For each of the radial and longitudinal velocities, two systolic and two diastolic parameters were computed: systolic peak velocity, systolic time to peak velocity, diastolic peak velocity and diastolic time to peak velocity. These parameters were computed for averaged global mid-ventricular velocities. In addition, the relative speed of motion between the basal and apical slice was plotted over the cardiac cycle as the difference between the circumferential (torsion-rate [$rad.s^{-1}.cm^{-1}$] defined as the rate of change of angular velocity along the heart) and longitudinal (longitudinal strain-rate [s^{-1}]) velocities of the global basal and apical slices normalized to mid-ventricular short axis diameter and to ventricular length. Peak systolic torsion-rate, peak diastolic torsion-rate, systolic time to peak torsion-rate, diastolic time to peak torsion-

rate and peak systolic longitudinal strain-rate, peak diastolic longitudinal strain-rate, systolic time to peak systolic longitudinal strain-rate and diastolic time to peak longitudinal strain-rate were then derived from those graphs.

Statistical Analysis

All data are presented as mean ± standard deviation (SD) unless stated otherwise. A univariate general linear model with fixed effects for sex and training (athlete vs. sedentary control) was used to test whether differences between age-and sex-matched athletes and sedentary controls were sex-specific. Throughout the analyses, a two-sided p-value of <0.05 was considered statistically significant. All computations were performed with SPSS 11.5 (SPSS Inc., Chicago, US).

5.3 Results

Study population

Sedentary controls were well matched to elite athletes with regards to age, weight, body mass index, body surface area and systolic blood pressure. Athletes had a slower heart rate than sedentary controls (p for training =0.01). The decrease in diastolic blood pressure observed in male athletes (75±7 mmHg) compared to male controls (64±9 mmHg) was sex-specific and was not observed in females (p for interaction =0.014). Baseline characteristics of all subjects are shown in **Table 5.1**.

Table 5.1: *Baseline Characteristics of elite athletes and sedentary healthy controls.*

	Male		**Female**		**P value**		
	Sedentary (n=21)	**Athletes (n=23)**	**Sedentary (n=17)**	**Athletes (n=20)**	*Training*	*Sex*	*Interaction*
Weight (kg)	80±11	79±12	63±10	66±6	0.61	**<0.001**	0.38
Height (cm)	182±6	185±10	169±5	174±5	**0.03**	**<0.001**	0.58
BMI (kg/m^2)	24.1±3.2	23.1±2.8	21.9±2.9	21.9±1.9	0.43	**0.007**	0.39
BSA (m^2)	2.01±0.15	2.01±0.20	1.72±0.16	1.79±0.10	0.26	**<0.001**	0.37
Training (hours/week)	N/A	22±7	N/A	19±5	N/A	0.15	N/A
Training (years at elite level)	N/A	9±5	N/A	9±5	N/A	0.70	N/A
Systolic blood pressure (mmHg)	121±8	117±8	111±8	115±10	0.70	**0.003**	0.07
Diastolic blood pressure (mmHg)	75±7	64±9	66±4	66±8	**0.008**	0.12	**0.014**
Mean blood pressure (mmHg)	91±7	82±7	81±4	82±8	0.06	**0.02**	**0.009**
Heart rate (bpm)	63±10	61±9	66±10	56±9	**0.01**	0.60	0.11

Left and right ventricular volumes, mass and global function

When compared to sedentary controls, athletes, as expected, had significantly increased left and right ventricular end-diastolic, end-systolic and stroke volumes and mass indices (**Figure 5.1**), reflecting a training effect of 15 to 42%. In contrast, LV and RV ejection fractions remained unchanged. We observed increased LV and RV volume indices in male compared to female subjects, but none of the parameters for LV and RV volumes, mass

and ejection fraction showed any sex-specific changes to exercise training ($p>0.05$ for all interactions, **Table 5.2**).

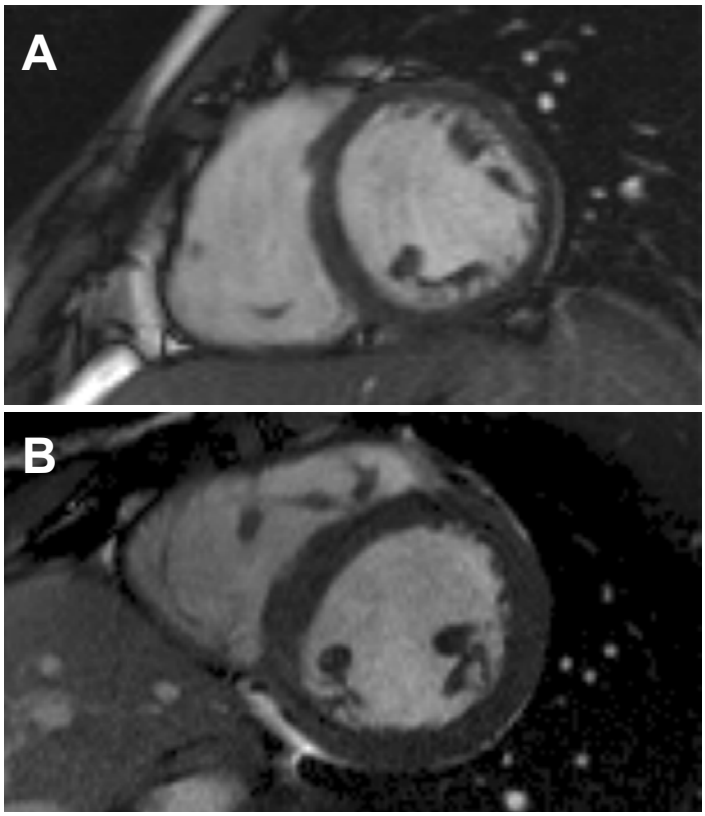

Figure 5.1: *End-diastolic still frames of steady-state free precession cines in a male sedentary control (A: Body surface area 1.84 m^2, LV end-diastolic volume 158 ml, LV mass 98 g) and a male elite athlete (B: Body surface area 2.37 m^2, LV end-diastolic volume 317 ml , LV mass 345 g)*

Table 5. 2: *Left and right ventricular volume parameters of elite athletes and sedentary controls.*

	Male			**Female**			**P value**		
	SC (n=21)	**Athletes (n=23)**	**Training effect (%)**	**SC (n=17)**	**Athletes (n=20)**	**Training effect (%)**	*Training*	*Sex*	*Interaction*
LV ejection fraction (%)	67±6	70±6	4	68±7	68±6	0	0.54	0.71	0.32
LV end-diastolic volume index (ml/m^2)	89±10	108±10	21	80±10	94±9	18	**<0.001**	**<0.001**	0.27
LV end-systolic volume index (ml/m^2)	29±7	33±8	14	25±5	31±7	24	**0.005**	0.054	0.662
LV stroke volume index (ml/m^2)	60±7	75±9	25	54±9	64±7	19	**<0.001**	**<0.001**	0.09
LV mass index (g/m^2)	66±9	94±20	42	52±9	70±9	35	**<0.001**	**<0.001**	0.09
RV ejection fraction (%)	58±6	59±7	2	60±5	58±5	-3	0.69	0.54	0.09
RV end-diastolic volume index (ml/m^2)	103±13	119±16	16	88±12	106±15	20	**<0.001**	**<0.001**	0.78
RV end-systolic volume index (ml/m^2)	44±9	48±7	9	35±6	45±9	29	**<0.001**	**0.001**	0.10
RV stroke volume index (ml/m^2)	59±9	71±14	20	53±9	61±9	15	**<0.001**	**0.002**	0.40
RV mass index (g/m^2)	23±5	28±3	22	21±3	25±3	19	**<0.001**	**0.013**	0.66

SC = sedentary control;

The ratios between the LV and RV volumes, masses and ejection fractions (**Table 5.3**) can be used to assess whether LV and RV dilatation and hypertrophy are balanced when compared to sedentary controls (Scharhag et al., 2002). Both male and female athletes show balanced cardiac dilatation (LV/RV ratios for end-diastolic volume, end-systolic and stroke volume index). The LV/RV ratio for mass index was significantly increased in athletes compared to controls (p for training = 0.006) and in males compared to female subjects (p for sex <0.001), but there was no sex-specific difference for the changes observed to due exercise training (p for interaction =0.35).

Table 5.3: *Left-to right ventricular volume parameters of elite athletes and sedentary controls.*

	Male			**Female**			**P value**		
	SC (n=21)	**Athletes (n=23)**	**Training effect (%)**	**SC (n=17)**	**Athletes (n=20)**	**Training effect (%)**	*Training*	*Sex*	*Inter-action*
LV/RV ejection fraction (%)	1.2±0.1	1.2±0.2	0	1.1±0.1	1.2±0.1	9	0.27	0.26	0.51
LV/RV end-diastolic volume index (ml/m^2)	0.9±0.1	0.9±0.1	0	0.9±0.1	0.9±0.1	0	0.30	0.61	0.11
LV/RV end-systolic volume index (ml/m^2)	0.7±0.1	0.7±0.2	0	0.7±0.2	0.7±0.1	0	0.74	0.27	0.26
LV/RV stroke volume index (ml/m^2)	1.0±0.1	1.1±0.2	10	1.0±0.1	1.1±0.1	10	0.13	0.53	0.50
LV/RV mass index (g/m^2)	3.0±0.5	3.5±0.7	17	2.5±0.5	2.8±0.5	12	**0.006**	**<0.001**	0.35

SC = sedentary controls;

Systolic and diastolic myocardial contraction patterns

Athletes had similar systolic and diastolic contraction patterns when compared to sedentary controls (p for training >0.05 for 7 of the 8 systolic and diastolic parameters), with the exception of the prolonged time to peak systolic longitudinal velocity in athletes (p for training =0.003), and the shortened time to peak diastolic longitudinal strain-rate (p for training =0.03). Male and female subjects showed similar systolic and diastolic relaxation patterns (p for sex >0.05 for all diastolic and for 6 of 8 systolic parameters).

Higher peak systolic radial velocities and prolonged time to peak systolic longitudinal strain-rate were observed in male compared to female subjects (p for sex <0.001 and 0.04, respectively). No sex-specific differences of training effect on systolic and diastolic myocardial contraction patterns were observed (all p for interaction >0.05, **Table 5.4**).

Table 5.4: *Mean± SD myocardial velocities at mid-ventricular level, myocardial torsion-rate and longitudinal strain-rate in elite athletes and sedentary controls.*

	Male			**Female**			**P value**		
	Sedentary (n=21)	**Athletes (n=23)**	**Training effect (%)**	**Sedentary (n=17)**	**Athletes (n=20)**	**Training effect (%)**	*Train-ing*	*Sex*	*Inter-action*
Peak systolic radial velocity [cm.s^{-1}]	3.64±0.58	3.74±0.91	-3	3.09±0.64	3.09±0.51	0	0.73	**<0.001**	0.75
Peak systolic longitudinal velocity [cm.s^{-1}]	-4.74±1.97	-4.64±2.49	2	-3.91±-1.51	-4.28±2.39	-9	0.79	0.27	0.66
Peak systolic torsion-rate [deg. s^{-1}. cm^{-1}]	15.07±4.86	15.50±3.41	-3	16.02±4.36	13.01±3.30	23	0.17	0.41	0.07
Peak systolic longitudinal strain-rate [s^{-1}]	-1.12±0.33	-1.03±0.39	9	-1.09±0.27	-0.89±0.28	22	0.09	0.29	0.49
Peak diastolic radial velocity [cm.s^{-1}]	-4.21±0.83	-4.55±0.88	-8	-3.91±1.56	-4.42±1.01	-13	0.09	0.39	0.74
Peak diastolic longitudinal velocity [cm.s^{-1}]	8.10±2.00	9.30±1.71	-15	8.81±1.70	8.96±1.85	-2	0.13	0.68	0.24
Peak diastolic torsion-rate [deg. s^{-1}. cm^{-1}]	-11.61±4.97	-14.52±3.90	-25	-11.87±4.18	-12.70±4.61	-7	0.07	0.45	0.31
Peak diastolic longitudinal strain-rate [s^{-1}]	1.52±0.62	1.39±0.46	9	1.73±0.65	1.44±0.69	20	0.16	0.39	0.61
Time to peak systolic radial velocity [%ES]	39±7	39±7	0	41±12	42±7	-2	0.72	0.19	0.64
Time to peak systolic longitudinal velocity [%ES]	16±27	39±46	-144	13±20	47±45	-262	**0.003**	0.73	0.56
Time to peak systolic torsion-rate [%ES]	69±43	53±24	30	69±36	54±23	28	0.96	0.93	0.053
Time to peak systolic longitudinal strain-rate [%ES]	45±15	50±25	-11	55±13	61±24	-11	0.27	**0.04**	0.86
Time to peak diastolic radial velocity [%ED]	18±4	19±6	-6	20±10	19±4	5	0.97	0.60	0.58
Time to peak diastolic longitudinal velocity [%ED]	19±7	20±5	-5	19±6	18±14	6	0.87	0.67	0.71
Time to peak diastolic torsion-rate [%ED]	8±6	7±10	14	13±12	9±4	44	0.23	0.10	0.58
Time to peak diastolic longitudinal strain-rate [%ED]	19±7	18±7	-6	22±7	15±9	-47	**0.03**	0.98	0.21

5.4 Discussion

Our principal finding is that young adult elite athletes show no sex-specific adaptive structural and functional changes to chronic physiological cardiac remodelling. This is in contrast to findings observed in models of chronic pathological remodelling thought to be modulated by the sex-specific hormonal milieu (Marsh et al., 1998; Xin et al., 2002; Cavasin et al., 2003; Nahrendorf et al., 2003; Skavdahl et al., 2005). This study, therefore, provides further evidence for the benign nature of the hypertrophy associated with athlete's heart.

Sex-specific structural cardiac changes to exercise training

Our finding that athletes, mainly engaged in rowing, swimming and triathlon, show an unbalanced left and right ventricular hypertrophy, favouring the LV, contrasts with a report by Scharhag and colleagues in male endurance athletes (Scharhag et al., 2002). This discrepancy might reflect differential effects to exercise type or severity as well as duration of training. The LV mass (and index) increase in male athletes was comparable for both studies (42% in our study vs. 36%), whereas the RV mass (and index) increased only by 22% in our study as compared to 37% in theirs. We report LV to RV volume and mass ratios for the first time in female athletes, demonstrating absence of sex-specific differences to exercise training.

Our results show balanced left and right ventricular dilatation in both male and female athletes, as determined by the LV to RV ratio of end-diastolic, end-systolic and stroke volume. These findings confirm previous observations for male athletes and extend them to female athletes (Scharhag

et al., 2002). Our findings suggest that there is no sex-specific difference of balanced cardiac dilatation due to chronic physiological dilatation.

The absence of sex-specific structural changes in chronic physiological cardiac remodelling is in contrast with observations made in models of chronic pathological remodelling. These sex-specific changes in pathological remodelling have been attributed to estrogens preventing and androgens facilitating cardiac hypertrophy (Marsh et al., 1998; Xin et al., 2002; Cavasin et al., 2003; Nahrendorf et al., 2003; Skavdahl et al., 2005). However, recent molecular studies have indicated a fundamental difference in calcium-sensitive signalling pathways leading to pathological (including calcineurin-NFAT) and physiological (via the activation of Akt through a phosphoinositide 3-kinase pathway) hypertrophy (McMullen et al., 2003). Therefore, the most likely explanation for the lack of sex-specific adaptive cardiac structural changes due to exercise training is the underlying difference in the pathophysiological mechanisms leading to cardiac hypertrophy and dilatation. In our study we have not documented androgen and oestrogen levels in sedentary controls and athletes. Therefore, a change of the hormonal balance due to extensive training in male and female athletes contributing to the lack of sex-specific cardiac changes cannot be ruled out (Steinacker et al., 1993; Uusitalo et al., 1998).

Sex-specific changes of cardiac contraction and relaxation to exercise training

Our results indicate essentially normal contraction and relaxation in highly-trained athletes. Furthermore, there were no sex-specific changes to exercise training on these systolic and diastolic parameters. While our and

previous studies agree on normal systolic function (Pluim et al., 2000; Whyte et al., 2004a), previous studies have been conflicting with regards to diastolic function in athletes. Doppler-echocardiography and tissue Doppler imaging studies have shown either normal (Varani et al., 1989; Lewis et al., 1992; Lai et al., 1998; Jungblut et al., 2000; Hoogsteen et al., 2004; Whyte et al., 2004a; Whyte et al., 2004b) or augmented diastolic function (Douglas and O'Toole, 1992; Palazzuoli et al., 2001; D'Andrea et al., 2002; Hoogsteen et al., 2003). A disadvantage of some of the previous studies is the lack of age- and sex-matched groups of sedentary controls (D'Andrea et al., 2002; Hoogsteen et al., 2003; Hoogsteen et al., 2004).

Human and experimental studies indicate that estrogens can positively modulate myocardial function. A number of studies have shown that healthy pre-menopausal women have higher ejection fractions compared to healthy age-matched men (Buonanno et al., 1982; Hayward et al., 2000) or to post-menopausal women (Pines et al., 1992). Similarly, papillary muscles from female rats have higher rates of shortening than male (Capasso et al., 1983) and than gonadectomised female rats (Schaible and Scheuer, 1984). The absence of sex-specific adaptive functional changes in our study suggests that this oestrogen effect may be important for baseline cardiovascular characteristics, but not for adaptive functional cardiac changes due to exercise training.

In conclusion, young adult elite athletes do not show sex-specific adaptive structural and functional changes to exercise training. Our data give further evidence of the benign nature of athlete’s heart.

CHAPTER 6: Differentiation of athlete's heart from pathological forms of cardiac hypertrophy by means of geometric indices derived from cardiovascular magnetic resonance

6.1 Introduction

Determining the underlying aetiology of left ventricular (LV) hypertrophy in patients is often a challenging clinical problem. Various pathological forms of LV hypertrophy, such as due to hypertrophic cardiomyopathy (HCM), hypertensive heart disease or aortic stenosis, and physiological forms of LV hypertrophy, such as in athlete's hearts, can present with overlapping cardiac hypertrophy phenotypes as determined by 2D-echocardiography or ECG. However, in clinical practice, the distinction between physiological hypertrophy occurring in athletes and pathological hypertrophy is critical because HCM accounts for about one-third of exercise-related sudden deaths in young competitive athletes (Maron et al., 1980; Maron et al., 1986; Burke et al., 1991; Corrado et al., 1998) . Furthermore, in athletes with hypertension, the relative contributions of increased blood pressure and physical training to the degree of LV hypertrophy detected need to be clarified, and this has implications as to the recommendation of treatment with antihypertensive agents in this situation.

Various pathophysiological mechanisms are responsible for the development of LV hypertrophy. In aortic stenosis and hypertensive heart disease, the resulting chronic LV pressure overload leads to compensatory concentric hypertrophy. Athlete's heart is thought to represent a physiological adaptation either to pressure overload (strength-trained athletes) or volume

overload (endurance-trained athletes), leading to concentric or eccentric LV hypertrophy, respectively. Most sport disciplines yield a combination of both mechanisms (Morganroth et al., 1975; Pelliccia et al., 1991; Maron et al., 1995; Pelliccia et al., 1999; Pluim et al., 2000; Maron, 2003; Whyte et al., 2004b). The precise pathophysiological mechanisms underlying LV hypertrophy in patients with HCM remain controversial (Ashrafian et al., 2003): However, in contrast to pressure or volume overload LV hypertrophy, the hypertrophic stimulus in HCM is intrinsic to the myocardium.

We therefore hypothesized that these differences in pathophysiology lead to subtle differences in the cardiac hypertrophy phenotype, which can be detected by a highly sensitive imaging technique (Grothues et al., 2002). Cardiac magnetic resonance (CMR) provides high image quality and is intrinsically three-dimensional, not relying on geometric assumptions, and is, thus, the currently accepted gold standard method for the measurement of cardiac volumes and mass (Bellenger et al., 2000).

Therefore, we employed CMR imaging to test whether CMR-derived LV volume parameters and geometric indices accurately predict the underlying etiology of LV hypertrophy. This hypothesis was tested in groups of patients with HCM, hypertension, and aortic stenosis, and in athletes.

6.2 Methods

Study participants

A total of 120 subjects were studied. Patients with LV hypertrophy and a preserved LV ejection fraction (greater than 50%) were enrolled (n=102).

Each participant with LV hypertrophy fell into one of the following groups: Competitive athletes (n=25; 25±4 years), hypertrophic cardiomyopathy (n=35; 43±17 years), hypertensive heart disease (n=18; 52±12 years), and aortic stenosis (n=24; 67±15 years). 18 healthy volunteers served as a reference group (41±13 years).

Athletes were recruited solely on the basis of participation in high-level competitive sports, which were principally rowing, swimming, running and cycling for at least the previous 18 months, with an average of 19.2±6.8 hours training per week for the last 8.5± 4.9 years. None of the athletes were hypertensive or had any cardiovascular disease or risk factors. HCM patients were recruited from the University of Oxford Cardiomyopathy and Heart Failure Clinic at the John Radcliffe Hospital, and the clinical diagnosis of HCM was based on family history, standard electrocardiographic and echocardiographic criteria (end-diastolic wall thickness of greater 13 mm) in the absence of secondary causes for left ventricular hypertrophy. None of the HCM patients had hypertension. Hypertensive patients were enrolled if they showed an end-diastolic wall thickness of greater 13 mm on echocardiography. Additionally, a history of longstanding hypertension, documentation of hypertension on 24 hour ambulatory blood pressure readings (>140/90 mmHg) and at least one antihypertensive medication were required. The average number of antihypertensive drugs was 3.3±1.5. In patients with aortic stenosis, the peak instantaneous aortic valve gradient was 71±27 mmHg. In addition, all aortic stenosis patients showed echocardiographic evidence of LV hypertrophy (end-diastolic wall thickness of greater 13 mm). Although aortic stenosis is clinically easily diagnosed by

examination and echocardiography, this group was included in our study to compare the LV morphologic phenotype arising from this form of pressure overload with the phenotypes caused by other forms of pathological and physiological LV hypertrophy. All groups other than athletes did not perform physical training at a level or duration that would be expected to cause LV hypertrophy. Baseline characteristics of subjects are also given in **Table 6.1**.

Table 6.1: *Baseline characteristics and left ventricular volume results*

		Groups with LVH				
Diagnosis (∑ n=120)	**Healthy Volunteers (n=18)**	**AH (n=25)**	**HCM (n=35)**	**HHD (n=18)**	**AS (n=24)**	**p-value**
Age [years]	41 ± 13 (26-68)	25 ± 4* (20-35)	43 ± 17 (15-78)	52 ± 12 (20-71)	67 ± 15* (33-89)	P<0.01
Gender	6m/12f	12m/13f	26m/9f	15m/3f	15m/9f	n.s.§
BSA [m^{-2}]	1.75 ± 0.19 (1.28-2.07)	1.87 ± 0.15 (1.61-2.28)	1.98 ± 0.29 (1.14-2.48)	2.07 ± 0.25 (1.69-2.47)	1.94 ± 0.23 (1.51-2.40)	n.s.
Body weight [kg]	66 ± 12 (38-88)	70 ± 10† (55-94)	82 ± 18 (36-119)	88 ± 19† (60-120)	80 ± 15 (55-117)	P<0.01
Heart rate [bpm]	67 ± 16 (50-112)	61 ± 9 (46-78)	58 ± 11 (44-91)	65 ± 12 (49-100)	64 ± 9 (49-80)	n.s.
Mean BP [mmHg]	98 ± 7 (92-116)	82 ± 8‡ (67-106)	92 ± 10‡ (65-113)	112 ± 20* (90-170)	88 ± 14 (73-118)	P<0.01
LV mass index [g/ m^{-2}]	55.6 ± 9.9 (40.3-78.9)	75.8 ± 15.5 (55.0-125.7)	85.0 ± 27.3 (48.1-161.3)	75.6 ± 10.1 (51.4-93.6)	93.7 ± 40.1 (46.9-218.2)	n.s.
LVEF [%]	72 ± 6 (60-80)	68 ± 6* (58-88)	76 ± 6 (61-86)	76 ± 6 (67-86)	76 ± 10 (54-90)	P<0.01
LVEDVI [ml/ m^{-2}]	79 ± 12 (63-101)	99 ± 11* (80-115)	77 ± 14 (47-111)	76 ± 12 (58-94)	76 ± 25 (44-134)	P<0.01
LVESVI [ml/ m^{-2}]	23 ± 6 (14-34)	31 ± 7* (13-45)	19 ± 7 (9-41)	19 ± 6 (11-29)	20 ± 13 (6-56)	P<0.01
LVSVI [ml/ m^{-2}]	56 ± 9 (42-72)	68 ± 10* (51-96)	58 ± 10 (33-76)	58 ± 9 (44-73)	57 ± 16 (34-98)	P<0.01

HCM=hypertrophic cardiomyopathy; HHD=hypertensive heart disease; AS=aortic stenosis; AH=athlete's heart; BSA=body surface area; bpm=beats per minute; LV= left ventricular; LVEF=LV ejection fraction; LVEDVI= LV end-diastolic volume index; LVESVI= LV end-systolic volume index; LVSVI = LV stroke volume index. One-way ANOVA with Bonferroni post-hoc corrections was applied for the four groups of left ventricular hypertrophy unless stated otherwise. Results of healthy volunteers' are presented for reference purposes. As the aim of this study was the identification of differences in various forms of LV hypertrophy, only these groups were used for statistical analysis. * p<0.01 versus all other cardiac hypertrophy groups;† p<0.01 between the groups with this symbol; ‡ p<0.05 between the groups with this symbol; § The Kruskal-Wallis-test for qualitative parameters was applied.

MR imaging

Steady state free precession cine images were acquired as described in chapter 2.

Data Analysis

Cine images were analysed as described in chapter 2, with an experienced analyser blinded to the diagnosis. For each set of Cine studies, standard LV volume parameters were generated: LV ejection fraction (LVEF), LV mass index, LV end-diastolic (LVEDVI), end-systolic (LVESVI) and stroke volume index (LVSVI). Geometric indices were computed to analyse the three-dimensional distribution of cardiac hypertrophy assessing all myocardial segments (Cerqueira et al., 2002). In each of the three diastolic long axis views and in a basal short axis slice at a level between the LV outflow tract and the papillary muscles (**Figure 6.1**) the segment with the thickest and the thinnest myocardial diameter was chosen for measurement. Only the maximal (i.e. thickest) and the minimal (i.e. thinnest) end-diastolic wall thickness were then used for analysis. These values were then used to calculate maximal end-diastolic wall thickness ("diastolic wall thickness") and end-diastolic maximal-to-minimal wall thickness ratios ("wall thickness ratio"). End-diastolic maximal wall thickness-to-LVEDVI ("diastolic wall-to-volume ratio"; a measure of wall thickness in relation to heart size) and end-systolic minimal wall thickness-to-LVESVI ("systolic wall-to-volume ratio"; a measure of contractility in the least hypertrophied region of the heart) were also calculated.

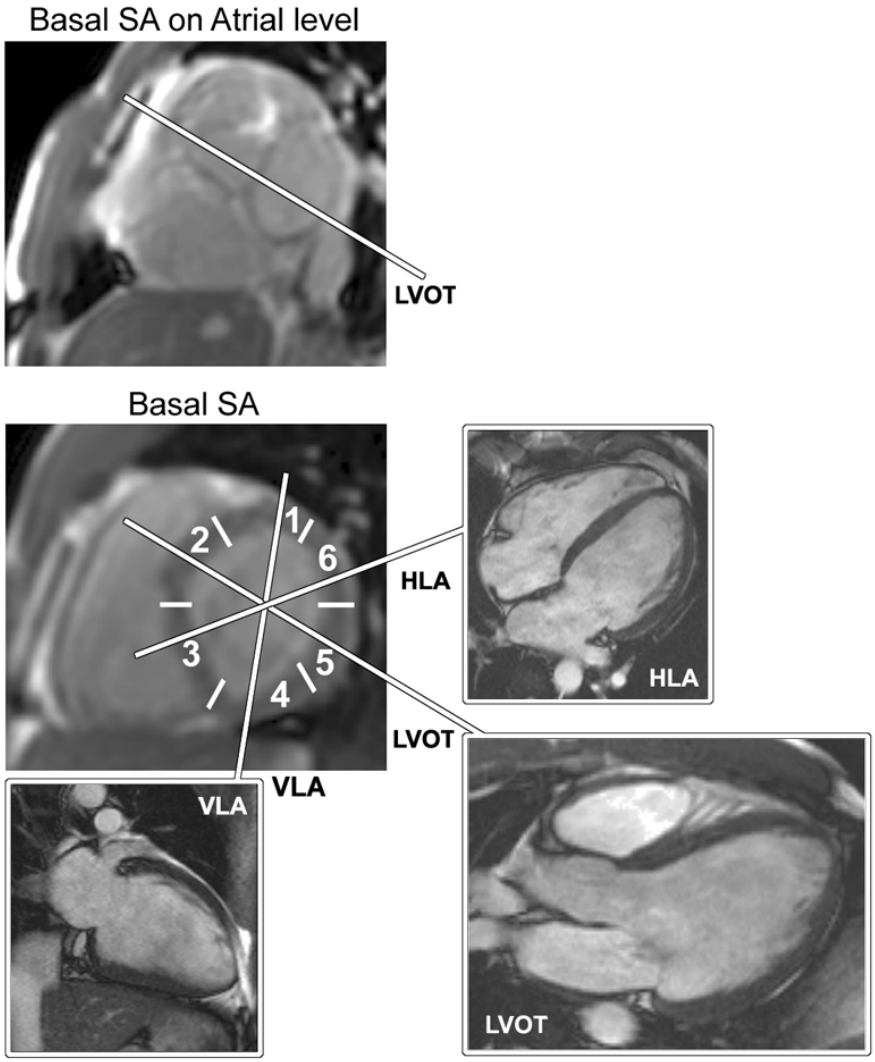

Figure 6.1: *Planning image positions to allow three-dimension analysis of wall thickness distribution. By rotating imaging planes by 60˚ around an imaginary axis at the centre of the left ventricular cavity in pilot short axis views (SA), the left ventricular outflow tract (LVOT) can be imaged, and horizontal (HLA) and vertical long axis (VLA) views can be generated. The basal short axis slice shows 6 segments according to the AHA convention.*

Statistical Analysis

Results of healthy volunteers are presented for reference purposes. As the aim of this study was the identification of differences amongst various forms of LV hypertrophy, only these groups were used for statistical analysis. All data are presented as mean±SD (range) unless stated otherwise. Nominal

data were tested for differences between multiple groups using the Kruskal-Wallis test. Continuous data were analysed using ANOVA with post-hoc Bonferroni analysis to establish differences between the individual groups. A p-value of <0.05 was considered statistically significant. Multiple logistic regression analysis was performed to identify the values of LV volume and geometric indices to allow correct diagnosis of LV hypertrophy. Receiver operating characteristics were used to generate cut-off values for optimised sensitivity and specificity to distinguish athlete's heart from pathological cardiac hypertrophy. All computations were done with SPSS 11.0 (SPSS Inc., Chicago, US).

6.3 Results

Characteristics of subject and patient groups

All groups with LV hypertrophy had similar LV mass indices (p>0.05 for all four LV hypertrophy groups), which were, on average, at least 35%higher than those obtained in healthy volunteers (p<0.05 for combined LV hypertrophy groups vs. healthy volunteers; t-test for unpaired variables, **Table 6.1**). The four LV hypertrophy groups were also similar with regard to gender, heart rate and body surface area (p>0.05 for all, **Table 6.1**). As expected, mean blood pressure was higher in hypertensive patients (p<0.01 vs. all groups). Hypertensive patients had a higher body weight compared to athletes (p<0.01). As is typical for athlete's heart, LV end-diastolic, end-systolic and stroke volume indices were all higher in the athletes group (p<0.01 for all three parameters vs. all groups). All ECG findings were normal in athletes.

Geometric indices

Diastolic wall thickness was significantly lower in athletes (Figure 6.2, Table 6.2) as compared to the other three groups with pathological cardiac hypertrophy ($p<0.01$). 10/25 (40%) athletes showed a diastolic wall thickness greater than 13 mm and 1/25 (4%) a wall thickness of greater than 16 mm. HCM patients showed the largest diastolic wall thickness, which was also significantly higher than wall thickness in hypertensive heart disease ($p<0.01$, Table 6.2). However, only 7 of 35 (20%) HCM patients presented with a wall thickness above the highest values of the other LV hypertrophy groups. Wall thickness ratio was highest for HCM ($p<0.01$ vs. AH, $p<0.05$ vs. AS), lowest for athletes and intermediate for hypertensive patients (n.s. vs. all other groups) and aortic stenosis. 2 of the 35 patients (6%) with HCM showed symmetric LV hypertrophy with a wall thickness ratio of less than 1.3. Diastolic wall-to-volume ratio was lowest in athletes ($p<0.01$ compared to all other groups) and was highest in HCM patients (**Table 6.2**). Athletes also had the lowest systolic wall-to-volume ratio ($p<0.01$ compared to all other groups), while aortic stenosis patients showed the highest ratio ($p<0.05$ compared to HCM, $p<0.01$ compared to athletes).

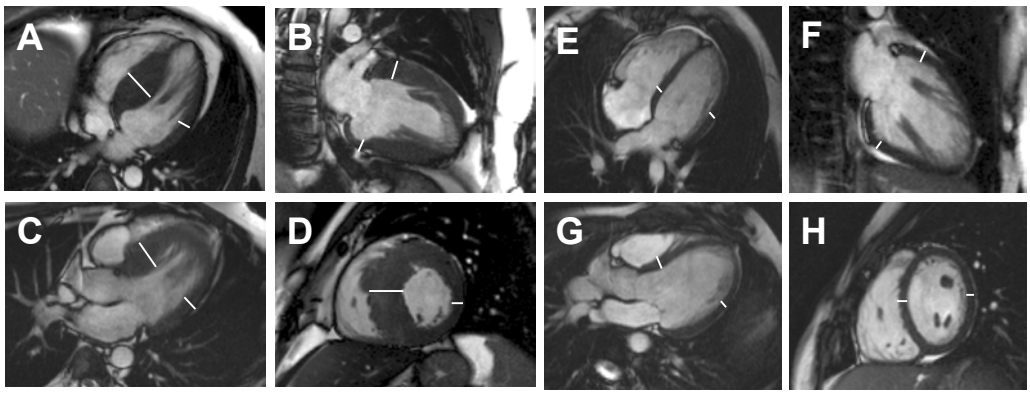

Figure 6.2: *End-diastolic steady-state free precession cine images in a patient with hypertrophic cardiomyopathy (A-D) and in a competitive athlete with athlete's heart (E-H). A/E: horizontal long axis, B/F: vertical long axis, C/G: left ventricular outflow tract and D/H: basal short axis view. In each of the three diastolic long axis views and in a basal short axis slice at a level between the LV outflow tract and the papillary muscles (Figure 1) the segment with the thickest and the thinnest myocardial diameter was chosen for measurement (white lines). Only the maximal (i.e. thickest) and the minimal (i.e. thinnest) end-diastolic wall thickness were then used for analysis. These values were then used to calculate maximal end-diastolic wall thickness ("diastolic wall thickness") and end-diastolic maximal-to-minimal wall thickness ratios ("wall thickness ratio").*

Table 6.2: *Geometric indices*

		Groups with LVH				
Diagnosis (∑ n=120)	**Healthy Volunteers (n=18)**	**AH (n=25)**	**HCM (n=35)**	**HHD (n=18)**	**AS (n=24)**	**p-value**
Diastolic wall thickness [mm]	11.1 ± 1.1 (9.3-12.6)	12.8 ± 1.8* (9.7-16.6)	21.5 ± 5.9† (14.3-36.5)	17.0 ± 2.6† (13.2-22.4)	19.4 ± 3.8 (13.1-26.6)	P<0.01
Wall thickness ratio [a.u.]	1.43 ± .22 (1.11-2.03)	1.42 ± 0.17† (1.09-1.87)	2.25 ± 1.07†,‡ (1.01-7.45)	1.77 ± 0.41 (1.27-2.77)	1.76 ± 0.35‡ (1.28-2.70)	P<0.01
Diastolic wall-to-volume ratio [mm*m^2/ml]	0.14 ± 0.03 (0.1-0.2)	0.13 ± 0.02* (0.1-0.2)	0.29 ± 0.10 (0.2-0.5)	0.23 ± 0.07 (0.2-0.4)	0.28 ± 0.10 (0.1-0.6)	P<0.01
Systolic wall-to-volume ratio [mm*m^2/ml]	0.56 ± 0.23 (0.3-1.0)	0.42 ± 0.15* (0.2-1.0)	0.86 ± 0.32‡ (0.4-1.9)	0.92 ± 0.36 (0.4-1.7)	1.22 ± 0.82‡ (0.3-3.3)	P<0.01

HCM=hypertrophic cardiomyopathy; HHD=hypertensive heart disease; AS=aortic stenosis; AH=athlete's heart; a.u.=arbitrary units; Diastolic wall thickness = maximal end-diastolic wall thickness; wall thickness ratio=ratio of maximal-to-minimal wall thickness; diastolic wall-to-volume ratio=maximal end-diastolic wall thickness-to-left ventricular end-diastolic volume index; systolic wall-to-volume ratio=minimal end-systolic wall thickness-to-left ventricular end-systolic volume index. The data are presented as mean ± standard deviation (range). One-way ANOVA with Bonferroni post-hoc corrections was applied for the four groups of left ventricular hypertrophy. Results of healthy volunteers' are presented for reference purposes. As the aim of this study was the identification of differences in various forms of LV hypertrophy, only these groups were used for statistical analysis.* $p<0.01$ versus all other cardiac hypertrophy groups; † $p<0.01$ between the groups with this symbol; ‡ $p<0.05$ between the groups with this symbol

Diagnostic accuracy of geometric indices to differentiate the underlying aetiology of cardiac hypertrophy

Receiver operating characteristics identified the diastolic wall-to-volume ratio as the best parameter (i.e. the highest area under the curve of 0.993) to differentiate athlete's heart from all other pathological hypertrophy forms. A cut-off value for diastolic wall-to-volume ratio of less than 0.15 $mm*m^2*ml^{-1}$ discriminated between physiological and pathological LV hypertrophy with a sensitivity of 80%, a specificity of 99%, a positive predictive value of 95% and a negative predictive value of 94% (**Table 6.3, Figure 6.3**).

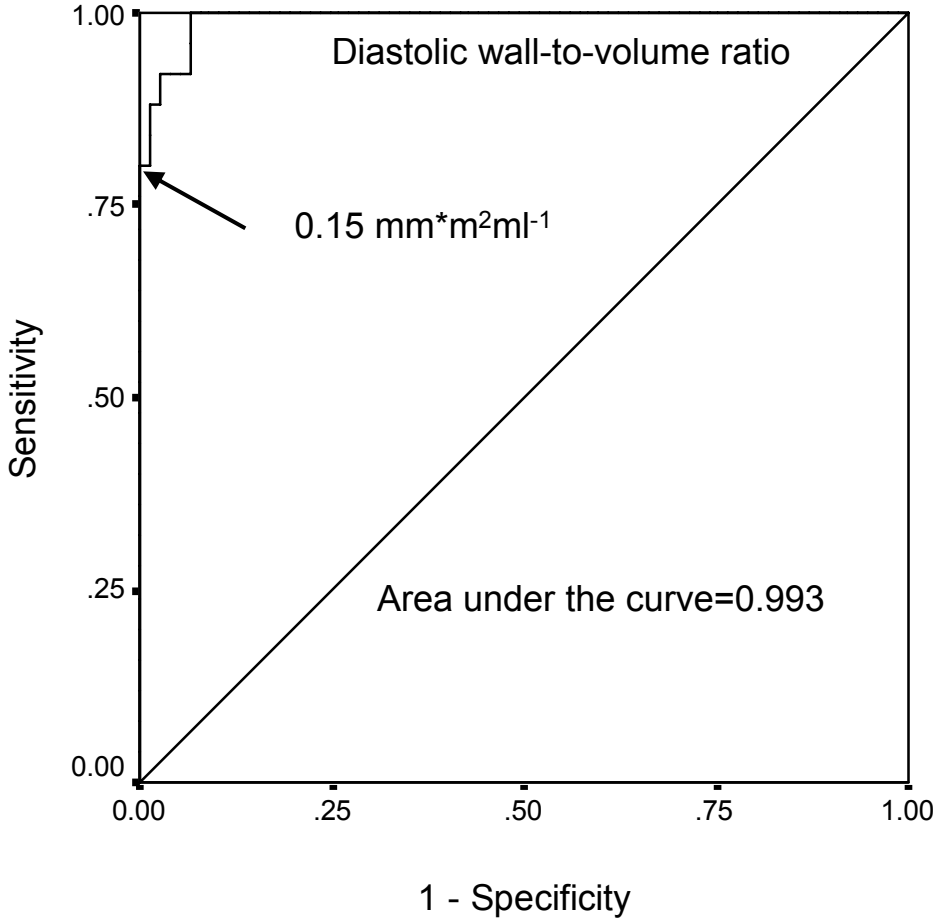

Figure 6.3: *Receiver operating characteristics of the diastolic wall-to-volume ratio to distinguish athlete's heart from pathological left ventricular hypertrophy. The area under the curve is 0.993, and for a cut-off value of 0.15 mm*m^2*ml^{-1} this parameter provides a sensitivity and specificity of 80% and 99%, respectively. The positive and negative predictive values were 95% and 94%, respectively.*

Table 6.3: *Diagnostic accuracy for differentiation of physiological from pathological LV hypertrophy*

	Sens	**Spec**	**pos pred**	**neg pred**	**AUC**
Diastolic wall thickness <13 mm	40%	100%	100%	84%	0.955
Wall thickness ratio<1.3	28%	95%	64%	95%	0.862
Diastolic wall-to-volume ratio <0.15 mm*m^2/ml	80%	99%	95%	94%	0.993
Systolic wall-to-volume ratio <0.26 mm*m^2/ml	4%	100%	100%	76%	0.926

Sens=sensitivity; spec=specificity; pos pred=positive predictive value; neg pred=negative predictive value; AUC=area under the curve for analysis based on receiver operating curves.

To analyse the diagnostic accuracy of CMR in differentiating between all four forms of cardiac hypertrophy studied, MR parameters derived from LV volume studies (LV mass index, LVEF, LVEDVI, LVESVI, LVSVI) and geometric indices (diastolic wall thickness, wall thickness ratio, diastolic wall-to-volume ratio and systolic wall-to-volume ratio) were subjected to multiple logistic regression analysis. The number and percentage of patients correctly classified with these parameters were computed (**Table 6.4**). Athlete's hearts were correctly classified in 100% of cases, HCM in 80%, aortic stenosis patients in 54% and hypertensive heart disease in 22%. Importantly, no athlete was misclassified as having HCM in spite of a maximal wall thickness of 16 mm and no patient with HCM as athlete's heart. Hypertensive heart disease was the most commonly misclassified condition, and could be

mistaken for any form of pathological cardiac hypertrophy, but, importantly, not for athlete's heart. Aortic stenosis was sometimes misclassified as hypertensive heart disease or HCM, but, again, never as athlete's heart. Thus, no single LV geometric index could identify athletes with 100% diagnostic accuracy, but multiple logistic regression analysis, taking into account all measured parameters, was 100% correct in distinguishing athlete's heart from all other forms of LV hypertrophy.

Table 6.4: *Classification table showing the prediction of diagnosis based on a multiple logistic regression analysis including left ventricular volume parameters (LVEF, LVEDVI, LVESVI, LVSVI, LV mass index) and geometric indices (diastolic wall thickness, wall thickness ratio, diastolic wall-to-volume ratio, systolic wall-to-volume ratio)*

Real Diagnosis	Predicted Diagnosis				
	HCM	**HHD**	**AS**	**AH**	**Percent correct**
HCM (n=35)	28 (80%)	3 (9%)	4 (11%)	0 (0%)	80%
HHD (n=18)	10 (56%)	4 (22%)	4 (22%)	0 (0%)	22%
AS (n=24)	8 (33%)	3 (13%)	13 (54%)	0 (0%)	54%
AH (n=25)	0 (0%)	0 (0%)	0 (0%)	25 (100%)	100%

6.4 Discussion

Our principal finding is that physiological LV hypertrophy can reliably be distinguished from pathological LV hypertrophy, such as in HCM, hypertensive heart disease and aortic stenosis, based on CMR-derived LV geometric indices. In contrast, these forms of pathological LV hypertrophy present with an overlapping cardiac hypertrophy phenotype.

Identification of Athlete's heart by CMR indices

Distinction of pathological and physiological LV hypertrophy remains a frequent clinical dilemma. In current clinical practice, one strategy of distinguishing athlete's heart from pathological LV hypertrophy is to document the deconditioning effect after training cessation for several months (Martin et al., 1986; Maron et al., 1993; Pelliccia et al., 2002). However, this is often not acceptable to athletes. Metabolic exercise testing has been shown to facilitate the differentiation between athlete's hearts and HCM (Sharma et al., 2000). Our study suggests a novel approach to distinguish athlete's heart from various forms of pathological LV hypertrophy by means of three-dimensional CMR-derived LV volume and geometric indices, obviating the need for 'de-training' to make this distinction.

Importantly, in our study, no athlete was misdiagnosed as having HCM in spite of a wall thickness of greater 16 mm, and no patient with HCM was diagnosed as having physiological LV hypertrophy. This is of clinical importance, as labelling athletes with a diagnosis of HCM would disqualify them from competitive exercise in addition to the psychological and socioeconomic impact of this diagnosis. On the other hand, missing HCM in athletes would expose them to a high risk of sudden cardiac death, as HCM is the most common cause of sudden death in the population under 35 years of age (Maron et al., 1980; Maron et al., 1986; Burke et al., 1991).

Our findings also confirm that cardiac morphologic changes in athletes are different from those induced by pressure overload LV hypertrophy. Athlete's hearts are characterised by larger LV volumes, smaller ejection

fractions, and less pronounced wall thickness, despite a similar LV mass index. The differentiation of athlete's heart from hypertensive heart disease is clinically relevant, and athletes with additional LV hypertrophy secondary to hypertension should be treated vigorously with antihypertensive medication. This is supported by a recent meta-analysis (Verdecchia et al., 2003) showing that regression of LV hypertrophy by antihypertensive treatment is associated with a marked reduction in risk for subsequent cardiovascular disease.

Our findings are in keeping with one previous study using echocardiography, which suggested that geometric indices are useful in distinguishing athlete's heart from hypertrophic cardiomyopathy (Devlin and Ostman-Smith, 2000). However, this study did not include other forms of pathological LV hypertrophy. In principle, CMR can detect changes of LV parameters with a much smaller sample size than echocardiography (for equivalent statistical power) due to the high inter-study reproducibility and the observer-independence of the method. As in our study, the measurements by Grothues and colleagues were based on manual detection of endo-and epicardial contours with coeffients of variability for inter-study reproducibility of 3.6% for CMR and 13.5% for echocardiography in LV hypertrophy patients (Grothues et al., 2002). Thus, to detect a 10 g difference in LV mass index, CMR allows a reduction of the sample size by 90%.

Pathological forms of LV hypertrophy

The differential diagnosis of patients with pathological cardiac hypertrophy remains difficult, even with a high-resolution, three-dimensional technique, such as CMR. The finding of similar patterns of cardiac

hypertrophy amongst different pathological hypertrophy etiologies is of clinical relevance. The ACC/ESC Expert consensus document (Maron et al., 2003) states that in HCM, LV wall thickening is found in the absence of another cardiac or systemic disease capable of producing the magnitude of hypertrophy evident. However, coexistence of pathologies, for example of hypertension and HCM, is not unusual. In addition, genotype-phenotype correlations have shown that virtually any LV wall thickness is compatible with HCM (Watkins et al., 1995). In our cohort, only 20% of HCM patients presented with a wall thickness above the maximal values seen in hypertension and aortic stenosis. Consequently, in the presence of coexisting pathologies that cause LV hypertrophy, a majority of the HCM patients in our study could not have been classified as affected by the ACC/ESC criteria. Genetic analysis to identify HCM mutations may be particularly valuable in patients with multiple potential causes of LV hypertrophy, such as in HCM family members with hypertension.

One possible explanation for the similarity of the cardiac muscle phenotypes in pathological hypertrophy may be a common intracellular signalling pathway mediating myocardial growth. A rise in intracellular calcium elicited by mechanical stretch (in aortic stenosis and hypertension) or altered bioenergetics (in HCM) (Frey et al., 2000; Ashrafian et al., 2003; Frey and Olson, 2003; Wilkins et al., 2004) has been identified as the key step leading to the activation of calcium-sensitive signalling pathways (including calcineurin-NFAT) and myocardial growth. Conversely, recent findings have indicated that physiological hypertrophy may result from the activation of Akt through a phosphoinositide 3-kinase (PI3K) pathway (McMullen et al., 2003).

Hypertrophy and cardiac asymmetry

Asymmetric LV hypertrophy is considered the hallmark of HCM, and traditionally, the wall thickness ratio has been widely used for the diagnosis of this disease. However, our results indicate that this parameter provides the least diagnostic accuracy for the differentiation of LV hypertrophy compared to the other geometric indices used. Cardiac muscle asymmetry, thus, is not solely associated with HCM. Furthermore, symmetric forms of HCM appear to be more common than may be appreciated; 6% of patients with HCM in our cohort showed symmetrical LV hypertrophy. For the distinction of physiological LV hypertrophy from HCM, this is particularly problematic as symmetrical HCM appears to be more common in the athletic HCM sub-population. Maron and colleagues found that up to 43% of athletes who suffered sudden death due to HCM had normal septum to LV wall ratios in the heart arrested in systole at autopsy (Maron et al., 1980).

Cardiac muscle asymmetry also shows a wide and overlapping spectrum in both athletes and in pathological cardiac hypertrophy. Furthermore, even in the absence of LV hypertrophy, our findings in healthy volunteers show a degree of asymmetry in line with previous reports (Kansal et al., 1979; Doi et al., 1980). Consequently, asymmetry as determined by high-resolution, three-dimensional CMR cannot reliably differentiate HCM from pressure overload LV hypertrophy. The pathoanatomical substrate underlying the phenomenon of asymmetric hypertrophy, as seen across the spectrum of groups studied, maybe denser sympathetic innvervation of the interventricular septum compared to the lateral wall (Ostman-Smith, 1981).

Limitations

Our study populations were, inevitably, dissimilar with regards to age (athletes were younger, aortic stenosis patients were older) and weight (despite a similar body surface area, the hypertensive patients were more obese). However, echocardiographically determined geometric indices have been shown to be independent of sex and body size (Ostman-Smith and Devlin, 2001). Additionally, we normalised all volume parameters to body surface area. Furthermore, our results were unchanged when we normalized LV parameters to body height instead of surface area (data not shown).

Athletes were ascertained if they participated in high-level physical training and athletic competition so as to be representative of the type of patient in whom the differential diagnosis of cardiac hypertrophy presents a problem. This selection resulted in similar elevation of mean LV mass index as was seen in the pathological hypertrophy groups but not all athletes had a diastolic wall thickness of greater than 13 mm. Thus the distribution of geometric measurements will be somewhat different in the athletes as wall thickness of greater than 13 mm was an inclusion criterion for HCM, hypertensive heart disease and aortic stenosis. Probably as a result of our very stringent selection, many of our elite athletes (40%) had a wall thickness of greater than 13 mm. CMR may tend to yield higher numbers for diastolic wall thickness than echocardiography. The inclusion of athletes with both, increased and normal wall thickness, but all with increased LV mass indices, appears important as HCM patients may be phenotype negative gene carriers.

While we cannot rule out HCM with absolute certainty in athletes with increased wall thickness, none of these athletes had an abnormal ECG, a positive family history or cardiovascular symptoms; therefore, a diagnosis of HCM is statistically highly unlikely.

Conclusions

We propose the use of CMR-derived LV volume and geometric indices for clinical practice to distinguish athlete's hearts from pathological forms LV hypertrophy. These indices, however, cannot differentiate HCM and LV hypertrophy secondary to systemic hypertension or aortic stenosis.

CHAPTER 7: Left ventricular non-compaction: Insights from cardiovascular magnetic resonance imaging

7.1 Introduction

Left ventricular non-compaction (LVNC) is characterized by the presence of an extensive non-compacted myocardial layer lining the cavity of the left ventricle, and potentially leads to cardiac failure, thromboembolism, and malignant arrhythmias (Ritter et al., 1997; Oechslin et al., 2000). It can be associated with neuromuscular disorders (Stollberger et al., 2002), and can co-exist with other cardiac malformations (Oechslin et al., 2000). Based on echocardiographic studies, its prevalence has been estimated at 0.05% in the general population (Ritter et al., 1997), and the finding of a ratio of greater than 2.0 between the thickness of the non-compacted and compacted myocardial layers in systole is considered diagnostic (Jenni et al., 2001). Echocardiography, however, poses inherent problems in assessing the LV apex, known to be the most commonly non-compacted area (Moon et al., 2004).

As high resolution imaging techniques, such as multi-detector CT, have shown the frequent presence of pronounced trabeculae within healthy myocardium (Axel, 2004), a similar finding may be expected with cardiovascular magnetic resonance (CMR) in both healthy and diseased hearts, which is increasingly used in clinical practice. Accordingly, it is necessary to establish specific CMR criteria for the diagnosis of pathological non-compaction. To this end, we examined healthy volunteers as well as patients with potential differential diagnoses for LVNC. Findings from this

group were compared with unequivocal LVNC cases in whom the diagnosis was supported by other clinical features.

7.2 Methods

The study was approved by our institutional ethics committee. Each participant gave written informed consent.

Participants

We enrolled 7 patients with the clinical diagnosis of LVNC based on either echocardiographic or CMR documentation of a distinct two layered appearance of trabeculated and compacted myocardium. An arbitrary threshold for the degree of non-compaction was not applied so as not to exclude patients with a partial expression of the disease (Sasse-Klaassen et al., 2004). The imaging findings had to be accompanied by one of the following to increase the pre-test probability for this diagnosis: documentation of a similar appearance in first degree relatives suggestive of autosomal dominant transmission, associated neuromuscular disorders, or complications, such as systemic embolization and regional wall motion abnormalities (**Table 7.1**). The remaining subjects were healthy volunteers without a history of cardiovascular symptoms or risk factors, or drawn from groups giving a potential differential diagnosis for LVNC: 25 competitive athletes, 14 patients with dilated cardiomyopathy (DCM), 39 with hypertrophic cardiomyopathy (HCM), 17 with left ventricular hypertrophy secondary to hypertension, and 30 with aortic stenosis.

Table 7.1: *Characteristics of patients diagnosed with left ventricular non-compaction (LVNC).*

LVNC patients	Age (years)	Gender	symptoms	FH	ECG changes	Regional wall motion abnormality	LV EF (%)	Neuro-muscular findings	NC/C ratio	N of segments with NC
1	14	M	Heart failure as baby	+	+	—	48	—	2.4	12
2	15	F	—	+	+	—	64	—	1.1	9
3	38	M	—	+	—	—	61	—	2.3	8
4	41	M	—	+	—	+	53	—	3.3	12
5	46	M	Systemic embolus	—		+	17	—	6.1	15
6	26	F	—	—	—	+	68	—	2.9	9
7	25	M	syncope	—	+	+	59	+	2.7	8

FH=family history; LVEF=left ventricular ejection fraction; NC=non-compaction;

High-level competitive athletes, with an average of 19±7 hours training per week were recruited. HCM patients were diagnosed based on family history, and standard electrocardiographic and echocardiographic criteria in the absence of a secondary cause for cardiac hypertrophy. The diagnosis of DCM was based on impaired global left ventricular function, with an ejection fraction of less than 40% on echocardiography, and exclusion of other causes of LV dysfunction. Hypertensive and aortic stenosis patients were enrolled if they showed an end-diastolic wall thickness of greater than 13 mm on echocardiography.

MR Imaging

Steady-state free precession cine images were acquired in 3 long-axis views (i.e. horizontal and vertical long axis and left ventricular outflow tract), planned on short axis (SA) pilots at 60˚ angles to each other to visualize all 17 segments according to the AHA recommendation (see also chapter 2 for details) (Cerqueira et al., 2002).

Data Analysis

Cine images were analyzed with CMRtools (Imperial College, London, UK), the observer being blinded to the diagnosis. The distribution of non-compaction was assessed by qualitative analysis of all 17 segments for presence or absence of any degree of non-compaction, i.e. for a distinct two-layered appearance of trabeculated and compacted myocardium. A segment was regarded as non-compacted, if the visual appearance clearly suggested the presence of two myocardial layers with different degrees of tissue compaction. In each of the three diastolic long axis views the segment with

the most pronounced trabeculations was chosen for measurement of the thickness of the non-compacted and the compacted myocardium perpendicular to the compacted myocardium. The ratio of non-compacted to compacted myocardium (NC/C ratio) in diastole was calculated for each of the three long axis views and only the maximal ratio was then used for analysis. The apex (segment 17) was excluded from the measurements, since the compacted myocardium is generally thinner in this area, and inclusion would have led to artificially high ratios.

Statistical Analysis

All data are presented as mean±standard deviation. Nominal data were tested using the Chi-square test. Continuous data were analyzed using ANOVA with post-hoc Bonferroni analysis to establish differences between LVNC and the six remaining groups individually. A p-value of less than 0.05 (after Bonferroni adjustment) was considered statistically significant. We used receiver operating characteristics (ROC) to generate cut-off values for optimized sensitivity and specificity to distinguish LVNC from all other groups of subjects.

7.3 Results

Non-compaction was more common in the apical segments of the healthy volunteers, being found in 91% of subjects, as compared to the mid-cavity levels (78%), and the basal segments (21%, **Figure 7.1**). Non-compaction was most common in the anterior segment, becoming less frequent in successive segments as viewed in a clockwise direction. Similar

patterns of distribution were seen in hearts of the patients with confirmed LVNC and in the other groups (**Figure 7.1**). Overall, patients with pathological non-compaction had involvement of significantly ($p<0.01$) more myocardial segments (10±3 segments) than did healthy volunteers (6±3 segments), athletes (6±4 segments), patients with hypertrophic (5±4 segments) and dilated cardiomyopathy (7±3 segments), and those with LV hypertrophy secondary to hypertension (4±4 segments) and aortic stenosis (6±4 segments).

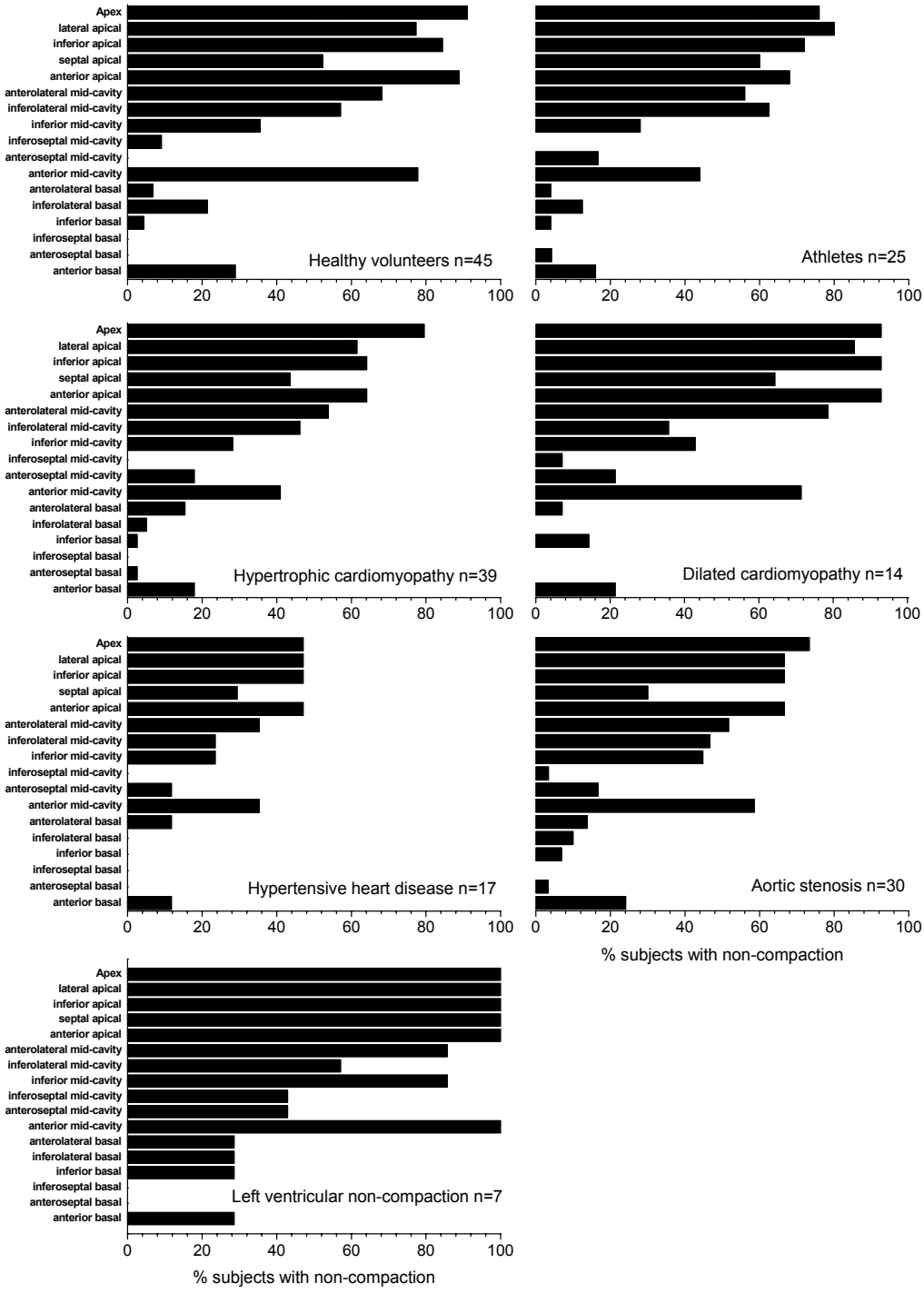

Figure 7.1: *Distribution of non-compaction. The bars represent the percentage of subjects in each group with non-compaction in given segments. The pattern of distribution of non-compaction does not separate the groups.*

The end-diastolic NC/C ratio was, on average, at least 60% greater in patients with LVNC (3.0 ±1.5) compared to all other groups ($p<0.01$ for all, **Figure 7.2**). ROC analysis identified the end-diastolic NC/C ratio as a valuable parameter to distinguish pathological non-compaction from the lesser degrees of non-compaction encountered in healthy, dilated and hypertrophied hearts. A NC/C ratio of greater than 2.3 in diastole distinguished pathological non-compaction, with values for sensitivity, specificity, positive, and negative predictions of 86%, 99%, 75% and 99%, respectively.

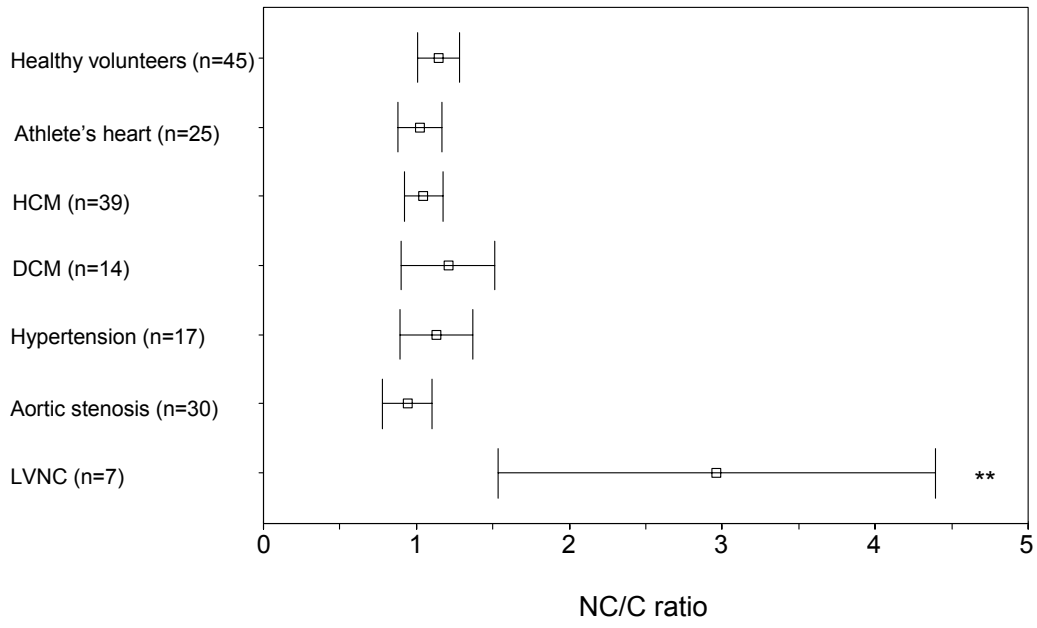

Figure 7.2: *Ratio of the end-diastolic thickness of the non-compacted and compacted layers of the myocardium (NC/C ratio). Data are presented as means (square) and 95% confidence interval (whiskers). ** denotes p<0.01.*

7.4 Discussion

We found that a degree of non-compaction of the left ventricle was far more frequent in healthy, dilated, and hypertrophied hearts than previously reported in cardiac imaging studies; presumably this is a manifestation of the increased sensitivity of CMR. Nevertheless, we have shown that the ratio between the trabecular and compact layers of the myocardium as measured by CMR in diastole is accurate in detecting pathological LVNC.

The segmental distribution of non-compaction was similar in healthy, dilated, and hypertrophied hearts to that found in the patients with confirmed LVNC. However, the ratio between the myocardial thicknesses was at least 60% greater in those with LVNC. We are, therefore, unable to lend support to the recent suggestion that the segmental distribution can be used to clarify the diagnosis of LVNC (Oechslin et al., 2000; Jenni et al., 2001).

The trabecular layer of the developing ventricular walls is known to compact during its development from base to apex, from epi- to endocardium, and from the septal to the lateral wall (Sedmera et al., 2000). Although the underlying pathophysiological mechanisms for lack of such compaction remain unresolved, varying degrees of arrest of this normal embryological process (Jenni et al., 2001) provide an attractive explanation for the typical pattern of distribution seen in all our subjects. Almost 70% of autopsied healthy hearts are reported to show some degree of non-compaction (Boyd et al., 1987), a finding endorsed by the prevalence observed in our study, and probably one with no prognostic relevance. Partial expression of pathological LVNC is illustrated by one patient (patient 2, **Table 7.1, Figure 7.3**) who has

only mild anatomical non-compaction, but supporting evidence for this diagnosis. This phenomenon is typical of autosomal dominant conditions and, has recently been reported in large families with autosomal dominant LVNC (Sasse-Klaassen et al., 2004).

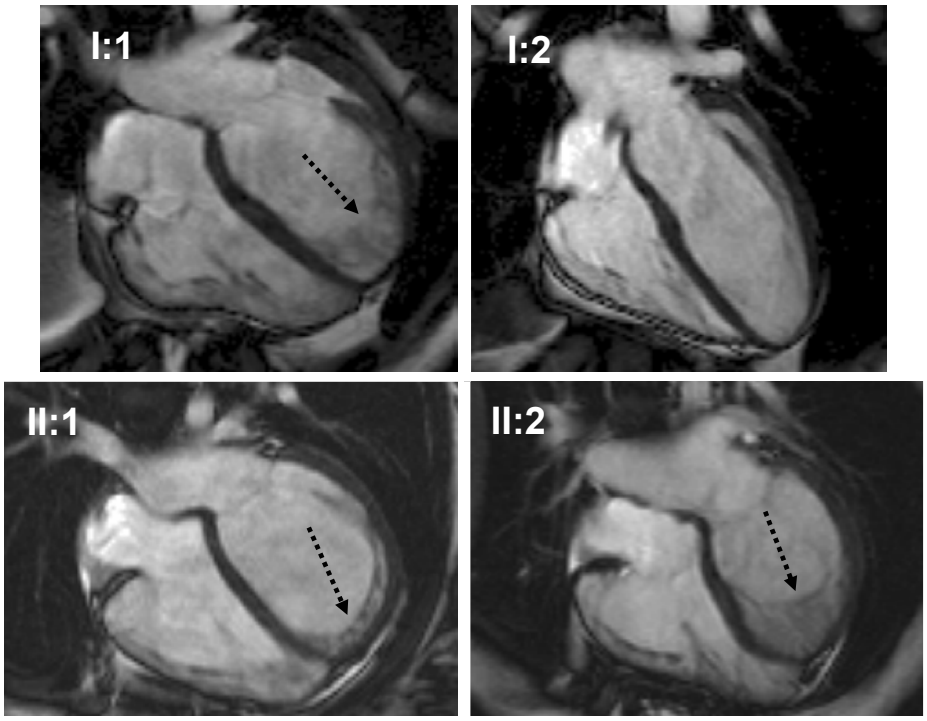

Figure 7.3: *The autosomal dominant pattern of inheritance in a family with pathological left ventricular non-compaction. Diastolic horizontal long axis views of parents (I:1 father and I:2 mother) and children (II:1-II.2) show variable degrees of non-compaction (black dotted arrows) in I:1 (patient 3, Table 7.1), II:1 (patient 2, Table 7.1) and II:2 (patient 1, Table 7.1). Patient II:1 likely illustrates partial expression of pathological non-compaction, as her ratio of end-diastolic thicknesses is less than 2.3 (1.1).*

Previous case studies using CMR imaging have usually considered echocardiographic criteria to represent the gold standard for diagnosis. One small study, mainly using older gradient echo sequences, suggested echocardiography to be superior to CMR at that time (Weiss et al., 2003). Advances in CMR have resulted in superior image quality. We used diastolic

steady-state free precession cine frames to determine the ratio of thickness of the trabecular and compact layers, the trabeculations being more easily identified by CMR in the relaxed heart. The diastolic ratio of greater than 2.3 showed high diagnostic accuracy for distinguishing pathological LVNC from the degrees of non-compaction observed in healthy, dilated, and hypertrophied hearts. This slightly higher cut-off value reflects that the measurement obtained with CMR is taken in diastole, while the echocardiographic values are taken in systole (cut-off value of 2.0) (Jenni et al., 2001).

Limitations

The main limitation of our study is the relatively small number of patients with features of LVNC in whom the diagnosis could be confirmed by the presence of other abnormalities. Isolated echocardiographic or CMR evidence of marked non-compaction was intentionally not considered sufficient for inclusion so as to avoid circular reasoning.

Conclusions

Based on the ratio of end-diastolic thickness of the non-compacted and compacted layers of the myocardium, we have shown that cardiovascular magnetic resonance imaging is accurate when diagnosing pathological left ventricular non-compaction. We propose that measurements are best made in diastole and that the cut-off values should be different from those used in echocardiography. Our findings support the clinical use of CMR in diagnosing LVNC, especially for those patients with poor echocardiographic windows.

CHAPTER 8: Derangement of cardiac high-energy phosphate metabolism in patients with left ventricular non-compaction and preserved ejection fraction

8.1 Introduction

Left ventricular non-compaction is characterised by the presence of an extensive non-compacted layer of myocardium, which can lead to malignant arrhythmias, thromboembolism and chronic cardiac failure (Chin et al., 1990; Ritter et al., 1997; Ichida et al., 1999; Oechslin et al., 2000; Stollberger et al., 2002). Raised awareness of the condition, coupled with improved diagnostic tools, such as contrast echocardiography and cardiovascular magnetic resonance imaging (Koo et al., 2002; Petersen et al., 2005), and emerging evidence of frequent autosomal dominant transmission (Sasse-Klaassen et al., 2003; Sasse-Klaassen et al., 2004), now lead to earlier diagnosis, even in patients who are asymptomatic. The non-compacted myocardial layer likely represents an arrest during development of normal compaction (Sedmera et al., 2000), albeit that the pathophysiological mechanisms leading to cardiac failure remain unknown. It is also unknown as to why some patients do, whilst others do not, develop cardiac failure.

One attractive mechanism which may underlie the progression into cardiac dysfunction may be altered metabolism of cardiac high-energy phosphates, since similar changes have been described in patients with hypertrophic (Jung et al., 1998; Crilley et al., 2003) or dilated cardiomyopathy (Neubauer et al., 1992; Beer et al., 2002). If this was the case, there would be two clinical implications: First, it would suggest treatment strategies aimed at improving myocardial energetics. Second, altered cardiac energetics may

potentially serve to distinguish patients with non-compaction at low and high risk of developing complications, analogous to the situation in dilated cardiomyopathy, where energetic impairment has been shown to be a powerful predictor of prognosis (Neubauer et al., 1997a). Thus, we aimed to investigate cardiac energy metabolism in a group of patients with preserved cardiac function in the setting of ventricular non-compaction.

8.2 Methods

Study Population

We studied 7 patients, 5 of male gender, with clear evidence of left ventricular non-compaction on cardiac magnetic resonance imaging, as defined by a ratio of non-compacted to compacted myocardium during diastole of greater than 2.3, or a distinct two-layered appearance of trabeculated and compacted myocardium with strong supporting clinical findings, such as electrocardiographic changes, as encountered in 2 of our patients with negative T waves, or family history, positive in 6 of the patients (Petersen et al., 2005). Of the 7 patients, 3 had been included in our previous publication describing the diagnostic accuracy of magnetic resonance imaging (Petersen et al., 2005). We were treating 2 patients with betablockers. We selected 7 age- and sex-matched healthy volunteers as controls. We excluded from the study any patients with contraindications for magnetic resonance imaging, or any with left ventricular ejection fractions of less than 50% as judged by magnetic resonance imaging. The study was carried out according to the principles of the Declaration of Helsinki, and was approved

by our institutional ethics committee. Each subject gave informed written consent.

Cardiovascular Magnetic Resonance Imaging and Spectroscopy Protocol

Steady-state free precession cine images (SSFP) and ^{31}P-MRS were acquired as outlined in detail in chapter 2.

Image and Spectroscopy Analysis

The diastolic ratio of non-compacted to compacted myocardium (NC/C ratio) was measured as described in chapter 7.

Analysis of SSFP cine images was performed with Argus software (Version 2002B, Siemens Medical Solutions, Erlangen, Germany), as outlined in chapter 2.

Cardiac high-energy phosphate metabolites (blood and T_1 corrected PCr/ATP ratio, an index of the energetic state of the heart) were measured at rest using ^{31}P-MR spectroscopy in the compacted basal anterior myocardium as outlined in chapter 2. In extensive preliminary studies, we attempted to measure PCr/ATP ratios in non-compacted apical myocardium, but this was not feasible due to insufficient signal-to-noise.

Statistical Analysis

All data are presented as means plus or minus standard deviations (SD), unless stated otherwise. Independent t-tests were used to test for differences between controls and those with non-compaction. Pearson's correlation analysis was performed for the end-diastolic volume of the left

ventricle, and the ratio of PCr to ATP. Throughout the analyses, a two-sided p-value of <0.05 was considered statistically significant. All computations were performed with SPSS 11.5 (SPSS Inc., Chicago, US).

8.3 Results

The mean ratio of the non-compacted to compacted myocardial layers during diastole in the patients diagnosed with non-compaction was 2.6 ± 0.9, with a range from 1.1 to 4.0. All the patients, on the basis of our criteria for inclusion, had preserved left ventricular ejection fractions and, which were measured at 68 ± 5, not significantly different from the values of 72 ± 4 in the control subjects (p=0.16, **Table 8.1**). There were no abnormalities of regional wall motion in any of the subjects. Compared to the controls, however, the patients with non-compaction had significantly dilated left ventricles, with both end-diastolic (146 ± 33 vs. 116 ± 16 ml, p=0.049) and end-systolic (46 ± 11 vs. 33 ± 8 ml, p=0.019) volumes increased compared to the control values (**Figure 8.1**). **Figure 8.2** shows typical ^{31}P-magnetic resonance spectra of a healthy volunteer and a patient with non-compaction with a decrease of the ratio of PCr to ATP in the patient. Individual and mean ratios are given in **Figure 8.3**. The ratio was significantly reduced by 19% in those with non-compaction compared to their controls (1.81 ± 0.10 vs. 2.25 ± 0.36, p=0.005). Furthermore, the ratio did not correlate significantly (p=0.32) with left ventricular volumes, suggesting that the cavity dilation, which leads to increased wall stress, is not related to the derangement in cardiac energetics.

Table 8.1: *Baseline characteristics of healthy controls and patients with left ventricular non-compaction (LVNC).*

	Healthy control (n=7)	**LVNC (n=7)**	**P value**
Age (years)	39±13	37±16	0.79
Gender	5 male/ 2 female	5 male/ 2 female	N/A
BSA (m^2)	2.02±0.20	1.82±0.23	0.11
Mean blood pressure (mmHg)	98±12	100±10	0.72
Family history of LVNC	0	6 (86%)	NA
ECG changes	0	2 (29%)	NA
Heart rate (bpm)	68±13	66±12	0.74
LV ejection fraction (%)	72±4	68±5	0.16
LV stroke volume (ml)	83±12	100±27	0.16
LV mass (g)	99±15	105±32	0.67

Values are presented as mean ± standard deviation. BMI = body mass index, BSA = body surface area, LV = left ventricle/ventricular. NA = not applicable

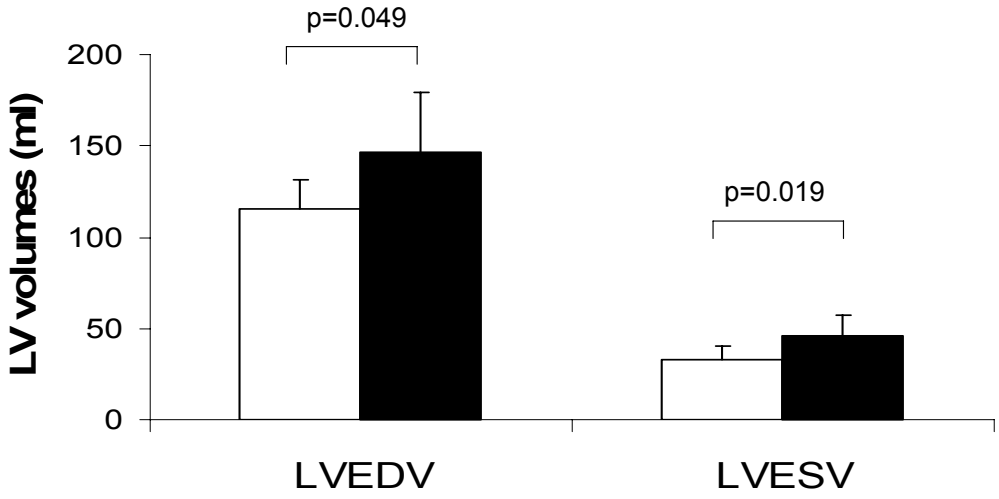

Figure 8.1: *Increased left ventricular end-diastolic (LVEDV) and end-systolic (LVESV) volumes in patients with left ventricular non-compaction (LVNC, black bars) and preserved systolic LV function compared to healthy controls (white bars).*

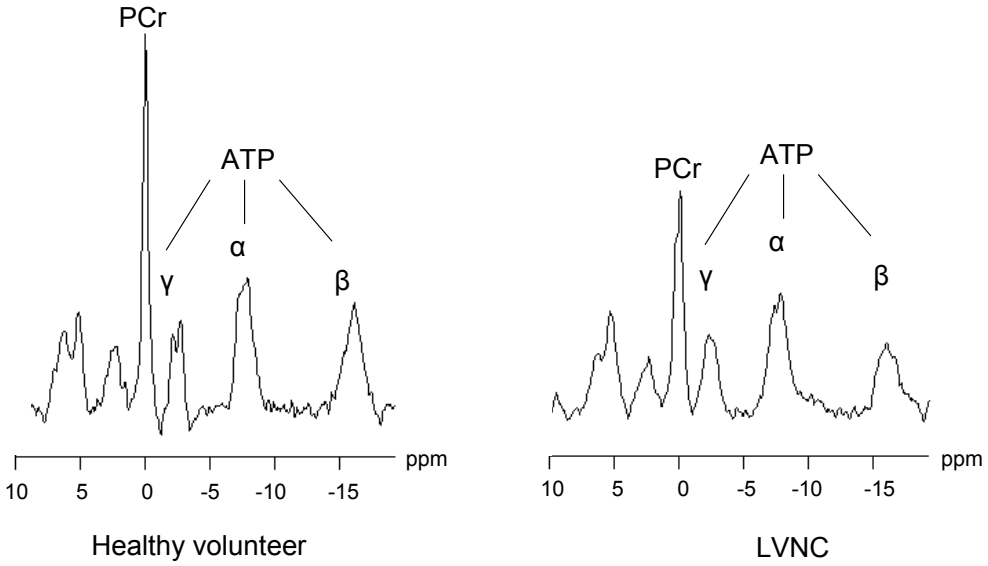

Figure 8.2: *Typical spectra of a healthy volunteer (A) and a patient with left ventricular non-compaction (LVNC) and preserved systolic LV function (B). Please note the substantially reduced PCr/ATP ratio in LVNC.*

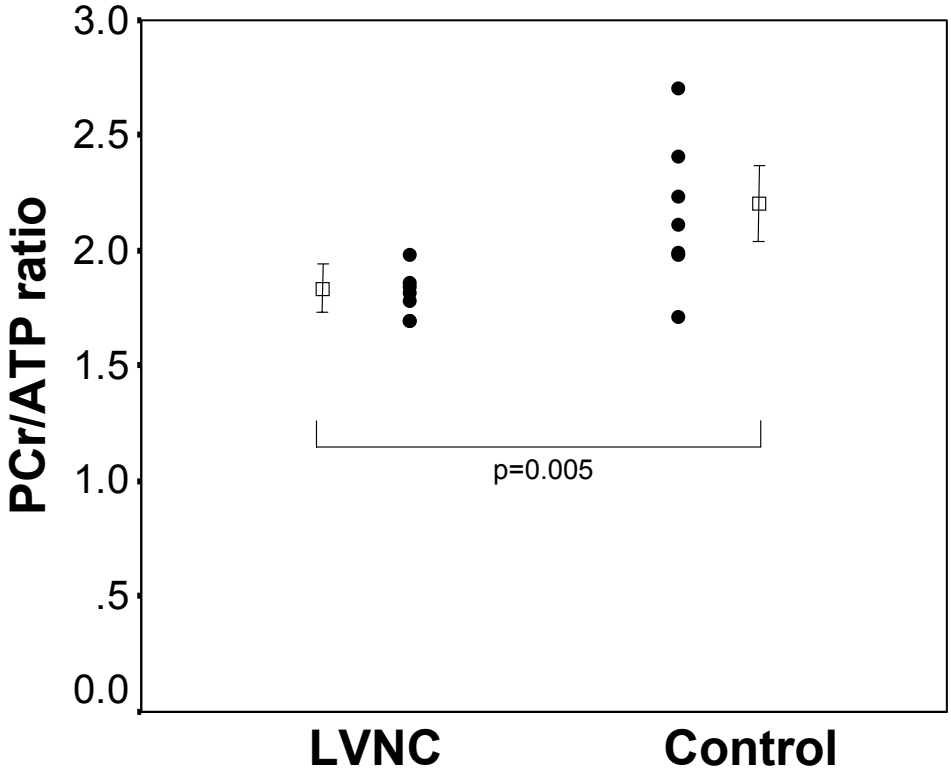

Figure 8.3: *Reduced PCr/ATP ratio in patients with left ventricular non-compaction (LVNC) compared to healthy controls. Dots represent individual PCr/ATP ratios and square and whiskers the mean ± standard deviation.*

8.4 Discussion

To the best of our knowledge, ours is the first study to show that levels of high-energy phosphates are reduced in the myocardium of patients with left ventricular non-compaction and maintained left ventricular systolic function. Our demonstrated reduction in the ratio of PCr to ATP by almost one-fifth is similar to those described in asymptomatic patients with hypertrophic cardiomyopathy, where reductions of one-quarter have been shown (Jung et al., 1998), and in genotyped patients with and without hypertrophy, with reductions shown of up to three-tenths (Crilley et al., 2003). In hypertrophic cardiomyopathy, the deranged cardiac energetics are considered to be intrinsic rather than secondary, in other words the consequence of reduced

perfusion or fibrosis. This hypothesis is supported by the identification of a primary metabolic mutation in AMP-activated protein kinase, a major regulator of energy metabolism, leading to a hypertrophic cardiomyopathic phenotype (Blair et al., 2001). Reduced ratios in dilated cardiomyopathy are again of similar magnitude to that found in our study, being decreased by one-quarter (Beer et al., 2002). Interestingly, we found reduced ratios despite preservation of left ventricular ejection fractions, a finding which has previously been described in patients with Becker muscular dystrophy and their female carriers (Crilley et al., 2000), as well as in patients with type 2 diabetes mellitus (Scheuermann-Freestone et al., 2003). The authors of these studies concluded that the depletion of cardiac energy occurred early in the process of the disease, and may have contributed to the development of cardiac contractile failure. Thus, such deranged mechanisms of cardiac energy in patients with non-compaction may also precede the development of cardiac contractile dysfunction. These findings may have important clinical implications, as energy sparing medications, such as betablockers, may help to prevent or improve the development of chronic heart failure in the patients with non-compaction, while energy costly drugs, such as beta-agonists, might prove detrimental. These hypotheses remain to be tested, but a small study in six patients with dilated cardiomyopathy studied before and after treatment of cardiac failure showed an increase in the ratio of PCr to ATP at three months follow-up compared to baseline (Neubauer et al., 1992).

High contrast imaging modalities now permit allow early diagnosis of non-compaction as an incidental finding in asymptomatic patients. For such patients, there is currently no consensus on strategies for treatment.

Measuring the ratio of PCr to ATP could well serve as a discriminator of a benign as opposed to a malignant course, as was shown in dilated cardiomyopathy (Neubauer et al., 1997a). Such a prognostic value also needs to be investigated in long-term follow-up studies.

While we have demonstrated reduced ratios of PCr to ATP in patients with left ventricular non-compaction, our data do not allow us to identify the molecular mechanisms that lead to the intrinsic metabolic derangements in cardiac energetics. Future studies are needed to investigate these molecular mechanisms.

Conclusions

In summary, the metabolism of high-energy phosphate is deranged in the non-compacted left ventricular myocardium of patients with maintained ejection fractions. The most likely mechanism is an intrinsic derangement of cardiac energetics. Our data suggest a new mechanism leading to development of chronic heart failure in such patients, and provide a potential target for therapeutic strategies. Future long-term follow-up studies are needed to test whether the deranged metabolism may have prognostic value.

CHAPTER 9: General conclusions and outlook

We have produced a large database for left and right ventricular and left atrial volumes of healthy volunteers using SSFP cine images and three-dimensional, endo- and epicardial, systolic and diastolic myocardial velocities using tissue phase mapping. This will be of particular use for reference in both clinical and research studies. We found further evidence for the benign nature of athlete's hearts and were able to provide MR-specific diagnostic criteria for the differentiation of physiological from pathological LV hypertrophy. Left ventricular non-compaction can be diagnosed accurately by magnetic resonance imaging and we identified an altered cardiac energy metabolism as a potential contributing factor towards progression into heart failure in such patients. This novel mechanism may present a potential target for treatment strategies.

Building on the cardiovascular magnetic imaging and spectroscopy protocol developed here, we are now planning to extend the work presented in this thesis, incorporating additional MR measurements of absolute perfusion at rest and stress, as well as measuring the extent of myocardial regional fibrosis by contrast-enhanced MRI. Cardiac PCr and ATP concentrations at rest in three groups of patients with HCM phenocopies due to known mutations where there is uncertainty about the involvement of myocardial energetics will be investigated: Anderson Fabry disease, Noonan's syndrome and patients with PRKAG2 mutations. The metabolic data will be analysed for regional differences and will be correlated to regional variations in wall thickness, wall thickening, tissue contractility, absolute

perfusion at rest and stress, and to the extent of regional fibrosis. These studies should allow us to determine whether these genetically unrelated conditions share aspects of pathogenesis, and are thus informative for understanding hypertrophic cardiomyopathy disease mechanisms, or are indeed only superficially similar.

Such CMR imaging and MRS protocol can also be applied to patients with hypertrophic cardiomyopathy to investigate whether the energetic deficit is a primary phenomenon, or whether it is explained by myocardial fibrosis or by altered perfusion.

Last but not least, we plan to establish a substantial database of CMR imaging and spectroscopy parameters in genotyped hypertrophic cardiomyopathy patients to allow novel insights into genotype-phenotype correlations.

We predict that CMR will become the central modality for the characterisation of the remodelled heart, both in research and in clinical practice.

References

Abraham, TP, Belohlavek, M, Thomson, HL, Pislaru, C, Khandheria, B, Seward, JB and Pellikka, PA (2002). Time to onset of regional relaxation: feasibility, variability and utility of a novel index of regional myocardial function by strain rate imaging. J Am Coll Cardiol 39(9): 1531-7.

Aletras, AH, Balaban, RS and Wen, H (1999a). High-resolution strain analysis of the human heart with fast-DENSE. J Magn Reson 140(1): 41-57.

Aletras, AH, Ding, S, Balaban, RS and Wen, H (1999b). DENSE: displacement encoding with stimulated echoes in cardiac functional MRI. J Magn Reson 137(1): 247-52.

Alfakih, K, Plein, S, Thiele, H, Jones, T, Ridgway, JP and Sivananthan, MU (2003). Normal human left and right ventricular dimensions for MRI as assessed by turbo gradient echo and steady-state free precession imaging sequences. J Magn Reson Imaging 17(3): 323-9.

Amartur, SC and Vesselle, HJ (1993). A new approach to study cardiac motion: the optical flow of cine MR images. Magn Reson Med 29(1): 59-67.

Angelini, A, Melacini, P, Barbero, F and Thiene, G (1999). Evolutionary persistence of spongy myocardium in humans. Circulation 99(18): 2475.

Ashrafian, H, Redwood, C, Blair, E and Watkins, H (2003). Hypertrophic cardiomyopathy:a paradigm for myocardial energy depletion. Trends Genet 19(5): 263-8.

Axel, L (2004). Papillary muscles do not attach directly to the solid heart wall. Circulation 109(25): 3145-8.

Babiker, FA, De Windt, LJ, van Eickels, M, Thijssen, V, Bronsaer, RJ, Grohe, C, van Bilsen, M and Doevendans, PA (2004). 17beta-estradiol antagonizes cardiomyocyte hypertrophy by autocrine/paracrine stimulation of a guanylyl cyclase A receptor-cyclic guanosine monophosphate-dependent protein kinase pathway. Circulation 109(2): 269-76.

Bache, RJ, Vrobel, TR, Ring, WS, Emery, RW and Andersen, RW (1981). Regional myocardial blood flow during exercise in dogs with chronic left ventricular hypertrophy. Circ Res 48(1): 76-87.

Barth, PG, Scholte, HR, Berden, JA, Van der Klei-Van Moorsel, JM, Luyt-Houwen, IE, Van 't Veer-Korthof, ET, Van der Harten, JJ and Sobotka-Plojhar, MA (1983). An X-linked mitochondrial disease affecting cardiac muscle, skeletal muscle and neutrophil leucocytes. J Neurol Sci 62(1-3): 327-55.

Beer, M, Seyfarth, T, Sandstede, J, Landschutz, W, Lipke, C, Kostler, H, von Kienlin, M, Harre, K, Hahn, D and Neubauer, S (2002). Absolute concentrations of high-energy phosphate metabolites in normal, hypertrophied, and failing human myocardium measured noninvasively with

(31)P-SLOOP magnetic resonance spectroscopy. J Am Coll Cardiol 40(7): 1267-74.

Bellenger, NG, Burgess, MI, Ray, SG, Lahiri, A, Coats, AJ, Cleland, JG and Pennell, DJ (2000). Comparison of left ventricular ejection fraction and volumes in heart failure by echocardiography, radionuclide ventriculography and cardiovascular magnetic resonance; are they interchangeable? Eur Heart J 21(16): 1387-96.

Beyerbacht, HP, Lamb, HJ, van Der Laarse, A, Vliegen, HW, Leujes, F, Hazekamp, MG, de Roos, A and van Der Wall, EE (2001). Aortic valve replacement in patients with aortic valve stenosis improves myocardial metabolism and diastolic function. Radiology 219(3): 637-43.

Bione, S, D'Adamo, P, Maestrini, E, Gedeon, AK, Bolhuis, PA and Toniolo, D (1996). A novel X-linked gene, G4.5. is responsible for Barth syndrome. Nat Genet 12(4): 385-9.

Blair, E, Redwood, C, Ashrafian, H, Oliveira, M, Broxholme, J, Kerr, B, Salmon, A, Ostman-Smith, I and Watkins, H (2001). Mutations in the gamma(2) subunit of AMP-activated protein kinase cause familial hypertrophic cardiomyopathy: evidence for the central role of energy compromise in disease pathogenesis. Hum Mol Genet 10(11): 1215-20.

Bland, JM and Altman, DG (1986). Statistical methods for assessing agreement between two methods of clinical measurement. Lancet 1(8476): 307-10.

Bleyl, SB, Mumford, BR, Brown-Harrison, MC, Pagotto, LT, Carey, JC, Pysher, TJ, Ward, K and Chin, TK (1997a). Xq28-linked noncompaction of the left ventricular myocardium: prenatal diagnosis and pathologic analysis of affected individuals. Am J Med Genet 72(3): 257-65.

Bleyl, SB, Mumford, BR, Thompson, V, Carey, JC, Pysher, TJ, Chin, TK and Ward, K (1997b). Neonatal, lethal noncompaction of the left ventricular myocardium is allelic with Barth syndrome. Am J Hum Genet 61(4): 868-72.

Bloch, F (1946). Nuclear induction. Physical Review (Physics): 460-473.

Bonow, RO, Carabello, B, de Leon, AC, Edmunds, LH, Jr., Fedderly, BJ, Freed, MD, Gaasch, WH, McKay, CR, Nishimura, RA, O'Gara, PT, O'Rourke, RA, Rahimtoola, SH, Ritchie, JL, Cheitlin, MD, Eagle, KA, Gardner, TJ, Garson, A, Jr., Gibbons, RJ, Russell, RO, Ryan, TJ and Smith, SC, Jr. (1998). ACC/AHA Guidelines for the Management of Patients With Valvular Heart Disease. Executive Summary. A report of the American College of Cardiology/American Heart Association Task Force on Practice Guidelines (Committee on Management of Patients With Valvular Heart Disease). J Heart Valve Dis 7(6): 672-707.

Bottomley, PA (1994). MR spectroscopy of the human heart: the status and the challenges. Radiology 191(3): 593-612.

Boyd, MT, Seward, JB, Tajik, AJ and Edwards, WD (1987). Frequency and location of prominent left ventricular trabeculations at autopsy in 474 normal human hearts: implications for evaluation of mural thrombi by two-dimensional echocardiography. J Am Coll Cardiol 9(2): 323-6.

Bryant, DJ, Payne, JA, Firmin, DN and Longmore, DB (1984). Measurement of flow with NMR imaging using a gradient pulse and phase difference technique. J Comput Assist Tomogr 8(4): 588-93.

Buonanno, C, Arbustini, E, Rossi, L, Dander, B, Vassanelli, C, Paris, B and Poppi, A (1982). Left ventricular function in men and women. Another difference between sexes. Eur Heart J 3(6): 525-8.

Burke, AP, Farb, A, Virmani, R, Goodin, J and Smialek, JE (1991). Sports-related and non-sports-related sudden cardiac death in young adults. Am Heart J 121(2 Pt 1): 568-75.

Capasso, JM, Remily, RM, Smith, RH and Sonnenblick, EH (1983). Sex differences in myocardial contractility in the rat. Basic Res Cardiol 78(2): 156-71.

Cavasin, MA, Sankey, SS, Yu, AL, Menon, S and Yang, XP (2003). Estrogen and testosterone have opposing effects on chronic cardiac remodeling and function in mice with myocardial infarction. Am J Physiol Heart Circ Physiol 284(5): H1560-9.

Cerqueira, MD, Weissman, NJ, Dilsizian, V, Jacobs, AK, Kaul, S, Laskey, WK, Pennell, DJ, Rumberger, JA, Ryan, T and Verani, MS (2002). Standardized myocardial segmentation and nomenclature for tomographic imaging of the heart: a statement for healthcare professionals from the Cardiac Imaging Committee of the Council on Clinical Cardiology of the American Heart Association. Circulation 105(4): 539-42.

Chen, R, Tsuji, T, Ichida, F, Bowles, KR, Yu, X, Watanabe, S, Hirono, K, Tsubata, S, Hamamichi, Y, Ohta, J, Imai, Y, Bowles, NE, Miyawaki, T and Towbin, JA (2002). Mutation analysis of the G4.5 gene in patients with isolated left ventricular noncompaction. Mol Genet Metab 77(4): 319-25.

Chin, TK, Perloff, JK, Williams, RG, Jue, K and Mohrmann, R (1990). Isolated noncompaction of left ventricular myocardium. A study of eight cases. Circulation 82(2): 507-13.

Chobanian, AV, Bakris, GL, Black, HR, Cushman, WC, Green, LA, Izzo, JL, Jr., Jones, DW, Materson, BJ, Oparil, S, Wright, JT, Jr. and Roccella, EJ (2003). The Seventh Report of the Joint National Committee on Prevention, Detection, Evaluation, and Treatment of High Blood Pressure: the JNC 7 report. Jama 289(19): 2560-72.

Cohn, JN, Ferrari, R and Sharpe, N (2000). Cardiac remodeling--concepts and clinical implications: a consensus paper from an international forum on

cardiac remodeling. Behalf of an International Forum on Cardiac Remodeling. J Am Coll Cardiol 35(3): 569-82.

Conrady, AO, Rudomanov, OG, Zaharov, DV, Krutikov, AN, Vahrameeva, NV, Yakovleva, OI, Alexeeva, NP and Shlyakhto, EV (2004). Prevalence and determinants of left ventricular hypertrophy and remodelling patterns in hypertensive patients: the St. Petersburg study. Blood Press 13(2): 101-9.

Conway, MA, Allis, J, Ouwerkerk, R, Niioka, T, Rajagopalan, B and Radda, GK (1991). Detection of low phosphocreatine to ATP ratio in failing hypertrophied human myocardium by 31P magnetic resonance spectroscopy. Lancet 338(8773): 973-6.

Corrado, D, Basso, C, Schiavon, M and Thiene, G (1998). Screening for hypertrophic cardiomyopathy in young athletes. N Engl J Med 339(6): 364-9.

Crilley, JG, Boehm, EA, Blair, E, Rajagopalan, B, Blamire, AM, Styles, P, McKenna, WJ, Ostman-Smith, I, Clarke, K and Watkins, H (2003). Hypertrophic cardiomyopathy due to sarcomeric gene mutations is characterized by impaired energy metabolism irrespective of the degree of hypertrophy. J Am Coll Cardiol 41(10): 1776-82.

Crilley, JG, Boehm, EA, Rajagopalan, B, Blamire, AM, Styles, P, Muntoni, F, Hilton-Jones, D and Clarke, K (2000). Magnetic resonance spectroscopy evidence of abnormal cardiac energetics in Xp21 muscular dystrophy. J Am Coll Cardiol 36(6): 1953-8.

D'Andrea, A, Caso, P, Sarubbi, B, Limongelli, G, Liccardo, B, Cice, G, D'Andrea, L, Scherillo, M, Cotrufo, M and Calabro, R (2003a). Right ventricular myocardial adaptation to different training protocols in top-level athletes. Echocardiography 20(4): 329-36.

D'Andrea, A, Caso, P, Severino, S, Galderisi, M, Sarubbi, B, Limongelli, G, Cice, G, D'Andrea, L, Scherillo, M, Mininni, N and Calabro, R (2002). Effects of different training protocols on left ventricular myocardial function in competitive athletes: a Doppler tissue imaging study. Ital Heart J 3(1): 34-40.

D'Andrea, A, Caso, P, Severino, S, Sarubbi, B, Forni, A, Cice, G, Esposito, N, Scherillo, M, Cotrufo, M and Calabro, R (2003b). Different involvement of right ventricular myocardial function in either physiologic or pathologic left ventricular hypertrophy: a Doppler tissue study. J Am Soc Echocardiogr 16(2): 154-61.

Devlin, AM and Ostman-Smith, I (2000). Diagnosis of hypertrophic cardiomyopathy and screening for the phenotype suggestive of gene carriage in familial disease: a simple echocardiographic procedure. J Med Screen 7(2): 82-90.

Digilio, MC, Marino, B, Bevilacqua, M, Musolino, AM, Giannotti, A and Dallapiccola, B (1999). Genetic heterogeneity of isolated noncompaction of the left ventricular myocardium. Am J Med Genet 85(1): 90-1.

Doi, YL, McKenna, WJ, Gehrke, J, Oakley, CM and Goodwin, JF (1980). M mode echocardiography in hypertrophic cardiomyopathy: diagnostic criteria and prediction of obstruction. Am J Cardiol 45(1): 6-14.

Douglas, PS and O'Toole, M (1992). Aging and physical activity determine cardiac structure and function in the older athlete. J Appl Physiol 72(5): 1969-73.

Dulce, MC, Mostbeck, GH, Friese, KK, Caputo, GR and Higgins, CB (1993). Quantification of the left ventricular volumes and function with cine MR imaging: comparison of geometric models with three-dimensional data. Radiology 188(2): 371-6.

Dusek, J, Ostadal, B and Duskova, M (1975). Postnatal persistence of spongy myocardium with embryonic blood supply. Arch Pathol 99(6): 312-7.

Elster, AD and Burdette, JH (2001). Questions and answers in magnetic resonance imaging. St. Louis, Mosby.

Feldt, RH, Rahimtoola, SH, Davis, GD, Swan, HJ and Titus, JL (1969). Anomalous ventricular myocardial patterns in a child with complex congenital heart disease. Am J Cardiol 23(5): 732-4.

Finsterer, J, Stollberger, C and Feichtinger, H (2002). Histological appearance of left ventricular hypertrabeculation/noncompaction. Cardiology 98(3): 162-4.

Finsterer, J, Stollberger, C and Feichtinger, H (2003a). Non-compaction on echocardiography and autopsy. Acta Cardiol 58(2): 165-8.

Finsterer, J, Stollberger, C and Kopsa, W (2003b). Noncompaction on cardiac MRI in a patient with nail-patella syndrome and mitochondriopathy. Cardiology 100(1): 48-9.

Finsterer, J, Stollberger, C, Wegmann, R, Jarius, C and Janssen, B (2001). Left ventricular hypertrabeculation in myotonic dystrophy type 1. Herz 26(4): 287-90.

Frey, N, McKinsey, TA and Olson, EN (2000). Decoding calcium signals involved in cardiac growth and function. Nat Med 6(11): 1221-7.

Frey, N and Olson, EN (2003). Cardiac hypertrophy: the good, the bad, and the ugly. Annu Rev Physiol 65: 45-79.

Galiuto, L, Ignone, G and DeMaria, AN (1998). Contraction and relaxation velocities of the normal left ventricle using pulsed-wave tissue Doppler echocardiography. Am J Cardiol 81(5): 609-14.

Gardin, JM, Savage, DD, Ware, JH and Henry, WL (1987). Effect of age, sex, and body surface area on echocardiographic left ventricular wall mass in normal subjects. Hypertension 9(2 Pt 2): II36-9.

Garlick, PB, Radda, GK and Seeley, PJ (1977). Phosphorus NMR studies on perfused heart. Biochem Biophys Res Commun 74(3): 1256-62.

Garot, J, Bluemke, DA, Osman, NF, Rochitte, CE, McVeigh, ER, Zerhouni, EA, Prince, JL and Lima, JA (2000). Fast determination of regional myocardial strain fields from tagged cardiac images using harmonic phase MRI. Circulation 101(9): 981-8.

Grothues, F, Moon, JC, Bellenger, NG, Smith, GS, Klein, HU and Pennell, DJ (2004). Interstudy reproducibility of right ventricular volumes, function, and mass with cardiovascular magnetic resonance. Am Heart J 147(2): 218-23.

Grothues, F, Smith, GC, Moon, JC, Bellenger, NG, Collins, P, Klein, HU and Pennell, DJ (2002). Comparison of interstudy reproducibility of cardiovascular magnetic resonance with two-dimensional echocardiography in normal subjects and in patients with heart failure or left ventricular hypertrophy. Am J Cardiol 90(1): 29-34.

Hashimoto, I, Li, X, Hejmadi Bhat, A, Jones, M, Zetts, AD and Sahn, DJ (2003). Myocardial strain rate is a superior method for evaluation of left ventricular subendocardial function compared with tissue Doppler imaging. J Am Coll Cardiol 42(9): 1574-83.

Hayward, CS, Kelly, RP and Collins, P (2000). The roles of gender, the menopause and hormone replacement on cardiovascular function. Cardiovasc Res 46(1): 28-49.

Hennig, J, Markl, M, Schneider, B and Peschl, S (1998a). Regional myocardial function with tissue phase mapping. Magma 6(2-3): 145-6.

Hennig, J, Schneider, B, Peschl, S, Markl, M, Krause, T and Laubenberger, J (1998b). Analysis of myocardial motion based on velocity measurements with a black blood prepared segmented gradient-echo sequence: methodology and applications to normal volunteers and patients. J Magn Reson Imaging 8(4): 868-77.

Henry, WL, Gardin, JM and Ware, JH (1980). Echocardiographic measurements in normal subjects from infancy to old age. Circulation 62(5): 1054-61.

Henson, RE, Song, SK, Pastorek, JS, Ackerman, JJ and Lorenz, CH (2000). Left ventricular torsion is equal in mice and humans. Am J Physiol Heart Circ Physiol 278(4): H1117-23.

Hermida-Prieto, M, Monserrat, L, Castro-Beiras, A, Laredo, R, Soler, R, Peteiro, J, Rodriguez, E, Bouzas, B, Alvarez, N, Muniz, J and Crespo-Leiro, M (2004). Familial dilated cardiomyopathy and isolated left ventricular noncompaction associated with lamin A/C gene mutations. Am J Cardiol 94(1): 50-4.

Hoogsteen, J, Hoogeveen, A, Schaffers, H, Wijn, PF and van der Wall, EE (2003). Left atrial and ventricular dimensions in highly trained cyclists. Int J Cardiovasc Imaging 19(3): 211-7.

Hoogsteen, J, Hoogeveen, A, Schaffers, H, Wijn, PF, van Hemel, NM and van der Wall, EE (2004). Myocardial adaptation in different endurance sports: an echocardiographic study. Int J Cardiovasc Imaging 20(1): 19-26.

Ichida, F, Hamamichi, Y, Miyawaki, T, Ono, Y, Kamiya, T, Akagi, T, Hamada, H, Hirose, O, Isobe, T, Yamada, K, Kurotobi, S, Mito, H, Miyake, T, Murakami, Y, Nishi, T, Shinohara, M, Seguchi, M, Tashiro, S and Tomimatsu, H (1999). Clinical features of isolated noncompaction of the ventricular myocardium: long-term clinical course, hemodynamic properties, and genetic background. J Am Coll Cardiol 34(1): 233-40.

Ichida, F, Tsubata, S, Bowles, KR, Haneda, N, Uese, K, Miyawaki, T, Dreyer, WJ, Messina, J, Li, H, Bowles, NE and Towbin, JA (2001). Novel gene mutations in patients with left ventricular noncompaction or Barth syndrome. Circulation 103(9): 1256-63.

Ino, T, Yabuta, K and Yamauchi, K (1993). Heart disease screening in Japanese children. Bmj 306(6885): 1128.

Jacobus, WE, Taylor, GJt, Hollis, DP and Nunnally, RL (1977). Phosphorus nuclear magnetic resonance of perfused working rat hearts. Nature 265(5596): 756-8.

Javadpour, MM, Tardiff, JC, Pinz, I and Ingwall, JS (2003). Decreased energetics in murine hearts bearing the R92Q mutation in cardiac troponin T. J Clin Invest 112(5): 768-75.

Jenni, R, Oechslin, E, Schneider, J, Jost, CA and Kaufmann, PA (2001). Echocardiographic and pathoanatomical characteristics of isolated left ventricular non-compaction: a step towards classification as a distinct cardiomyopathy. Heart 86(6): 666-71.

Jenni, R, Rojas, J and Oechslin, E (1999). Isolated noncompaction of the myocardium. N Engl J Med 340(12): 966-7.

Jung, WI, Sieverding, L, Breuer, J, Hoess, T, Widmaier, S, Schmidt, O, Bunse, M, van Erckelens, F, Apitz, J, Lutz, O and Dietze, GJ (1998). 31P NMR spectroscopy detects metabolic abnormalities in asymptomatic patients with hypertrophic cardiomyopathy. Circulation 97(25): 2536-42.

Jungblut, PR, Osborne, JA, Quigg, RJ, McNeal, MA, Clauser, J, Muster, AJ and McPherson, DD (2000). Echocardiographic Doppler evaluation of left ventricular diastolic filling in older, highly trained male endurance athletes. Echocardiography 17(1): 7-16.

Kansal, S, Roitman, D and Sheffield, LT (1979). Interventricular septal thickness and left ventricular hypertrophy. An echocardiographic study. Circulation 60(5): 1058-65.

Karjalainen, J, Kujala, UM, Stolt, A, Mantysaari, M, Viitasalo, M, Kainulainen, K and Kontula, K (1999). Angiotensinogen gene M235T polymorphism predicts left ventricular hypertrophy in endurance athletes. J Am Coll Cardiol 34(2): 494-9.

Karwatowski, SP, Mohiaddin, R, Yang, GZ, Firmin, DN, Sutton, MS, Underwood, SR and Longmore, DB (1994a). Assessment of regional left ventricular long-axis motion with MR velocity mapping in healthy subjects. J Magn Reson Imaging 4(2): 151-5.

Karwatowski, SP, Mohiaddin, RH, Yang, GZ, Firmin, DN, St John Sutton, M and Underwood, SR (1994b). Regional myocardial velocity imaged by magnetic resonance in patients with ischaemic heart disease. Br Heart J 72(4): 332-8.

Kenton, AB, Sanchez, X, Coveler, KJ, Makar, KA, Jimenez, S, Ichida, F, Murphy, RT, Elliott, PM, McKenna, W, Bowles, NE, Towbin, JA and Bowles, KR (2004). Isolated left ventricular noncompaction is rarely caused by mutations in G4.5, alpha-dystrobrevin and FK Binding Protein-12. Mol Genet Metab 82(2): 162-6.

Kim, D, Gilson, WD, Kramer, CM and Epstein, FH (2004). Myocardial tissue tracking with two-dimensional cine displacement-encoded MR imaging: development and initial evaluation. Radiology 230(3): 862-71.

Koo, BK, Choi, D, Ha, JW, Kang, SM, Chung, N and Cho, SY (2002). Isolated noncompaction of the ventricular myocardium: contrast echocardiographic findings and review of the literature. Echocardiography 19(2): 153-6.

Kukulski, T, Jamal, F, D'Hooge, J, Bijnens, B, De Scheerder, I and Sutherland, GR (2002). Acute changes in systolic and diastolic events during clinical coronary angioplasty: a comparison of regional velocity, strain rate, and strain measurement. J Am Soc Echocardiogr 15(1): 1-12.

Lai, ZY, Chang, NC, Tsai, MC, Lin, CS, Chang, SH and Wang, TC (1998). Left ventricular filling profiles and angiotensin system activity in elite baseball players. Int J Cardiol 67(2): 155-60.

Lamb, HJ, Beyerbacht, HP, van der Laarse, A, Stoel, BC, Doornbos, J, van der Wall, EE and de Roos, A (1999). Diastolic dysfunction in hypertensive heart disease is associated with altered myocardial metabolism. Circulation 99(17): 2261-7.

Lauterbur, P (1973). Image formation by induced local interactions: examples employing nuclear magnetic reosnance. Nature 242: 190-191.

Lewis, JF, Spirito, P, Pelliccia, A and Maron, BJ (1992). Usefulness of Doppler echocardiographic assessment of diastolic filling in distinguishing "athlete's heart" from hypertrophic cardiomyopathy. Br Heart J 68(3): 296-300.

Lorenz, CH, Walker, ES, Morgan, VL, Klein, SS and Graham, TP, Jr. (1999). Normal human right and left ventricular mass, systolic function, and gender

differences by cine magnetic resonance imaging. J Cardiovasc Magn Reson 1(1): 7-21.

Maier, SE, Fischer, SE, McKinnon, GC, Hess, OM, Krayenbuehl, HP and Boesiger, P (1992). Evaluation of left ventricular segmental wall motion in hypertrophic cardiomyopathy with myocardial tagging. Circulation 86(6): 1919-28.

Marcus, ML, Doty, DB, Hiratzka, LF, Wright, CB and Eastham, CL (1982). Decreased coronary reserve: a mechanism for angina pectoris in patients with aortic stenosis and normal coronary arteries. N Engl J Med 307(22): 1362-6.

Markl, M and Hennig, J (2001). Phase contrast MRI with improved temporal resolution by view sharing: k-space related velocity mapping properties. Magn Reson Imaging 19(5): 669-76.

Markl, M, Schneider, B and Hennig, J (2002). Fast phase contrast cardiac magnetic resonance imaging: Improved assessment and analysis of left ventricular wall motion. J Magn Reson Imaging 15(6): 642-53.

Markl, M, Schneider, B, Hennig, J, Peschl, S, Winterer, J, Krause, T and Laubenberger, J (1999). Cardiac phase contrast gradient echo MRI: measurement of myocardial wall motion in healthy volunteers and patients. Int J Card Imaging 15(6): 441-52.

Maron, BJ (2003). Sudden death in young athletes. N Engl J Med 349(11): 1064-75.

Maron, BJ, Epstein, SE and Roberts, WC (1986). Causes of sudden death in competitive athletes. J Am Coll Cardiol 7(1): 204-14.

Maron, BJ, McKenna, WJ, Danielson, GK, Kappenberger, LJ, Kuhn, HJ, Seidman, CE, Shah, PM, Spencer, WH, 3rd, Spirito, P, Ten Cate, FJ, Wigle, ED, Vogel, RA, Abrams, J, Bates, ER, Brodie, BR, Danias, PG, Gregoratos, G, Hlatky, MA, Hochman, JS, Kaul, S, Lichtenberg, RC, Lindner, JR, O'Rourke, RA, Pohost, GM, Schofield, RS, Tracy, CM, Winters, WL, Jr., Klein, WW, Priori, SG, Alonso-Garcia, A, Blomstrom-Lundqvist, C, De Backer, G, Deckers, J, Flather, M, Hradec, J, Oto, A, Parkhomenko, A, Silber, S and Torbicki, A (2003). American College of Cardiology/European Society of Cardiology Clinical Expert Consensus Document on Hypertrophic Cardiomyopathy. A report of the American College of Cardiology Foundation Task Force on Clinical Expert Consensus Documents and the European Society of Cardiology Committee for Practice Guidelines. Eur Heart J 24(21): 1965-91.

Maron, BJ, Pelliccia, A, Spataro, A and Granata, M (1993). Reduction in left ventricular wall thickness after deconditioning in highly trained Olympic athletes. Br Heart J 69(2): 125-8.

Maron, BJ, Pelliccia, A and Spirito, P (1995). Cardiac disease in young trained athletes. Insights into methods for distinguishing athlete's heart from

structural heart disease, with particular emphasis on hypertrophic cardiomyopathy. Circulation 91(5): 1596-601.

Maron, BJ, Roberts, WC, McAllister, HA, Rosing, DR and Epstein, SE (1980). Sudden death in young athletes. Circulation 62(2): 218-29.

Maron, BJ, Shirani, J, Poliac, LC, Mathenge, R, Roberts, WC and Mueller, FO (1996). Sudden death in young competitive athletes. Clinical, demographic, and pathological profiles. Jama 276(3): 199-204.

Marsh, JD, Lehmann, MH, Ritchie, RH, Gwathmey, JK, Green, GE and Schiebinger, RJ (1998). Androgen receptors mediate hypertrophy in cardiac myocytes. Circulation 98(3): 256-61.

Martin, WH, 3rd, Coyle, EF, Bloomfield, SA and Ehsani, AA (1986). Effects of physical deconditioning after intense endurance training on left ventricular dimensions and stroke volume. J Am Coll Cardiol 7(5): 982-9.

Matsuda, M, Tsukahara, M, Kondoh, O and Mito, H (1999). Familial isolated noncompaction of ventricular myocardium. J Hum Genet 44(2): 126-8.

Matsuoka, H, Hamada, M, Honda, T, Kobayashi, T, Suzuki, M, Ohtani, T, Takezaki, M, Abe, M, Fujiwara, Y, Sumimoto, T and et al. (1993). Measurement of cardiac chamber volumes by cine magnetic resonance imaging. Angiology 44(4): 321-7.

Mazur, W and Nagueh, SF (2001). Myocardial viability: recent developments in detection and clinical significance. Curr Opin Cardiol 16(5): 277-81.

McMullen, JR, Shioi, T, Zhang, L, Tarnavski, O, Sherwood, MC, Kang, PM and Izumo, S (2003). Phosphoinositide 3-kinase(p110alpha) plays a critical role for the induction of physiological, but not pathological, cardiac hypertrophy. Proc Natl Acad Sci U S A 100(21): 12355-60.

McVeigh, ER and Atalar, E (1992). Cardiac tagging with breath-hold cine MRI. Magn Reson Med 28(2): 318-27.

Michel, RS, Carpenter, MA and Lovell, MA (1998). Pathological case of the month. Noncompaction of the left ventricular myocardium. Arch Pediatr Adolesc Med 152(7): 709-10.

Montgomery, DE, Tardiff, JC and Chandra, M (2001). Cardiac troponin T mutations: correlation between the type of mutation and the nature of myofilament dysfunction in transgenic mice. J Physiol 536(Pt 2): 583-92.

Montgomery, HE, Clarkson, P, Dollery, CM, Prasad, K, Losi, MA, Hemingway, H, Statters, D, Jubb, M, Girvain, M, Varnava, A, World, M, Deanfield, J, Talmud, P, McEwan, JR, McKenna, WJ and Humphries, S (1997). Association of angiotensin-converting enzyme gene I/D polymorphism with change in left ventricular mass in response to physical training. Circulation 96(3): 741-7.

Moon, JC, Fisher, NG, McKenna, WJ and Pennell, DJ (2004). Detection of apical hypertrophic cardiomyopathy by cardiovascular magnetic resonance in patients with non-diagnostic echocardiography. Heart 90(6): 645-9.

Moon, JC, Lorenz, CH, Francis, JM, Smith, GC and Pennell, DJ (2002). Breath-hold FLASH and FISP cardiovascular MR imaging: left ventricular volume differences and reproducibility. Radiology 223(3): 789-97.

Moore, CC, Lugo-Olivieri, CH, McVeigh, ER and Zerhouni, EA (2000). Three-dimensional systolic strain patterns in the normal human left ventricle: characterization with tagged MR imaging. Radiology 214(2): 453-66.

Morganroth, J, Maron, BJ, Henry, WL and Epstein, SE (1975). Comparative left ventricular dimensions in trained athletes. Ann Intern Med 82(4): 521-4.

Nagel, E, Lehmkuhl, HB, Bocksch, W, Klein, C, Vogel, U, Frantz, E, Ellmer, A, Dreysse, S and Fleck, E (1999). Noninvasive diagnosis of ischemia-induced wall motion abnormalities with the use of high-dose dobutamine stress MRI: comparison with dobutamine stress echocardiography. Circulation 99(6): 763-70.

Nahrendorf, M, Frantz, S, Hu, K, von zur Muhlen, C, Tomaszewski, M, Scheuermann, H, Kaiser, R, Jazbutyte, V, Beer, S, Bauer, W, Neubauer, S, Ertl, G, Allolio, B and Callies, F (2003). Effect of testosterone on post-myocardial infarction remodeling and function. Cardiovasc Res 57(2): 370-8.

Neubauer, S (2003). Cardiac magnetic resonance spectroscopy. Curr Cardiol Rep 5(1): 75-82.

Neubauer, S and Clarke, K (2003). Cardiac energy metabolism in heart failure. Cardiac Metabolism and ischemic cardiomyopathy. M. Marber. Puteaux, Wolters Kluwer Health**:** 45-61.

Neubauer, S, Horn, M, Cramer, M, Harre, K, Newell, JB, Peters, W, Pabst, T, Ertl, G, Hahn, D, Ingwall, JS and Kochsiek, K (1997a). Myocardial phosphocreatine-to-ATP ratio is a predictor of mortality in patients with dilated cardiomyopathy. Circulation 96(7): 2190-6.

Neubauer, S, Horn, M, Pabst, T, Harre, K, Stromer, H, Bertsch, G, Sandstede, J, Ertl, G, Hahn, D and Kochsiek, K (1997b). Cardiac high-energy phosphate metabolism in patients with aortic valve disease assessed by 31P-magnetic resonance spectroscopy. J Investig Med 45(8): 453-62.

Neubauer, S, Krahe, T, Schindler, R, Horn, M, Hillenbrand, H, Entzeroth, C, Mader, H, Kromer, EP, Riegger, GA, Lackner, K and et al. (1992). 31P magnetic resonance spectroscopy in dilated cardiomyopathy and coronary artery disease. Altered cardiac high-energy phosphate metabolism in heart failure. Circulation 86(6): 1810-8.

Neudorf, UE, Hussein, A, Trowitzsch, E and Schmaltz, AA (2001). Clinical features of isolated noncompaction of the myocardium in children. Cardiol Young 11(4): 439-42.

Neustein, HB, Lurie, PR, Dahms, B and Takahashi, M (1979). An X-linked recessive cardiomyopathy with abnormal mitochondria. Pediatrics 64(1): 24-9.

Oechslin, E and Jenni, R (2002). Isolated left ventricular non-compaction: increasing recognition of this distinct, yet 'unclassified' cardiomyopathy. Eur J Echocardiogr 3(4): 250-1.

Oechslin, EN, Attenhofer Jost, CH, Rojas, JR, Kaufmann, PA and Jenni, R (2000). Long-term follow-up of 34 adults with isolated left ventricular noncompaction: a distinct cardiomyopathy with poor prognosis. J Am Coll Cardiol 36(2): 493-500.

Okada, M, Mitsunami, K, Inubushi, T and Kinoshita, M (1998). Influence of aging or left ventricular hypertrophy on the human heart: contents of phosphorus metabolites measured by 31P MRS. Magn Reson Med 39(5): 772-82.

Olivetti, G, Giordano, G, Corradi, D, Melissari, M, Lagrasta, C, Gambert, SR and Anversa, P (1995). Gender differences and aging: effects on the human heart. J Am Coll Cardiol 26(4): 1068-79.

Osman, NF, Kerwin, WS, McVeigh, ER and Prince, JL (1999). Cardiac motion tracking using CINE harmonic phase (HARP) magnetic resonance imaging. Magn Reson Med 42(6): 1048-60.

Ostman-Smith, I (1981). Cardiac sympathetic nerves as the final common pathway in the induction of adaptive cardiac hypertrophy. Clin Sci (Lond) 61(3): 265-72.

Ostman-Smith, I and Devlin, AM (2001). A simple method for assessing the regression or progression of ventricular hypertrophy in the growing child and adult: the value of left ventricular wall-to-cavity ratios. Eur J Echocardiogr 2(1): 22-30.

Palazzuoli, A, Puccetti, L, Bruni, F, Pasqui, AL and Auteri, A (2001). Diastolic filling in hypertrophied hearts of elite runners: an echo-Doppler study. Eur Rev Med Pharmacol Sci 5(2): 65-9.

Pauli, RM, Scheib-Wixted, S, Cripe, L, Izumo, S and Sekhon, GS (1999). Ventricular noncompaction and distal chromosome 5q deletion. Am J Med Genet 85(4): 419-23.

Pedram, A, Razandi, M, Aitkenhead, M and Levin, ER (2005). Estrogen inhibits cardiomyocyte hypertrophy in-vitro: Antagonism of calcineurin-related hypertrophy through induction of MCIP1. J Biol Chem.

Pelc, LR, Sayre, J, Yun, K, Castro, LJ, Herfkens, RJ, Miller, DC and Pelc, NJ (1994). Evaluation of myocardial motion tracking with cine-phase contrast magnetic resonance imaging. Invest Radiol 29(12): 1038-42.

Pellerin, D, Sharma, R, Elliott, P and Veyrat, C (2003). Tissue Doppler, strain, and strain rate echocardiography for the assessment of left and right systolic ventricular function. Heart 89 Suppl 3: iii9-17.

Pelliccia, A, Culasso, F, Di Paolo, FM and Maron, BJ (1999). Physiologic left ventricular cavity dilatation in elite athletes. Ann Intern Med 130(1): 23-31.

Pelliccia, A, Maron, BJ, Culasso, F, Spataro, A and Caselli, G (1996). Athlete's heart in women. Echocardiographic characterization of highly trained elite female athletes. Jama 276(3): 211-5.

Pelliccia, A, Maron, BJ, De Luca, R, Di Paolo, FM, Spataro, A and Culasso, F (2002). Remodeling of left ventricular hypertrophy in elite athletes after long-term deconditioning. Circulation 105(8): 944-9.

Pelliccia, A, Maron, BJ, Spataro, A, Proschan, MA and Spirito, P (1991). The upper limit of physiologic cardiac hypertrophy in highly trained elite athletes. N Engl J Med 324(5): 295-301.

Pennell, DJ (2003). Cardiovascular magnetic resonance: twenty-first century solutions in cardiology. Clin Med 3(3): 273-8.

Perings, SM, Schulze, K, Decking, U, Kelm, M and Strauer, BE (2000). Age-related decline of PCr/ATP-ratio in progressively hypertrophied hearts of spontaneously hypertensive rats. Heart Vessels 15(4): 197-202.

Petersen, SE, Selvanayagam, JB, Wiesmann, F, Robson, MD, Francis, JM, Anderson, RH, Watkins, H and Neubauer, S (2005). Left ventricular non-compaction: insights from cardiovascular magnetic resonance imaging. J Am Coll Cardiol 46(1): 101-5.

Pines, A, Fisman, EZ, Shemesh, J, Levo, Y, Ayalon, D, Kellermann, JJ, Motro, M and Drory, Y (1992). Menopause-related changes in left ventricular function in healthy women. Cardiology 80(5-6): 413-6.

Pluim, BM, Chin, JC, De Roos, A, Doornbos, J, Siebelink, HM, Van der Laarse, A, Vliegen, HW, Lamerichs, RM, Bruschke, AV and Van der Wall, EE (1996). Cardiac anatomy, function and metabolism in elite cyclists assessed by magnetic resonance imaging and spectroscopy. Eur Heart J 17(8): 1271-8.

Pluim, BM, Lamb, HJ, Kayser, HW, Leujes, F, Beyerbacht, HP, Zwinderman, AH, van der Laarse, A, Vliegen, HW, de Roos, A and van der Wall, EE (1998). Functional and metabolic evaluation of the athlete's heart by magnetic resonance imaging and dobutamine stress magnetic resonance spectroscopy. Circulation 97(7): 666-72.

Pluim, BM, Zwinderman, AH, van der Laarse, A and van der Wall, EE (2000). The athlete's heart. A meta-analysis of cardiac structure and function. Circulation 101(3): 336-44.

Pohmann, R and von Kienlin, M (2001). Accurate phosphorus metabolite images of the human heart by 3D acquisition-weighted CSI. Magn Reson Med 45(5): 817-26.

Purcell, E, Torrey, H and Pound, R (1946). Resonance adsorption by nuclear magnetic moments in a solid. Physical Review (Physics): 37-38.

Rademakers, FE, Rogers, WJ, Guier, WH, Hutchins, GM, Siu, CO, Weisfeldt, ML, Weiss, JL and Shapiro, EP (1994). Relation of regional cross-fiber shortening to wall thickening in the intact heart. Three-dimensional strain analysis by NMR tagging. Circulation 89(3): 1174-82.

Redwood, CS, Moolman-Smook, JC and Watkins, H (1999). Properties of mutant contractile proteins that cause hypertrophic cardiomyopathy. Cardiovasc Res 44(1): 20-36.

Reichek, N (1999). MRI myocardial tagging. J Magn Reson Imaging 10(5): 609-16.

Richardson, P, McKenna, W, Bristow, M, Maisch, B, Mautner, B, O'Connell, J, Olsen, E, Thiene, G, Goodwin, J, Gyarfas, I, Martin, I and Nordet, P (1996). Report of the 1995 World Health Organization/International Society and Federation of Cardiology Task Force on the Definition and Classification of cardiomyopathies. Circulation 93(5): 841-2.

Ritter, M, Oechslin, E, Sutsch, G, Attenhofer, C, Schneider, J and Jenni, R (1997). Isolated noncompaction of the myocardium in adults. Mayo Clin Proc 72(1): 26-31.

Rominger, MB, Bachmann, GF, Geuer, M, Puzik, M, Boedeker, RH, Ricken, WW and Rau, WS (1999). [Accuracy of right and left ventricular heart volume and left ventricular muscle mass determination with cine MRI in breath holding technique]. Rofo 170(1): 54-60.

Rost, R and Hollmann, W (1983). Athlete's heart--a review of its historical assessment and new aspects. Int J Sports Med 4(3): 147-65.

Rushmer, RF, Crystal, DK and Wagner, C (1953). The functional anatomy of ventricular contraction. Circ Res 1(2): 162-70.

Sandstede, J, Lipke, C, Beer, M, Hofmann, S, Pabst, T, Kenn, W, Neubauer, S and Hahn, D (2000). Age- and gender-specific differences in left and right ventricular cardiac function and mass determined by cine magnetic resonance imaging. Eur Radiol 10(3): 438-42.

Sasse-Klaassen, S, Gerull, B, Oechslin, E, Jenni, R and Thierfelder, L (2003). Isolated noncompaction of the left ventricular myocardium in the adult is an autosomal dominant disorder in the majority of patients. Am J Med Genet 119A(2): 162-7.

Sasse-Klaassen, S, Probst, S, Gerull, B, Oechslin, E, Nurnberg, P, Heuser, A, Jenni, R, Hennies, HC and Thierfelder, L (2004). Novel gene locus for

autosomal dominant left ventricular noncompaction maps to chromosome 11p15. Circulation 109(22): 2720-3.

Schaible, TF and Scheuer, J (1984). Comparison of heart function in male and female rats. Basic Res Cardiol 79(4): 402-12.

Scharhag, J, Schneider, G, Urhausen, A, Rochette, V, Kramann, B and Kindermann, W (2002). Athlete's heart: right and left ventricular mass and function in male endurance athletes and untrained individuals determined by magnetic resonance imaging. J Am Coll Cardiol 40(10): 1856-63.

Scheuermann-Freestone, M, Madsen, PL, Manners, D, Blamire, AM, Buckingham, RE, Styles, P, Radda, GK, Neubauer, S and Clarke, K (2003). Abnormal cardiac and skeletal muscle energy metabolism in patients with type 2 diabetes. Circulation 107(24): 3040-6.

Sedmera, D, Pexieder, T, Vuillemin, M, Thompson, RP and Anderson, RH (2000). Developmental patterning of the myocardium. Anat Rec 258(4): 319-37.

Seidman, JG and Seidman, C (2001). The genetic basis for cardiomyopathy: from mutation identification to mechanistic paradigms. Cell 104(4): 557-67.

Sharma, S, Elliott, P, Whyte, G, Jones, S, Mahon, N, Whipp, B and McKenna, WJ (2000). Utility of cardiopulmonary exercise in the assessment of clinical determinants of functional capacity in hypertrophic cardiomyopathy. Am J Cardiol 86(2): 162-8.

Shou, W, Aghdasi, B, Armstrong, DL, Guo, Q, Bao, S, Charng, MJ, Mathews, LM, Schneider, MD, Hamilton, SL and Matzuk, MM (1998). Cardiac defects and altered ryanodine receptor function in mice lacking FKBP12. Nature 391(6666): 489-92.

Sievers, B, Kirchberg, S, Addo, M, Bakan, A, Brandts, B and Trappe, HJ (2004). Assessment of left atrial volumes in sinus rhythm and atrial fibrillation using the biplane area-length method and cardiovascular magnetic resonance imaging with TrueFISP. J Cardiovasc Magn Reson 6(4): 855-63.

Silver, M (1991). Cardiovascular Pathology. New York, NY, Churchill Livingstone.

Simpson, IA (1997). Echocardiographic assessment of long axis function: a simple solution to a complex problem? Heart 78(3): 211-2.

Skavdahl, M, Steenbergen, C, Clark, J, Myers, P, Demianenko, T, Mao, L, Rockman, HA, Korach, KS and Murphy, E (2005). Estrogen receptor-beta mediates male-female differences in the development of pressure overload hypertrophy. Am J Physiol Heart Circ Physiol 288(2): H469-76.

Spencer, RG, Buttrick, PM and Ingwall, JS (1997). Function and bioenergetics in isolated perfused trained rat hearts. Am J Physiol 272(1 Pt 2): H409-17.

Spindler, M, Saupe, KW, Christe, ME, Sweeney, HL, Seidman, CE, Seidman, JG and Ingwall, JS (1998). Diastolic dysfunction and altered energetics in the alphaMHC403/+ mouse model of familial hypertrophic cardiomyopathy. J Clin Invest 101(8): 1775-83.

Spirito, P, Seidman, CE, McKenna, WJ and Maron, BJ (1997). The management of hypertrophic cardiomyopathy. N Engl J Med 336(11): 775-85.

Steinacker, JM, Laske, R, Hetzel, WD, Lormes, W, Liu, Y and Stauch, M (1993). Metabolic and hormonal reactions during training in junior oarsmen. Int J Sports Med 14 Suppl 1: S24-8.

Steiner, I, Hrubecky, J, Pleskot, J and Kokstejn, Z (1996). Persistence of spongy myocardium with embryonic blood supply in an adult. Cardiovasc Pathol 5: 47-53.

Stollberger, C and Finsterer, J (2004). Left ventricular hypertrabeculation/noncompaction. J Am Soc Echocardiogr 17(1): 91-100.

Stollberger, C, Finsterer, J and Blazek, G (2002). Left ventricular hypertrabeculation/noncompaction and association with additional cardiac abnormalities and neuromuscular disorders. Am J Cardiol 90(8): 899-902.

Stollberger, C, Finsterer, J, Blazek, G and Bittner, RE (1996). Left ventricular non-compaction in a patient with becker's muscular dystrophy. Heart 76(4): 380.

Sweeney, HL, Feng, HS, Yang, Z and Watkins, H (1998). Functional analyses of troponin T mutations that cause hypertrophic cardiomyopathy: insights into disease pathogenesis and troponin function. Proc Natl Acad Sci U S A 95(24): 14406-10.

Thierfelder, L, Watkins, H, MacRae, C, Lamas, R, McKenna, W, Vosberg, HP, Seidman, JG and Seidman, CE (1994). Alpha-tropomyosin and cardiac troponin T mutations cause familial hypertrophic cardiomyopathy: a disease of the sarcomere. Cell 77(5): 701-12.

Torrent-Guasp, FF, Whimster, WF and Redmann, K (1997). A silicone rubber mould of the heart. Technol Health Care 5(1-2): 13-20.

Urheim, S, Edvardsen, T, Torp, H, Angelsen, B and Smiseth, OA (2000). Myocardial strain by Doppler echocardiography. Validation of a new method to quantify regional myocardial function. Circulation 102(10): 1158-64.

Uusitalo, AL, Huttunen, P, Hanin, Y, Uusitalo, AJ and Rusko, HK (1998). Hormonal responses to endurance training and overtraining in female athletes. Clin J Sport Med 8(3): 178-86.

Varani, E, Rapezzi, C, Binetti, G, Ferlito, M, Maiello, L, Tartagni, F, Bacchi Reggiani, ML, Ortolani, P and Magnani, B (1989). [Analysis of the diastolic function of the left ventricle by Doppler echocardiography in athletes engaged in competitive sports activities]. Cardiologia 34(10): 855-60.

Vatta, M, Mohapatra, B, Jimenez, S, Sanchez, X, Faulkner, G, Perles, Z, Sinagra, G, Lin, JH, Vu, TM, Zhou, Q, Bowles, KR, Di Lenarda, A, Schimmenti, L, Fox, M, Chrisco, MA, Murphy, RT, McKenna, W, Elliott, P, Bowles, NE, Chen, J, Valle, G and Towbin, JA (2003). Mutations in Cypher/ZASP in patients with dilated cardiomyopathy and left ventricular non-compaction. J Am Coll Cardiol 42(11): 2014-27.

Verdecchia, P, Angeli, F, Borgioni, C, Gattobigio, R, de Simone, G, Devereux, RB and Porcellati, C (2003). Changes in cardiovascular risk by reduction of left ventricular mass in hypertension: a meta-analysis. Am J Hypertens 16(11 Pt 1): 895-9.

Victor, S, Nayak, VM and Rajasingh, R (1999). Evolution of the ventricles. Tex Heart Inst J 26(3): 168-75; discussion 175-6.

Voigt, JU, Arnold, MF, Karlsson, M, Hubbert, L, Kukulski, T, Hatle, L and Sutherland, GR (2000). Assessment of regional longitudinal myocardial strain rate derived from doppler myocardial imaging indexes in normal and infarcted myocardium. J Am Soc Echocardiogr 13(6): 588-98.

Voigt, JU and Flachskampf, FA (2004). Strain and strain rate. New and clinically relevant echo parameters of regional myocardial function. Z Kardiol 93(4): 249-58.

Wald, R, Veldtman, G, Golding, F, Kirsh, J, McCrindle, B and Benson, L (2004). Determinants of outcome in isolated ventricular noncompaction in childhood. Am J Cardiol 94(12): 1581-4.

Watkins, H, McKenna, WJ, Thierfelder, L, Suk, HJ, Anan, R, O'Donoghue, A, Spirito, P, Matsumori, A, Moravec, CS, Seidman, JG and et al. (1995). Mutations in the genes for cardiac troponin T and alpha-tropomyosin in hypertrophic cardiomyopathy. N Engl J Med 332(16): 1058-64.

Weiford, BC, Subbarao, VD and Mulhern, KM (2004). Noncompaction of the ventricular myocardium. Circulation 109(24): 2965-71.

Weiss, F, Habermann, CR, Lilje, C, Razek, W, Sievers, J, Weil, J and Adam, G (2003). [MRI in the diagnosis of non-compacted ventricular myocardium (NCVM) compared to echocardiography]. Rofo Fortschr Geb Rontgenstr Neuen Bildgeb Verfahr 175(9): 1214-9.

Wexler, LF, Lorell, BH, Momomura, S, Weinberg, EO, Ingwall, JS and Apstein, CS (1988). Enhanced sensitivity to hypoxia-induced diastolic dysfunction in pressure-overload left ventricular hypertrophy in the rat: role of high-energy phosphate depletion. Circ Res 62(4): 766-75.

Whyte, GP, George, K, Nevill, A, Shave, R, Sharma, S and McKenna, WJ (2004a). Left ventricular morphology and function in female athletes: a meta-analysis. Int J Sports Med 25(5): 380-3.

Whyte, GP, George, K, Sharma, S, Firoozi, S, Stephens, N, Senior, R and McKenna, WJ (2004b). The upper limit of physiological cardiac hypertrophy in elite male and female athletes: the British experience. Eur J Appl Physiol.

Wilkins, BJ, Dai, YS, Bueno, OF, Parsons, SA, Xu, J, Plank, DM, Jones, F, Kimball, TR and Molkentin, JD (2004). Calcineurin/NFAT coupling participates in pathological, but not physiological, cardiac hypertrophy. Circ Res 94(1): 110-8.

Xin, HB, Senbonmatsu, T, Cheng, DS, Wang, YX, Copello, JA, Ji, GJ, Collier, ML, Deng, KY, Jeyakumar, LH, Magnuson, MA, Inagami, T, Kotlikoff, MI and Fleischer, S (2002). Oestrogen protects FKBP12.6 null mice from cardiac hypertrophy. Nature 416(6878): 334-8.

Young, AA, Imai, H, Chang, CN and Axel, L (1994a). Two-dimensional left ventricular deformation during systole using magnetic resonance imaging with spatial modulation of magnetization. Circulation 89(2): 740-52.

Young, AA, Kramer, CM, Ferrari, VA, Axel, L and Reichek, N (1994b). Three-dimensional left ventricular deformation in hypertrophic cardiomyopathy. Circulation 90(2): 854-67.

Zambrano, E, Marshalko, SJ, Jaffe, CC and Hui, P (2002). Isolated noncompaction of the ventricular myocardium: clinical and molecular aspects of a rare cardiomyopathy. Lab Invest 82(2): 117-22.

Zerhouni, EA, Parish, DM, Rogers, WJ, Yang, A and Shapiro, EP (1988). Human heart: tagging with MR imaging--a method for noninvasive assessment of myocardial motion. Radiology 169(1): 59-63.

Zhang, J, Merkle, H, Hendrich, K, Garwood, M, From, AH, Ugurbil, K and Bache, RJ (1993). Bioenergetic abnormalities associated with severe left ventricular hypertrophy. J Clin Invest 92(2): 993-1003.

Index of Figures

Index of Tables